AN ABSTRACT OF THE THESIS OF

Waylon T. Bowers for the degree of Master of Science in Electrical and Computer Engineering presented on June 8, 2004.
Title: Hybrid Electric Vehicle Converter Harmonics

Abstract approved:

_____

Annette von Jouanne, Alan K. Wallace

Hybrid electric vehicles (HEV's) are a very important part of today's transportation system as they are bridging the gap between fully electric vehicles and conventional internal combustion vehicles (ICV's). They have much higher efficiencies and lower emissions than ICV's, while still having the ability to travel long range and refuel conveniently. The advantages offered by HEV's have caused several major automobile manufacturers to develop HEV's for public use and they are also being developed for military use. With the necessity of high performance vehicles the need arises for investigations on the converter generated harmonics which may become increasingly important. This is because there are several problems associated with harmonics including, high frequency interference, additional heat, mechanical stresses and audible noise (vibration) that may shorten the life of the equipment involved in HEV's and lower their reliability.

This thesis models, predicts, and mitigates the dc bus harmonics that are reflected by power electronic converters. It includes the investigation of dc bus harmonics through sine-triangle pulse width modulation (SPWM) analytical derivations

(open and closed form) and switching function approaches, as well as verification through Simulink and PSpice simulations, which all showed very good correlation. The resulting dc bus harmonics were also compared against MIL-STD-461 distortion limits. In the case where MIL-STD-461 was not met, mitigation techniques involved increasing the size of the dc bus capacitor. For further comparison, the space vector PWM (SVM) switching function approach has also been implemented in the simulations. Next, an experimental verification is presented and compared with a Simulink simulation which operates at approximately the same parameters. The final section of this report presents an overall comparison of the output line-to-line voltage harmonics, and the dc currents, for all of the above approaches.

Hybrid Electric Vehicle Converter Harmonics

By
Waylon T. Bowers

A THESIS

Submitted to

Oregon State University

In partial fulfillment of
the requirements for the
degree of

Master of Science

Presented June 8, 2004
Commencement June 2005

Master of Science thesis of Waylon T. Bowers presented on June 8, 2004

APPROVED:

Co-Major Professor, representing Electrical and Computer Engineering

---

Co-Major Professor, representing Electrical and Computer Engineering

---

Director, School of Electrical Engineering and Computer Science

---

Dean of the Graduate School

I understand that my thesis will become part of the permanent collection of Oregon State University libraries. My signature below authorizes release of my thesis to any reader upon request.

Waylon T. Bowers, Author

Master of Science thesis of Waylon T. Bowers presented on June 8, 2004

APPROVED:

Co-Major Professor, representing Electrical and Computer Engineering

---

Co-Major Professor, representing Electrical and Computer Engineering

---

Associate Director, School of Electrical Engineering and Computer Science

---

Dean of the Graduate School

I understand that my thesis will become part of the permanent collection of Oregon State University libraries. My signature below authorizes release of my thesis to any reader upon request.

Waylon T. Bowers, Author

ACKNOWLEDGMENTS

I would like to thank my advising professors Dr. Annette von Jouanne and Dr. Alan Wallace for the opportunity to pursue this degree and for their expertise, mentoring, encouragement and patience. I also would like to thank the other members of the Committee: Dr. Jimmy Eggerton and Dr. David Gobeli for their help. I want to express my appreciation to my fellow graduate students Anthony Schacher, Michael Mills-Price, Emmanuel Agamloh, Xiaolin Zhou, Jifeng Han and the entire Energy Systems group for their help and encouragement. A thanks goes out to Fuminao Kinjo and Andre Ramme for their enticement and charisma in the beginning.

Finally I am very grateful to my wife, Amanda, and my family for their love and support that kept me going through the years.

TABLE OF CONTENTS

LIST OF FIGURES

Figure Page

LIST OF FIGURES (Continued)

Figure Page

LIST OF TABLES

Table Page

LIST OF TABLES (Continued)

Table Page

1 Introduction

1.1 Hybrid Electric Vehicles

The typical hybrid electric vehicle (HEV) combines the conventional internal combustion engine with an electric motor and energy storage device(s) (batteries, flywheels, ultracapacitors, etc.). This combination drastically increases efficiency and reduces emissions. HEV's are becoming more common because they bridge the gap between conventional vehicles and fully electric vehicles (EV's). The problem with EV's is that with current battery technology they cannot be used for applications where long driving time is a requirement. HEV's are capable of going twice the distance of conventional vehicles and use the same convenient refueling system while producing many of the same environmental benefits as EV's. The advantages offered by HEV's have caused several major automobile manufacturers to develop HEV's for public use and they are also being developed to improve the range of military vehicles.

As the advantages of HEV's drive advanced applications with high performance requirements, investigations on the dc bus harmonics become increasingly important. This is because there are several problems associated with harmonics including, high frequency interference, capacitor degradation, skewing of digital clocks, potential interference with communication command and control, additional heat, mechanical stresses and audible noise (vibration) that may shorten the life of the equipment involved in HEV's and lower their reliability. The high power demands of HEV's

require advanced power electronic converters. For inverter controlled ac drive systems, two main strategies employed to minimize harmonic distortion of the supply to drive motors and other loads and eliminate harmonics are pulse width modulation (PWM) and multilevel topologies employing PWM, which will be discussed in this chapter. These strategies, however, result in harmonics being reflected back into the vehicles dc bus system.

1.2 PWM Strategies

PWM strategies, although synthesized through many different approaches, have some commonalities. First, the carrier frequency of the gate control should preferably be an integer multiple of the fundamental to the load such that the frequency spectrum of the output will consist of integer multiples of the fundamental output. Second, due to quarter-wave and half-wave symmetry, even-mode harmonics can be eliminated. Beyond this, techniques for PWM synthesis can be effectively described in the following categories [1].

1) Offline or pre-calculated PWM (also "Programmed PWM")

Selective harmonic elimination combines square-wave switching and PWM to control the fundamental output voltage and to eliminate selected lower-order harmonics from the output. Each angle corresponds to a degree of freedom from which a single odd order harmonic may be removed. Many of these PWM strategies use these degrees of freedom to cancel the critical lower odd-order harmonics.

2) Hysteresis Band PWM

A hysteresis band modulator calculates the error between the desired output and the measured output. The state of the switches is changed when this error leaves the hysteresis band so as to drive the error back within the band. The advantages to this technique are that it can respond to transients at the input or output quickly, and predict and bound the error (it is closed loop by nature).

3) Carrier Based PWM

Carrier based PWM methods are those where the switching decisions of the converter are made for each switching cycle either at the beginning or during that switch cycle. The PWM waveform is calculated on a cycle by cycle basis, either pulse by pulse, or edge by edge. This distinguishes it from offline PWM, where multiple switching edges are mapped out for the entire fundamental period or some fraction therein; and hysteretic PWM, where neither edges nor switch period are defined, calculated or even known in advance.

Sine-triangle PWM (SPWM) will be discussed in detail as part of the analytical derivations of this thesis. To effectively increase the modulation index for increased output voltage magnitudes, and to reduce the switching losses, "modified SPWM" can also be implemented. With "modified SPWM", the sine-triangle intersection is only performed for the first 60° and last 60° of each half of the waveform. Another method of increasing the effective modulation index and output voltage magnitude is by injecting (or "doping") the sinusoidal control waveform with 3^{rd} as well as 9^{th} harmonic to cause the

fundamental control waveform to be more “trapezoidal” with the major objective of reduced switching losses.

4) Space Vector PWM

The mathematical basis of Space Vector Modulation (SVM) Schemes requires that, the three-phase system, of many loads including propulsion motors, is transformed into its equivalent two-phase system in the d-q plane using Parks Transformation. This transformation removes the time dependency of load variables and enables the computation of inverter states in real time. The desired output voltage vector is synthesized as a function of the inverter switching states, as detailed in the developed SVM switching function approach later in this report.

Much of the current research focus addresses carrier based and space vector modulation techniques, which are implemented in this study. They provide good dynamic control, can be implemented in a digital or analog format with relative ease, and show adequate performance up through moderate switching frequencies. There are further refinement techniques in all these PWM schemes which allow for tradeoffs of certain desirable characteristics (low voltage ripple, low harmonic content, high power circuitry, etc.).

1.3 Multilevel Inverters

Multilevel inverters have shown promise in high power applications such as large HEV's. The attribute of high volt-ampere ratings in transformerless multilevel inverters makes them appropriate for applications in large HEV's [2]. The basic purpose of the multilevel inverter is to take many levels of dc voltages to synthesize the waveform of the desired output voltage. High voltages and low harmonics with no transformers and no series-connected, synchronized-switching devices are made possible by the use of multilevel inverters. For this reason, multilevel inverters can provide the high output quality power required by large HEV's. The best known multilevel inverter for this application (assuming an HEV with parallel connected traction drives) is the cascade H-bridge inverter [3]. This can use combinations of batteries, fuel cells, and ultracapacitors as the dc source. For military applications a significant advantage arises from the use of a cascade inverter, in that it will allow the HEV to "limp home" (it will still be able to operate with appropriate control and at reduced power even if some of the inverters are damaged) [4]. This requires the redundancy of each of the H-bridge inverters having its own separate dc source (SDCS) which can produce three different voltage levels $-V_{dc}$, 0, and $+ V_{dc}$. This is done by specific switching characteristics. The ac output of each H-bridge inverter is linked in series such that the system voltage waveform is the sum of each inverter's output. The larger the number of SDCS's there are in the system, the more sinusoidal the synthesized output voltage waveform will be. Fig. 1 shows an example of a single-phase cascade H-bridge inverter. In [5], the authors derive a way to eliminate

harmonics from varying levels of dc voltage sources as would be seen in the use of HEV's.

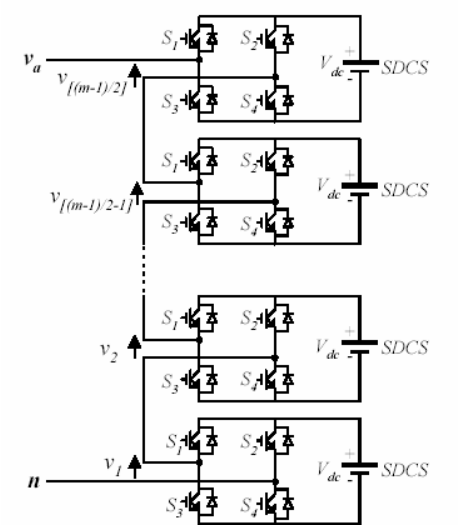

Fig. 1: Single-Phase Cascade H-Bridge Inverter

Fig. 2 shows an example of the output of an 11-level cascaded H-bridge multilevel inverter (it has five SDCS's). As mentioned previously, the output is $v_{an} = \sum_{i=1}^{5} v_{ai}$ and closely resembles a sinusoid.

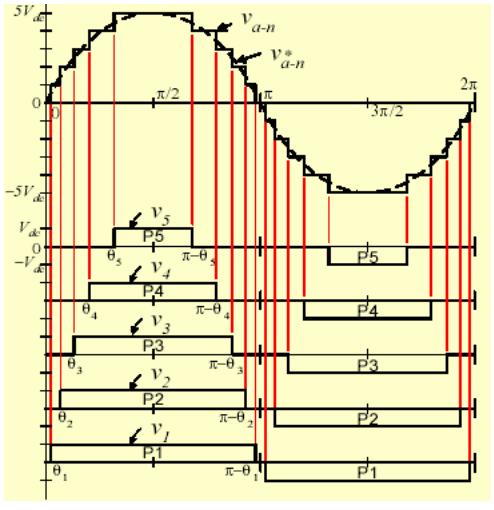

Fig. 2: Output of 11-Level Inverter

2 DC Bus Harmonic Study

The following material presents a summary of approaches, to converge on accurate results for dc bus harmonic currents and voltages. First, detailed open and closed form SPWM analytical approaches are conducted, followed by the SPWM Switching Function approach and SPWM simulations in Simulink and PSpice. All four of these approaches showed excellent correlation in the output line-to-line voltage harmonics, as well as close correlation of harmonics in the reflected the dc currents. The resulting dc bus harmonics were also compared against MIL-STD-461 distortion limits. In the case where MIL-STD-461 was not met, mitigation techniques involved increasing the size of the dc bus capacitor. For further comparison, the SVM Switching Function approach has also been implemented. The SVM approach employs a dramatically different method for generating the gating signals, thus the actual harmonics in the line-to-line voltages and the dc currents and voltages are different from the SPWM based approaches, however the predicted overall harmonic orders correlate well. Next, an experimental verification is presented and compared with a Simulink simulation which operates at approximately the same parameters. The final section of this report presents an overall Comparison Section of the output line-to-line voltage harmonics, and the dc currents, for all of the above approaches.

2.1 Analytical Approach

This section presents open form analysis and closed form solutions for the dc bus harmonics produced by three-phase PWM voltage source inverters (VSI's).

Transfer functions are frequently used as a means of describing the input/output relationship of a system. Although they are mainly used in linear systems, transfer functions can still be a very useful tool for describing switch mode converters. Basically, they can be used to evaluate a dependent variable in terms of its independent converter variable [6]. For example, the input dc bus current of a VSI (dependent input) depends on the converter transfer function and the output phase currents (independent outputs). Table 1 lists the various dependent and independent variables for VSI's. Inverters can be characterized by transfer functions, which are defined as:

$$TF = \frac{dependent\ electric\ variable}{independent\ electric\ variable} \quad [6]$$

Table 1: Variable Classification

Type	Input/Output	Current Variable	Voltage Variable
Voltage Source Inverter	Input (dc bus) Output (load)	Dependent (dc bus current) Independent (phase currents)	Independent (dc ripple free voltage) Dependent (ac line-to-neutral voltages)

Source: [6] pp. 237

The transfer functions differ according to the PWM scheme used. This initial analysis will be performed for sine-triangle PWM. The transfer function for SPWM in a VSI can be expressed as:

$$TF_v = \frac{[v_a, v_b, v_c]}{V_{dc}} = H(\omega t) \quad [6] \qquad (1)$$

where v_a, v_b, v_c are the corresponding phase voltages and V_{dc} is the dc input voltage. The line currents in the output of the inverter are reflected back to the input by means of this transfer function, such that:

$$I_{dc}(\omega t) = I_a(\omega t) \cdot H_a(\omega t) + I_b(\omega t) \cdot H_b(\omega t - 2.094) + I_c(\omega t) \cdot H_c(\omega t + 2.094)$$

Several SPWM parameters need to be defined to continue with this solution. The amplitude modulation ratio m_a, and the frequency modulation ration m_f, are defined as:

$$m_a = \frac{\hat{V}_{control}}{\hat{V}_{tri}} \qquad\qquad m_f = \frac{f_{sw}}{f_{fund}}$$

where $\hat{V}_{tri}$ is the amplitude of the triangle wave, $\hat{V}_{control}$ is the amplitude of the control sine wave (for the "sine-triangle intersection"), f_{sw} is the switching frequency for the triangle carrier wave, and f_{fund} is the fundamental frequency of the control sine wave [7]. For linear modulation, $m_a \leq 1.0$. To eliminate most of the dominant harmonics in the VSI output line-to-line voltages, m_f should be an odd multiple of 3, causing m_f and its multiples to be suppressed in the line-to-line voltages (only odd harmonics will exist as sidebands) [7]. For lower switching frequencies (f_{sw}) or higher fundamental/control frequencies (f_{fund}) which would result in $m_f < 21$, we typically use synchronous PWM where m_f is an integer, i.e. f_{sw} is an exact multiple of f_{fund}, to prevent large subharmonics of the fundamental frequency (e.g. close to 0 Hz). Therefore, as f_{fund} varies, f_{sw} varies, or m_f varies, or both to maintain synchronous operation [7]. The targeted switching frequency for this application is 5-10 kHz, while

f_{fund} can go up to 900Hz (with a range of slip frequency, near zero speed with a low slip induction machine, i.e. 2Hz, to 900Hz), thus the possibility exists for $m_f < 21$, therefore the harmonic results of asynchronous PWM (e.g. 500Hz) are investigated as a part of this study.

For $m_a \le 1.0$, the fundamental output voltages vary linearly with m_a, and we have no lower order harmonics close to the fundamental. It follows that the line-to-line rms voltage at the fundamental frequency, $(V_{LL})_1$, can be computed as:

$$(V_{LL})_1 = \frac{\sqrt{3}}{\sqrt{2}}(V_{LN})_1 = \frac{\sqrt{3}}{\sqrt{2}} m_a \frac{V_{dc}}{2} = 0.612 \cdot m_a V_{dc} \quad [7]$$

The line-to-line rms harmonic voltages can be computed similarly as:

$$(V_{LL})_h = m_h \cdot V_{dc} \quad [7] \qquad (2)$$

and the phase voltages will be:

$$(V_\phi)_h = \frac{(V_{LL})_h}{\sqrt{3}} = \frac{m_h \cdot V_{dc}}{\sqrt{3}}$$

where m_h is a coefficient listed in Table 2. Also listed in Table 2 is k_h, which is the actual harmonic order that will be used in the following calculations.

Table 2:Generalized Harmonic Coefficients for Three Phase PWM

h	k_h	m_a				
		0.2	0.4	0.6	**0.8**	1.0
		Coefficient m_h				
1	1	0.122	0.245	0.367	**0.490**	0.612
2	$m_f \pm 2$	0.010	0.037	0.080	**0.135**	0.195
3	$m_f \pm 4$				**0.005**	0.011
4	$2m_f \pm 1$	0.116	0.200	0.227	**0.192**	0.111
5	$2m_f \pm 5$				**0.008**	0.020
6	$3m_f \pm 2$	0.027	0.085	0.124	**0.108**	0.038
7	$3m_f \pm 4$		0.007	0.029	**0.064**	0.096
8	$4m_f \pm 1$	0.100	0.096	0.005	**0.064**	0.042
9	$4m_f \pm 5$			0.021	**0.051**	0.073
10	$4m_f \pm 7$				**0.010**	0.030

Source: [7] pp. 228

Closed Form Solution

For a closed form solution, the following parameters will be used:

$V_{dc} = 600$ V $\qquad f_{sw} = 9900$ Hz $\qquad f_{fund} = 60$ Hz

$m_f = \frac{f_{sw}}{f_{fund}} = 165$ $\qquad m_a = 0.8$ for 250kW (=1.0 for $P_{\max} = 400$ kW)

$P_{out} = 250$ kW $\qquad \cos(\theta) = p.f. = 0.9$ $\qquad \omega = 2\pi\ f_{fund} = 377$ rad/sec

$C = 2400\mu F$

Conversion of 30° voltage phase shift (line-to-line voltage leads the phase voltage by 30°), θ_{LL}, to radians: $\theta_{LL} = \frac{30^\circ}{180^\circ}\pi = 0.524$ rad

Conversion of 120° voltage phase shift, θ_V, to radians: $\theta_V = \frac{120^\circ}{180^\circ}\pi = 2.094$ rad

Voltages

With m_a = 0.8 and including the harmonic coefficients (m_h coefficient of $m_f \pm 2$, $m_f \pm 4$, $2m_f \pm 1, 2m_f \pm 5, 3m_f \pm 2$, $3m_f \pm 4$, $4m_f \pm 1$, $4m_f \pm 5$, and $4m_f \pm 7$ which are bolded in Table 2), the line-to-line voltage amplitudes are defined as:

$$v_{ab}(\omega t) = \sum_{h=1,2}^{10} \sqrt{2} \cdot V_{dc} \cdot m_h \sin\left(k_h(\omega t + \theta_{LL})\right)$$

$$\begin{aligned}
&= \sqrt{2} \cdot V_{dc}(m_1 \sin(\omega t + \theta_{LL}) \\
&+ m_2 \sin((m_f \pm 2)(\omega t + \theta_{LL})) + m_3 \sin((m_f \pm 4)(\omega t + \theta_{LL})) \\
&+ m_4 \sin((2m_f \pm 1)(\omega t + \theta_{LL})) + m_5 \sin((2m_f \pm 5)(\omega t + \theta_{LL})) \\
&+ m_6 \sin((3m_f \pm 2)(\omega t + \theta_{LL})) + m_7 \sin((3m_f \pm 4)(\omega t + \theta_{LL})) \\
&+ m_8 \sin((4m_f \pm 1)(\omega t + \theta_{LL})) + m_9 \sin((4m_f \pm 5)(\omega t + \theta_{LL})) \\
&+ m_{10} \sin((4m_f \pm 7)(\omega t + \theta_{LL})))
\end{aligned}$$

$$\begin{aligned}
&= \sqrt{2} \cdot 600 \cdot (0.490 \sin(377t + 0.524) \\
&+ 0.135 \sin(167 * (377t + 0.524)) + 0.135 \sin(163 * (377t + 0.524)) \\
&+ 0.005 \sin(169 * (377t + 0.524)) + 0.005 * \sin(161 * (377t + 0.524)) \\
&+ 0.192 \sin(331 * (377t + 0.524)) + 0.192 \sin(329 * (377t + 0.524)) \\
&+ 0.008 \sin(335 * (377t + 0.524)) + 0.008 \sin(325 * (377t + 0.524)) \\
&+ 0.108 \sin(497 * (377t + 0.524)) + 0.108 \sin(493 * (377t + 0.524)) \\
&+ 0.064 \sin(499 * (377t + 0.524)) + 0.064 \sin(491 * (377t + 0.524)) \\
&+ 0.064 \sin(661 * (377t + 0.524)) + 0.064 \sin(659 * (377t + 0.524)) \\
&+ 0.051 \sin(665 * (377t + 0.524)) + 0.051 \sin(655 * (377t + 0.524)) \\
&+ 0.010 \sin(667 * (377t + 0.524)) + 0.010 \sin(653 * (377t + 0.524)))
\end{aligned}$$

$$
\begin{aligned}
&= 415.77\sin(377t + 0.524) \\
&+ 114.55\sin(62959t + 87.51) + 114.5\sin(61451t + 85.41) \\
&+ 4.24\sin(63713t + 88.56) + 4.24\sin(60697t + 84.36) \\
&+ 162.92\sin(124787t + 173.44) + 162.92\sin(124033t + 172.39) \\
&+ 6.79\sin(126295t + 175.54) + 6.79\sin(122525t + 170.30) \\
&+ 91.64\sin(187369t + 260.43) + 91.64\sin(185861t + 258.33) \\
&+ 54.31\sin(188123t + 261.48) + 54.31\sin(185107t + 257.28) \\
&+ 54.31\sin(249197t + 346.36) + 54.31\sin(248443t + 345.32) \\
&+ 43.27\sin(250705t + 348.46) + 43.27\sin(246935t + 343.22) \\
&+ 8.49\sin(251459t + 349.51) + 8.49\sin(246181t + 342.17)
\end{aligned}
$$

$v_{ab}(\omega t)$ is shown in Fig. 3 (zoomed in, in Fig. 4) and its harmonic spectrum is shown in Fig. 5, which is also listed in Table 3.

$$v_{bc}(\omega t) = \sum_{h=1,2}^{10} \sqrt{2} \cdot V_{dc} \cdot m_h \sin\left(k_h(\omega t + \theta_{LL} - \theta_V)\right)$$

$$
\begin{aligned}
&= \sqrt{2} \cdot V_{dc}(m_1 \sin(\omega t + \theta_{LL} - \theta_V) \\
&+ m_2 \sin((m_f \pm 2)(\omega t + \theta_{LL} - \theta_V)) + m_3 \sin((m_f \pm 4)(\omega t + \theta_{LL} - \theta_V)) \\
&+ m_4 \sin((2m_f \pm 1)(\omega t + \theta_{LL} - \theta_V)) + m_5 \sin((2m_f \pm 5)(\omega t + \theta_{LL} - \theta_V)) \\
&+ m_6 \sin((3m_f \pm 2)(\omega t + \theta_{LL} - \theta_V)) + m_7 \sin((3m_f \pm 4)(\omega t + \theta_{LL} - \theta_V)) \\
&+ m_8 \sin((4m_f \pm 1)(\omega t + \theta_{LL} - \theta_V)) + m_9 \sin((4m_f \pm 5)(\omega t + \theta_{LL} - \theta_V)) \\
&+ m_{10} \sin((4m_f \pm 7)(\omega t + \theta_{LL} - \theta_V)))
\end{aligned}
$$

$$
\begin{aligned}
&= \sqrt{2} \cdot 600 \cdot (0.490\sin(377t - 2.094 + 0.524) \\
&+ 0.135\sin(167 * (377t - 2.094 + 0.524)) + 0.135\sin(163 * (377t - 2.094 + 0.524)) \\
&+ 0.005\sin(169 * (377t - 2.094 + 0.524)) + 0.100\sin(161 * (377t - 2.094 + 0.524)) \\
&+ 0.192\sin(331 * (377t - 2.094 + 0.524)) + 0.192\sin(329 * (377t - 2.094 + 0.524)) \\
&+ 0.008\sin(335 * (377t - 2.094 + 0.524)) + 0.008\sin(325 * (377t - 2.094 + 0.524)) \\
&+ 0.108\sin(497 * (377t - 2.094 + 0.524)) + 0.108\sin(493 * (377t - 2.094 + 0.524)) \\
&+ 0.064\sin(499 * (377t - 2.094 + 0.524)) + 0.064\sin(491 * (377t - 2.094 + 0.524)) \\
&+ 0.064\sin(661 * (377t - 2.094 + 0.524)) + 0.064\sin(659 * (377t - 2.094 + 0.524)) \\
&+ 0.051\sin(665 * (377t - 2.094 + 0.524)) + 0.051\sin(655 * (377t - 2.094 + 0.524)) \\
&+ 0.010\sin(667 * (377t - 2.094 + 0.524)) + 0.010\sin(653 * (377t - 2.094 + 0.524)))
\end{aligned}
$$

$$= 415.77\sin(377t - 1.57)$$
$$+ 114.55\sin(62959t - 262.19) + 114.5\sin(61451t - 255.91)$$
$$+ 4.24\sin(63713t - 265.33) + 4.24\sin(60697t - 252.77)$$
$$+ 162.92\sin(124787t - 519.67) + 162.92\sin(124033t - 516.53)$$
$$+ 6.79\sin(126295t - 525.95) + 6.79\sin(122525t - 510.25)$$
$$+ 91.64\sin(187369t - 780.29) + 91.64\sin(185861t - 774.01)$$
$$+ 54.31\sin(188123t - 783.43) + 54.31\sin(185107t - 770.87)$$
$$+ 54.31\sin(249197t - 1037.77) + 54.31\sin(248443t - 1034.63)$$
$$+ 43.27\sin(250705t - 1044.05) + 43.27\sin(246935t - 1028.35)$$
$$+ 8.49\sin(251459t - 1047.19) + 8.49\sin(246181t - 1025.21)$$

$$v_{ca}(\omega t) = \sum_{h=1,2}^{10} \sqrt{2} \cdot V_{dc} \cdot m_h \sin\left(k_h(\omega t + \theta_{LL} + \theta_V)\right)$$
$$= \sqrt{2} \cdot V_{dc}(m_1 \sin(\omega t + \theta_{LL} + \theta_V)$$
$$+ m_2 \sin((m_f \pm 2)(\omega t + \theta_{LL} + \theta_V)) + m_3 \sin((m_f \pm 4)(\omega t + \theta_{LL} + \theta_V))$$
$$+ m_4 \sin((2m_f \pm 1)(\omega t + \theta_{LL} + \theta_V)) + m_5 \sin((2m_f \pm 5)(\omega t + \theta_{LL} + \theta_V))$$
$$+ m_6 \sin((3m_f \pm 2)(\omega t + \theta_{LL} + \theta_V)) + m_7 \sin((3m_f \pm 4)(\omega t + \theta_{LL} + \theta_V))$$
$$+ m_8 \sin((4m_f \pm 1)(\omega t + \theta_{LL} + \theta_V)) + m_9 \sin((4m_f \pm 5)(\omega t + \theta_{LL} + \theta_V))$$
$$+ m_{10} \sin((4m_f \pm 7)(\omega t + \theta_{LL} + \theta_V)))$$

$$= \sqrt{2} \cdot 600 \cdot (0.490\sin(377t + 2.094 + 0.524)$$
$$+ 0.135\sin(167 * (377t + 2.094 + 0.524)) + 0.135\sin(163 * (377t + 2.094 + 0.524))$$
$$+ 0.005\sin(169 * (377t + 2.094 + 0.524)) + 0.100\sin(161 * (377t + 2.094 + 0.524))$$
$$+ 0.192\sin(331 * (377t + 2.094 + 0.524)) + 0.192\sin(329 * (377t + 2.094 + 0.524))$$
$$+ 0.008\sin(335 * (377t + 2.094 + 0.524)) + 0.008\sin(325 * (377t + 2.094 + 0.524))$$
$$+ 0.108\sin(497 * (377t + 2.094 + 0.524)) + 0.108\sin(493 * (377t + 2.094 + 0.524))$$
$$+ 0.064\sin(499 * (377t + 2.094 + 0.524)) + 0.064\sin(491 * (377t + 2.094 + 0.524))$$
$$+ 0.064\sin(661 * (377t + 2.094 + 0.524)) + 0.064\sin(659 * (377t + 2.094 + 0.524))$$
$$+ 0.051\sin(665 * (377t + 2.094 + 0.524)) + 0.051\sin(655 * (377t + 2.094 + 0.524))$$
$$+ 0.010\sin(667 * (377t + 2.094 + 0.524)) + 0.010\sin(653 * (377t + 2.094 + 0.524)))$$

$$
\begin{aligned}
&= 415.77\sin(377t + 2.618) \\
&+ 114.55\sin(62959t + 437.21) + 114.5\sin(61451t + 426.73) \\
&+ 4.24\sin(63713t + 442.44) + 4.24\sin(60697t + 421.49) \\
&+ 162.92\sin(124787t + 866.56) + 162.92\sin(124033t + 861.32) \\
&+ 6.79\sin(126295t + 877.03) + 6.79\sin(122525t + 850.85) \\
&+ 91.64\sin(187369t + 1301.15) + 91.64\sin(185861t + 1290.67) \\
&+ 54.31\sin(188123t + 1306.38) + 54.31\sin(185107t + 1285.44) \\
&+ 54.31\sin(249197t + 1730.49) + 54.31\sin(248443t + 1725.26) \\
&+ 43.27\sin(250705t + 1740.97) + 43.27\sin(246935t + 1714.79) \\
&+ 8.49\sin(251459t + 1746.21) + 8.49\sin(246181t + 1709.55)
\end{aligned}
$$

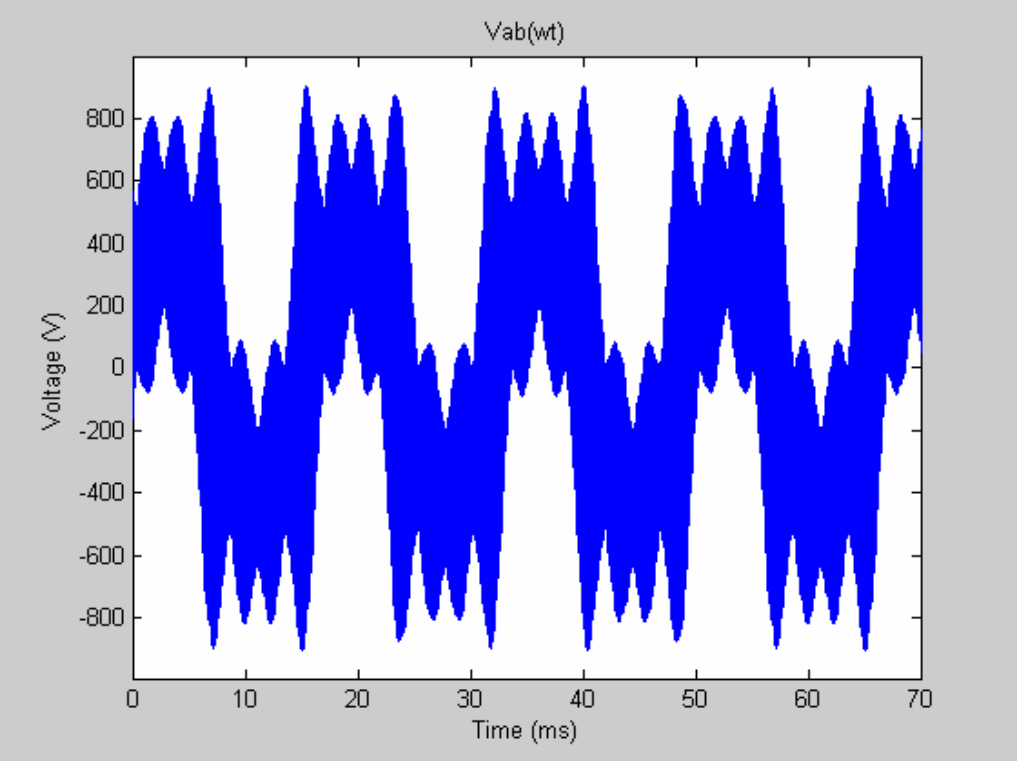

Fig. 3: Line-to-Line Voltage, $v_{ab}(\omega t)$

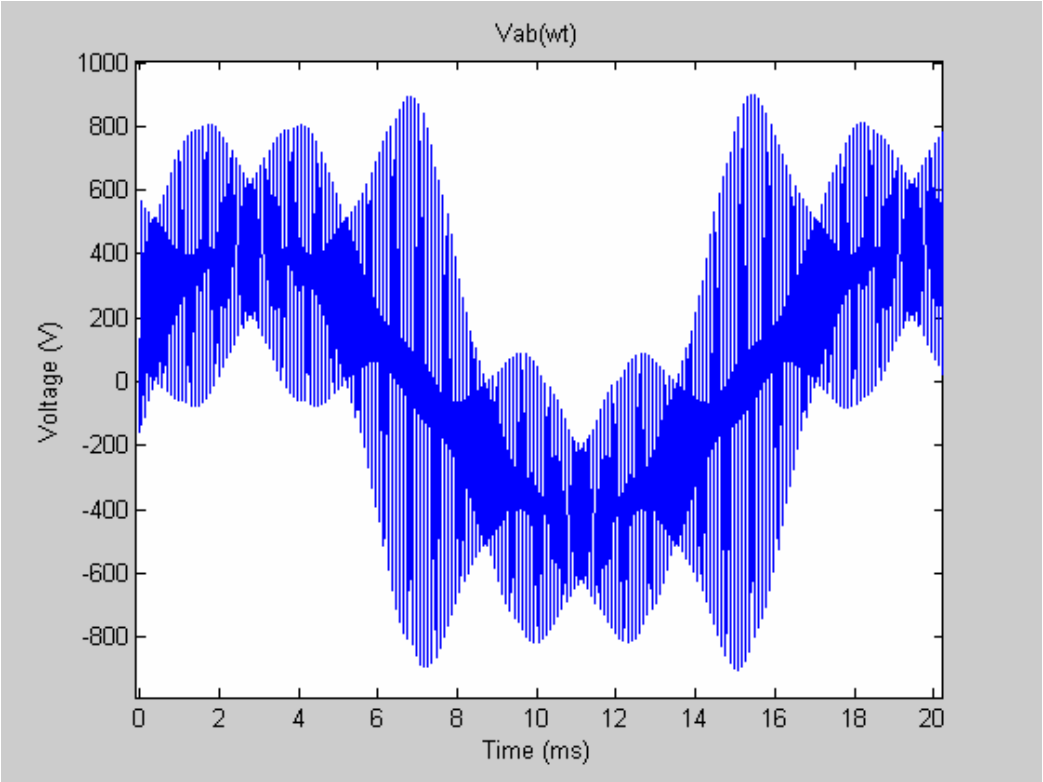

Fig. 4: Line-to-Line Voltage, $v_{ab}(\omega t)$, Zoomed In

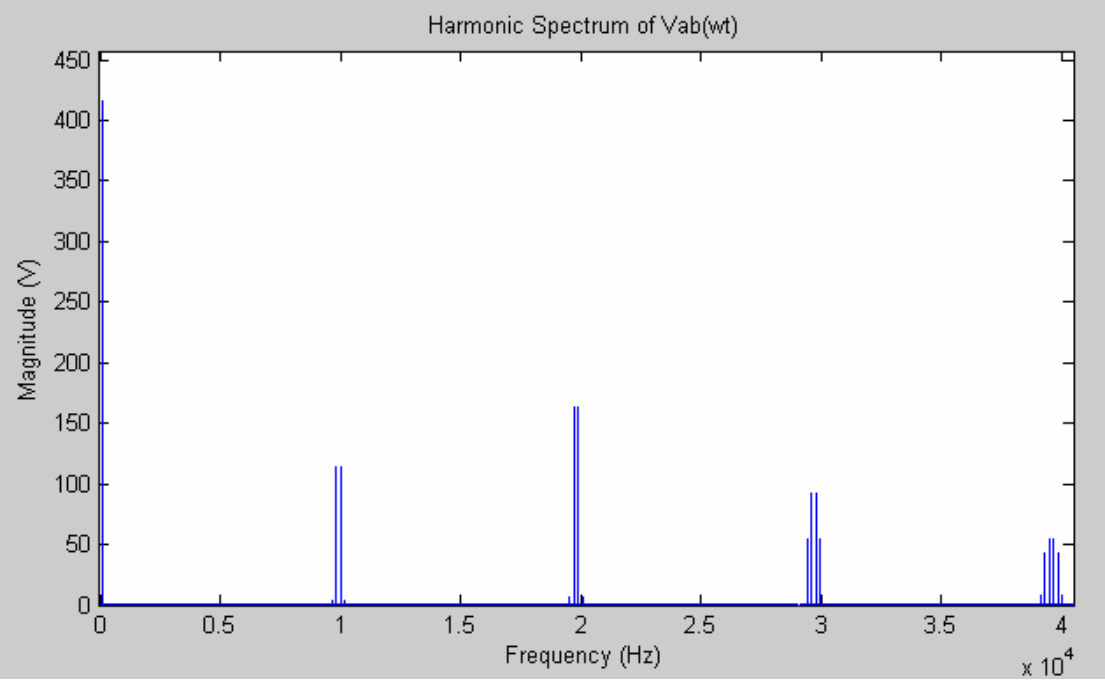

Fig. 5: Harmonic Spectrum of $v_{ab}(\omega t)$

Table 3: Harmonics of $v_{ab}(\omega t)$

Order	Freq (kHz)	Magn (% of Fund)
FUND	0.060	100.00
161	9.66	1.02
163	9.78	27.56
167	10.02	27.56
169	10.14	1.02
325	19.5	1.64
329	19.74	39.19
331	19.86	39.19
335	20.1	1.64
491	29.46	13.06
493	29.58	22.04
497	29.82	22.04
499	29.94	13.06
653	39.18	2.04
655	39.3	10.38
659	39.54	13.03
661	39.66	13.03
665	39.9	10.38
667	40.02	2.04

For the transfer function we need the phase voltages, which are:

$$v_a(\omega t) = \sum_{h=1,2}^{10} \frac{\sqrt{2}}{\sqrt{3}} \cdot V_{dc} \cdot m_h \sin(k_h \omega t)$$

$$\begin{aligned}
&= \frac{\sqrt{2}}{\sqrt{3}} \cdot V_{dc} (m_1 \sin(\omega t) \\
&+ m_2 \sin((m_f \pm 2)\omega t) + m_3 \sin((m_f \pm 4)\omega t) \\
&+ m_4 \sin((2m_f \pm 1)\omega t) + m_5 \sin((2m_f \pm 5)\omega t) \\
&+ m_6 \sin((3m_f \pm 2)\omega t) + m_7 \sin((3m_f \pm 4)\omega t) \\
&+ m_8 \sin((4m_f \pm 1)\omega t) + m_9 \sin((4m_f \pm 5)\omega t) \\
&+ m_{10} \sin((4m_f \pm 7)\omega t))
\end{aligned}$$

$$= \frac{\sqrt{2}}{\sqrt{3}} \cdot 600 \cdot (0.490\sin(377t)$$
$$+ 0.135\sin(167*377t) + 0.135\sin(163*377t)$$
$$+ 0.005\sin(169*377t) + 0.005*\sin(161*377t)$$
$$+ 0.192\sin(331*377t) + 0.192\sin(329*377t)$$
$$+ 0.008\sin(335*377t) + 0.008\sin(325*377t)$$
$$+ 0.108\sin(497*377t) + 0.108\sin(493*377t)$$
$$+ 0.064\sin(499*377t) + 0.064\sin(491*377t)$$
$$+ 0.064\sin(661*377t) + 0.064\sin(659*377t)$$
$$+ 0.051\sin(665*377t) + 0.051\sin(655*377t)$$
$$+ 0.010\sin(667*377t) + 0.010\sin(653*377t))$$

$$= 240.04\sin(377t)$$
$$+ 66.14\sin(62959t) + 66.14\sin(61451t)$$
$$+ 2.45\sin(63713t) + 2.45\sin(60697t)$$
$$+ 94.06\sin(124787t) + 94.06\sin(124033t)$$
$$+ 3.92\sin(126295t) + 3.92\sin(122525t)$$
$$+ 52.91\sin(187369t) + 52.91\sin(185861t)$$
$$+ 31.36\sin(188123t) + 31.36\sin(185107t)$$
$$+ 31.36\sin(249197t) + 31.36\sin(248443t)$$
$$+ 24.98\sin(250705t) + 24.98\sin(246935t)$$
$$+ 4.90\sin(251459t) + 4.90\sin(246181t)$$

$$v_b(\omega t) = \sum_{h=1,2}^{10} \frac{\sqrt{2}}{\sqrt{3}} \cdot V_{dc} \cdot m_h \sin\left(k_h(\omega t - \theta_V)\right)$$

$$= \frac{\sqrt{2}}{\sqrt{3}} \cdot V_{dc}(m_1 \sin(\omega t - \theta_V)$$
$$+ m_2 \sin((m_f \pm 2)(\omega t - \theta_V)) + m_3 \sin((m_f \pm 4)(\omega t - \theta_V))$$
$$+ m_4 \sin((2m_f \pm 1)(\omega t - \theta_V)) + m_5 \sin((2m_f \pm 5)(\omega t - \theta_V))$$
$$+ m_6 \sin((3m_f \pm 2)(\omega t - \theta_V)) + m_7 \sin((3m_f \pm 4)(\omega t - \theta_V))$$
$$+ m_8 \sin((4m_f \pm 1)(\omega t - \theta_V)) + m_9 \sin((4m_f \pm 5)(\omega t - \theta_V))$$
$$+ m_{10} \sin((4m_f \pm 7)(\omega t - \theta_V)))$$

$$= \frac{\sqrt{2}}{\sqrt{3}} \cdot 600 \cdot (0.490 \sin(377t - 2.094)$$
$$+ 0.135 \sin(167 * (377t - 2.094)) + 0.135 \sin(163 * (377t - 2.094))$$
$$+ 0.005 \sin(169 * (377t - 2.094)) + 0.100 \sin(161 * (377t - 2.094))$$
$$+ 0.192 \sin(331 * (377t - 2.094)) + 0.192 \sin(329 * (377t - 2.094))$$
$$+ 0.008 \sin(335 * (377t - 2.094)) + 0.008 \sin(325 * (377t - 2.094))$$
$$+ 0.108 \sin(497 * (377t - 2.094)) + 0.108 \sin(493 * (377t - 2.094))$$
$$+ 0.064 \sin(499 * (377t - 2.094)) + 0.064 \sin(491 * (377t - 2.094))$$
$$+ 0.064 \sin(661 * (377t - 2.094)) + 0.064 \sin(659 * (377t - 2.094))$$
$$+ 0.051 \sin(665 * (377t - 2.094)) + 0.051 \sin(655 * (377t - 2.094))$$
$$+ 0.010 \sin(667 * (377t - 2.094)) + 0.010 \sin(653 * (377t - 2.094)))$$

$$= 240.04 \sin(377t - 2.094)$$
$$+ 66.14 \sin(62959t - 349.69) + 66.14 \sin(61451t - 341.32)$$
$$+ 2.45 \sin(63713t - 353.89) + 2.45 \sin(60697t - 337.13)$$
$$+ 94.06 \sin(124787t - 693.11) + 94.06 \sin(124033t - 688.93)$$
$$+ 3.92 \sin(126295t - 701.49) + 3.92 \sin(122525t - 680.55)$$
$$+ 52.91 \sin(187369t - 1040.72) + 52.91 \sin(185861t - 1032.34)$$
$$+ 31.36 \sin(188123t - 1044.91) + 31.36 \sin(185107t - 1028.15)$$
$$+ 31.36 \sin(249197t - 1384.13) + 31.36 \sin(248443t - 1379.95)$$
$$+ 24.98 \sin(250705t - 1392.51) + 24.98 \sin(246935t - 1371.57)$$
$$+ 4.90 \sin(251459t - 1396.69) + 4.90 \sin(246181t - 1367.38)$$

$$v_c(\omega t) = \sum_{h=1,2}^{10} \frac{\sqrt{2}}{\sqrt{3}} \cdot V_{dc} \cdot m_h \sin\left(k_h(\omega t + \theta_V)\right)$$

$$= \frac{\sqrt{2}}{\sqrt{3}} \cdot V_{dc} (m_1 \sin(\omega t + \theta_V)$$
$$+ m_2 \sin((m_f \pm 2)(\omega t + \theta_V)) + m_3 \sin((m_f \pm 4)(\omega t + \theta_V))$$
$$+ m_4 \sin((2m_f \pm 1)(\omega t + \theta_V)) + m_5 \sin((2m_f \pm 5)(\omega t + \theta_V))$$
$$+ m_6 \sin((3m_f \pm 2)(\omega t + \theta_V)) + m_7 \sin((3m_f \pm 4)(\omega t + \theta_V))$$
$$+ m_8 \sin((4m_f \pm 1)(\omega t + \theta_V)) + m_9 \sin((4m_f \pm 5)(\omega t + \theta_V))$$
$$+ m_{10} \sin((4m_f \pm 7)(\omega t + \theta_V)))$$

$$= \frac{\sqrt{2}}{\sqrt{3}} \cdot 600 \cdot (0.490 \sin(377t + 2.094)$$
$$+ 0.135 \sin(167 * (377t + 2.094)) + 0.135 \sin(163 * (377t + 2.094))$$
$$+ 0.005 \sin(169 * (377t + 2.094)) + 0.100 \sin(161 * (377t + 2.094))$$
$$+ 0.192 \sin(331 * (377t + 2.094)) + 0.192 \sin(329 * (377t + 2.094))$$
$$+ 0.008 \sin(335 * (377t + 2.094)) + 0.008 \sin(325 * (377t + 2.094))$$
$$+ 0.108 \sin(497 * (377t + 2.094)) + 0.108 \sin(493 * (377t + 2.094))$$
$$+ 0.064 \sin(499 * (377t + 2.094)) + 0.064 \sin(491 * (377t + 2.094))$$
$$+ 0.064 \sin(661 * (377t + 2.094)) + 0.064 \sin(659 * (377t + 2.094))$$
$$+ 0.051 \sin(665 * (377t + 2.094)) + 0.051 \sin(655 * (377t + 2.094))$$
$$+ 0.010 \sin(667 * (377t + 2.094)) + 0.010 \sin(653 * (377t + 2.094)))$$

$$= 240.04 \sin(377t + 2.094)$$
$$+ 66.14 \sin(62959t + 349.69) + 66.14 \sin(61451t + 341.32)$$
$$+ 2.45 \sin(63713t + 353.89) + 2.45 \sin(60697t + 337.13)$$
$$+ 94.06 \sin(124787t + 693.11) + 94.06 \sin(124033t + 688.93)$$
$$+ 3.92 \sin(126295t + 701.49) + 3.92 \sin(122525t + 680.55)$$
$$+ 52.91 \sin(187369t + 1040.72) + 52.91 \sin(185861t + 1032.34)$$
$$+ 31.36 \sin(188123t + 1044.91) + 31.36 \sin(185107t + 1028.15)$$
$$+ 31.36 \sin(249197t + 1384.13) + 31.36 \sin(248443t + 1379.95)$$
$$+ 24.98 \sin(250705t + 1392.51) + 24.98 \sin(246935t + 1371.57)$$
$$+ 4.90 \sin(251459t + 1396.69) + 4.90 \sin(246181t + 1367.38)$$

Currents

Next, the line currents need to be solved for (the line current is assumed to be a pure sine wave due to the highly inductive motor load). The output power is defined as:

$$P_{out} = \sqrt{3} V_{LL} I_L \cos(\theta)$$

where at $m_a = 0.8$, $V_{LL,rms,1} = m_1 V_{dc} = 0.490 * 600 = 294.0$.

Thus, the magnitude of the rms line current is:

$$I_{L,rms} = \frac{P_{out}}{\sqrt{3}V_{LL,rms,1}\cos(\theta)}$$

$$= \frac{250000}{\sqrt{3} * 294.0 * 0.9}$$

$$= 545.49 \text{ A}$$

$$I_{L,\max} = \sqrt{2} \cdot I_{L,rms} = \sqrt{2} \cdot 545.49 = 771.44 \text{ A}$$

$v_a(\omega t)$ has a phase angle of $\theta_{LN} = 0^\circ$. Now, the phase angle of the line current can be computed by:

$$p.f. = \cos(\theta_{LN} - \theta_I)$$

$$\theta_I = \theta_{LN} - \cos^{-1}(p.f.)$$
$$= 0^\circ - 25.84^\circ$$
$$= -25.84^\circ = -0.451 \text{ rad}$$

Therefore,

$$I_a(\omega t) = 771.44 \sin(\omega t - 0.451)$$
$$= 771.44 \sin(377t - 0.451)$$

$$I_b(\omega t) = 771.44 \sin(\omega t - 0.451 - 2.094)$$
$$= 771.44 \sin(377t - 2.545)$$

$$I_c(\omega t) = 771.44 \sin(\omega t - 0.451 + 2.094)$$
$$= 771.44 \sin(377t + 1.643)$$

$I_a(\omega t)$, $I_b(\omega t)$, $I_c(\omega t)$ are shown in Fig. 6.

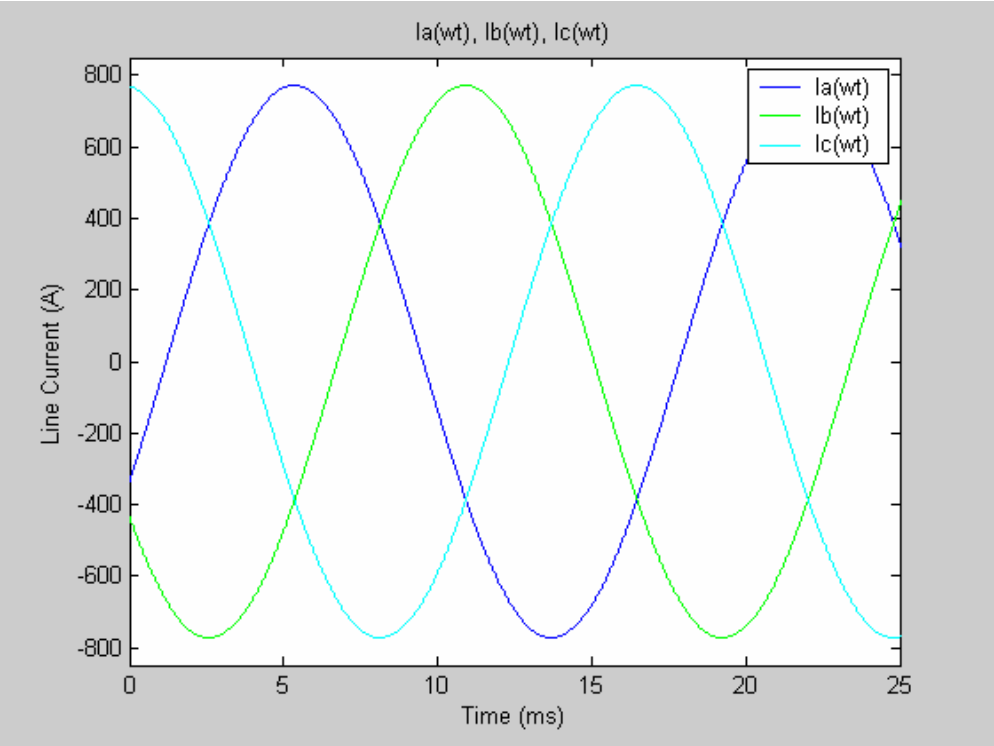

Fig. 6: Line Currents, $I_a(\omega t), I_b(\omega t), I_c(\omega t)$

The transfer function is now:

$$H(\omega t) = \frac{[v_a, v_b, v_c]}{V_{dc}} \quad [6]$$

where it can be broken up to its phase components:

$$\begin{aligned} H_a(\omega t) &= \frac{v_a(\omega t)}{V_{dc}} \\ &= \frac{\sqrt{2}}{\sqrt{3}}(m_1 \sin(\omega t) \\ &+ m_2 \sin((m_f \pm 2)\omega t) + m_3 \sin((m_f \pm 4)\omega t) \\ &+ m_4 \sin((2m_f \pm 1)\omega t) + m_5 \sin((2m_f \pm 5)\omega t) \\ &+ m_6 \sin((3m_f \pm 2)\omega t) + m_7 \sin((3m_f \pm 4)\omega t) \\ &+ m_8 \sin((4m_f \pm 1)\omega t) + m_9 \sin((4m_f \pm 5)\omega t) \\ &+ m_{10} \sin((4m_f \pm 7)\omega t)) \end{aligned}$$

$$= \frac{\sqrt{2}}{\sqrt{3}} \cdot (0.490\sin(377t)$$
$$+ 0.135\sin(167*377t) + 0.135\sin(163*377t)$$
$$+ 0.005\sin(169*377t) + 0.005*\sin(161*377t)$$
$$+ 0.192\sin(331*377t) + 0.192\sin(329*377t)$$
$$+ 0.008\sin(335*377t) + 0.008\sin(325*377t)$$
$$+ 0.108\sin(497*377t) + 0.108\sin(493*377t)$$
$$+ 0.064\sin(499*377t) + 0.064\sin(491*377t)$$
$$+ 0.064\sin(661*377t) + 0.064\sin(659*377t)$$
$$+ 0.051\sin(665*377t) + 0.051\sin(655*377t)$$
$$+ 0.010\sin(667*377t) + 0.010\sin(653*377t))$$

$$H_b(\omega t - 2.094) = \frac{v_b(\omega t)}{V_{dc}}$$
$$= \frac{\sqrt{2}}{\sqrt{3}}(m_1\sin(\omega t - 2.094)$$
$$+ m_2\sin((m_f \pm 2)(\omega t - 2.094)) + m_3\sin((m_f \pm 4)(\omega t - 2.094))$$
$$+ m_4\sin((2m_f \pm 1)(\omega t - 2.094)) + m_5\sin((2m_f \pm 5)(\omega t - 2.094))$$
$$+ m_6\sin((3m_f \pm 2)(\omega t - 2.094)) + m_7\sin((3m_f \pm 4)(\omega t - 2.094))$$
$$+ m_8\sin((4m_f \pm 1)(\omega t - 2.094)) + m_9\sin((4m_f \pm 5)(\omega t - 2.094))$$
$$+ m_{10}\sin((4m_f \pm 7)(\omega t - 2.094)))$$

$$= \frac{\sqrt{2}}{\sqrt{3}} \cdot (0.490\sin(377t - 2.094)$$
$$+ 0.135\sin(167*(377t - 2.094)) + 0.135\sin(163*(377t - 2.094))$$
$$+ 0.005\sin(169*(377t - 2.094)) + 0.100\sin(161*(377t - 2.094))$$
$$+ 0.192\sin(331*(377t - 2.094)) + 0.192\sin(329*(377t - 2.094))$$
$$+ 0.008\sin(335*(377t - 2.094)) + 0.008\sin(325*(377t - 2.094))$$
$$+ 0.108\sin(497*(377t - 2.094)) + 0.108\sin(493*(377t - 2.094))$$
$$+ 0.064\sin(499*(377t - 2.094)) + 0.064\sin(491*(377t - 2.094))$$
$$+ 0.064\sin(661*(377t - 2.094)) + 0.064\sin(659*(377t - 2.094))$$
$$+ 0.051\sin(665*(377t - 2.094)) + 0.051\sin(655*(377t - 2.094))$$
$$+ 0.010\sin(667*(377t - 2.094)) + 0.010\sin(653*(377t - 2.094)))$$

$$H_c(\omega t + 2.094) = \frac{v_c(\omega t)}{V_{dc}}$$

$$= \frac{\sqrt{2}}{\sqrt{3}}(m_1 \sin(\omega t + 2.094)$$
$$+ m_2 \sin((m_f \pm 2)(\omega t + 2.094)) + m_3 \sin((m_f \pm 4)(\omega t + 2.094))$$
$$+ m_4 \sin((2m_f \pm 1)(\omega t + 2.094)) + m_5 \sin((2m_f \pm 5)(\omega t + 2.094))$$
$$+ m_6 \sin((3m_f \pm 2)(\omega t + 2.094)) + m_7 \sin((3m_f \pm 4)(\omega t + 2.094))$$
$$+ m_8 \sin((4m_f \pm 1)(\omega t + 2.094)) + m_9 \sin((4m_f \pm 5)(\omega t + 2.094))$$
$$+ m_{10} \sin((4m_f \pm 7)(\omega t + 2.094)))$$

$$= \frac{\sqrt{2}}{\sqrt{3}} \cdot (0.490 \sin(377t + 2.094)$$
$$+ 0.135 \sin(167 * (377t + 2.094)) + 0.135 \sin(163 * (377t + 2.094))$$
$$+ 0.005 \sin(169 * (377t + 2.094)) + 0.100 \sin(161 * (377t + 2.094))$$
$$+ 0.192 \sin(331 * (377t + 2.094)) + 0.192 \sin(329 * (377t + 2.094))$$
$$+ 0.008 \sin(335 * (377t + 2.094)) + 0.008 \sin(325 * (377t + 2.094))$$
$$+ 0.108 \sin(497 * (377t + 2.094)) + 0.108 \sin(493 * (377t + 2.094))$$
$$+ 0.064 \sin(499 * (377t + 2.094)) + 0.064 \sin(491 * (377t + 2.094))$$
$$+ 0.064 \sin(661 * (377t + 2.094)) + 0.064 \sin(659 * (377t + 2.094))$$
$$+ 0.051 \sin(665 * (377t + 2.094)) + 0.051 \sin(655 * (377t + 2.094))$$
$$+ 0.010 \sin(667 * (377t + 2.094)) + 0.010 \sin(653 * (377t + 2.094)))$$

Finally, the total input dc bus current, $I_{dc}(\omega t)$, can be found by multiplying the output line currents by this transfer function [8], i.e.

$$I_{dc}(\omega t) = I_a(\omega t) \cdot H_a(\omega t) + I_b(\omega t) \cdot H_b(\omega t - 2.094) + I_c(\omega t) \cdot H_c(\omega t + 2.094) \qquad (3)$$

Thus,

$$I_a(\omega t)\cdot H_a(\omega t)=$$

$$\begin{aligned}
&= 771.44\sin(377t-0.451)\cdot\frac{\sqrt{2}}{\sqrt{3}}\cdot(0.490\sin(377t)\\
&+0.135\sin(167*377t)+0.135\sin(163*377t)\\
&+0.005\sin(169*377t)+0.005*\sin(161*377t)\\
&+0.192\sin(331*377t)+0.192\sin(329*377t)\\
&+0.008\sin(335*377t)+0.008\sin(325*377t)\\
&+0.108\sin(497*377t)+0.108\sin(493*377t)\\
&+0.064\sin(499*377t)+0.064\sin(491*377t)\\
&+0.064\sin(661*377t)+0.064\sin(659*377t)\\
&+0.051\sin(665*377t)+0.051\sin(655*377t)\\
&+0.010\sin(667*377t)+0.010\sin(653*377t))
\end{aligned}$$

$$I_b(\omega t)\cdot H_b(\omega t-2.094)=$$

$$\begin{aligned}
&= 771.44\sin(377t-2.545)\cdot\frac{\sqrt{2}}{\sqrt{3}}\cdot(0.490\sin(377t-2.094)\\
&+0.135\sin(167*(377t-2.094))+0.135\sin(163*(377t-2.094))\\
&+0.005\sin(169*(377t-2.094))+0.100\sin(161*(377t-2.094))\\
&+0.192\sin(331*(377t-2.094))+0.192\sin(329*(377t-2.094))\\
&+0.008\sin(335*(377t-2.094))+0.008\sin(325*(377t-2.094))\\
&+0.108\sin(497*(377t-2.094))+0.108\sin(493*(377t-2.094))\\
&+0.064\sin(499*(377t-2.094))+0.064\sin(491*(377t-2.094))\\
&+0.064\sin(661*(377t-2.094))+0.064\sin(659*(377t-2.094))\\
&+0.051\sin(665*(377t-2.094))+0.051\sin(655*(377t-2.094))\\
&+0.010\sin(667*(377t-2.094))+0.010\sin(653*(377t-2.094)))
\end{aligned}$$

$$I_c(\omega t)\cdot H_c(\omega t+2.094)=$$

$$=771.44\sin(377t+1.643)\cdot\frac{\sqrt{2}}{\sqrt{3}}\cdot(0.490\sin(377t+2.094)$$
$$+0.135\sin(167*(377t+2.094))+0.135\sin(163*(377t+2.094))$$
$$+0.005\sin(169*(377t+2.094))+0.100\sin(161*(377t+2.094))$$
$$+0.192\sin(331*(377t+2.094))+0.192\sin(329*(377t+2.094))$$
$$+0.008\sin(335*(377t+2.094))+0.008\sin(325*(377t+2.094))$$
$$+0.108\sin(497*(377t+2.094))+0.108\sin(493*(377t+2.094))$$
$$+0.064\sin(499*(377t+2.094))+0.064\sin(491*(377t+2.094))$$
$$+0.064\sin(661*(377t+2.094))+0.064\sin(659*(377t+2.094))$$
$$+0.051\sin(665*(377t+2.094))+0.051\sin(655*(377t+2.094))$$
$$+0.010\sin(667*(377t+2.094))+0.010\sin(653*(377t+2.094)))$$

$I_{dc}(\omega t)$ is shown in Fig. 7 (zoomed in, in Fig. 8) and its harmonic spectrum is shown in Fig. 9, which is also listed in Table 4.

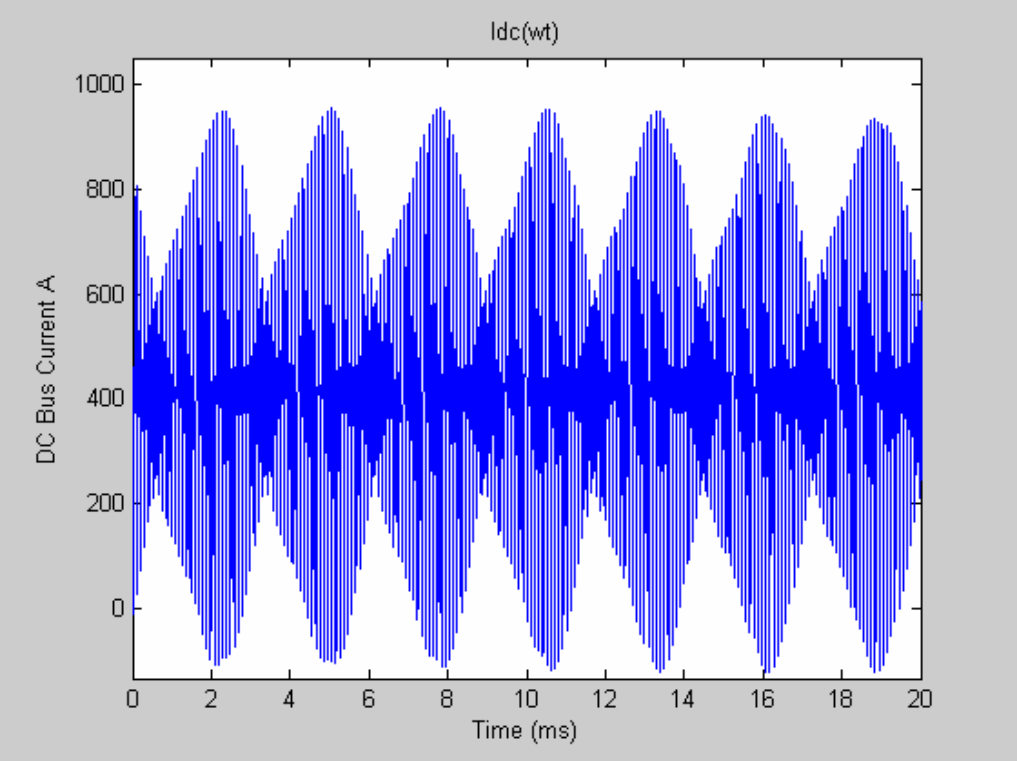

Fig. 7: DC Bus Current, $I_{dc}(\omega t)$

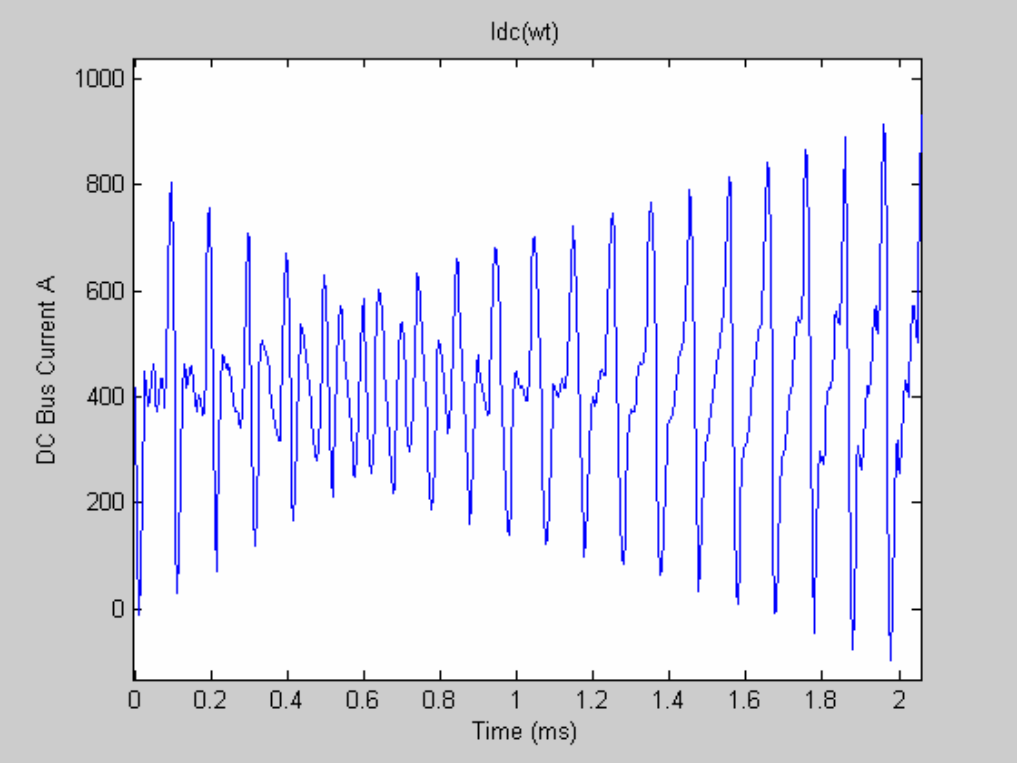

Fig. 8: DC Bus Current, $I_{dc}(\omega t)$, Zoomed In

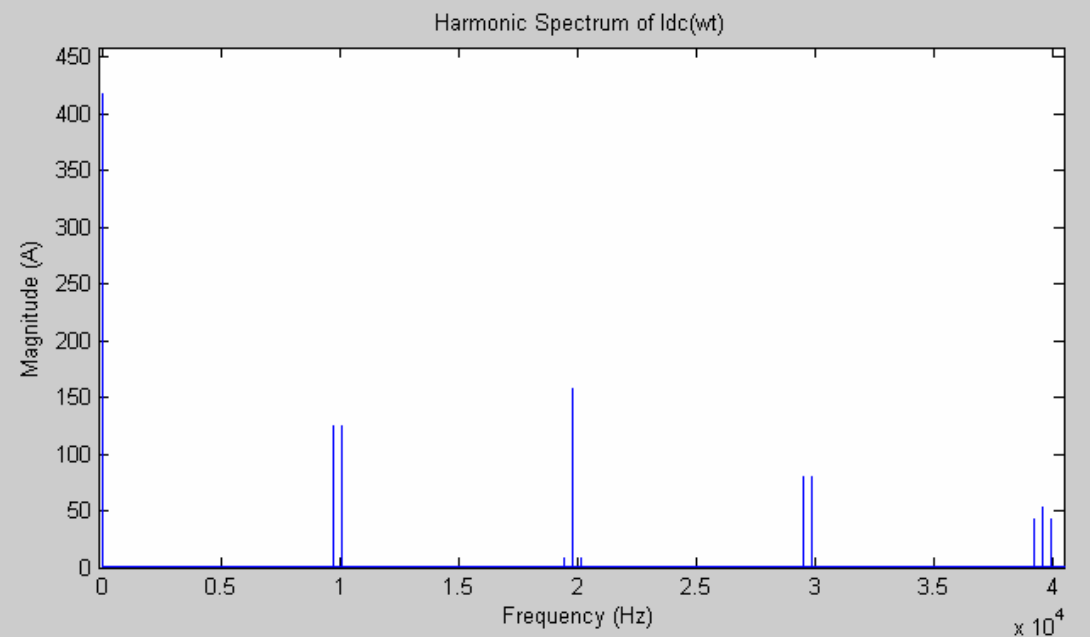

Fig. 9: Harmonic Spectrum of $I_{dc}(\omega t)$

Table 4: Harmonic Comparison of $I_{dc}(\omega t)$

Order	Freq (kHz)	Magn (% of DC)
DC	0	100.00
162	9.72	29.92
168	10.08	29.92
324	19.44	1.81
330	19.8	37.95
336	20.16	1.81
492	29.52	19.22
498	29.88	19.22
654	39.24	10.31
660	39.6	12.65
666	39.96	10.31

From the harmonic spectrum (Fig. 9), it can be seen that $I_{dc}(\omega t)$ has a dc component of magnitude 416.67 A ($P=V_{dc}I_{dc}$, thus I_{dc} = 250kW/600V = 416.67A confirming accuracy).

2.2 Switching Function Approach

In this approach we assume the dc current is made up of contributions of the line currents that the dc bus "sees" while each top switch is on [9], as seen in Fig. 10.

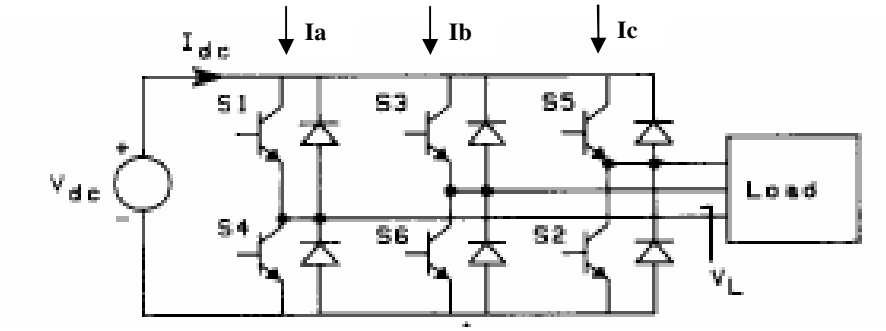

Fig. 10: Six Switch Inverter

Then the dc current would be the sum of each line current multiplied by its respective gating signal (normalized to "1" when on and "0" when off) [9]. These gating signals are generated in Simulink and are shown in Fig. 11 for 1/8 of a 60 Hz cycle.

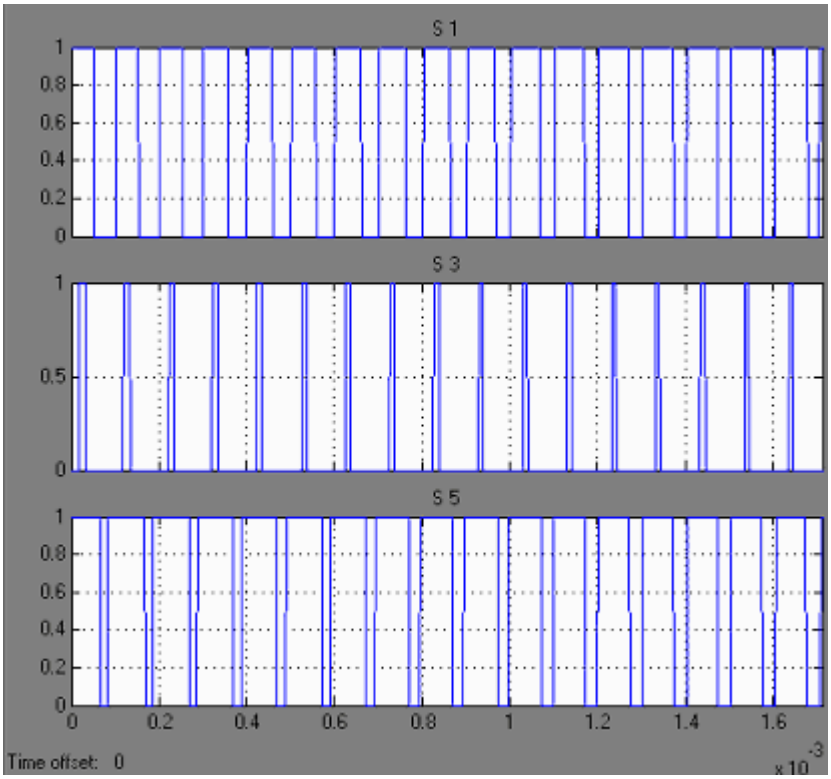

Fig. 11: Gating Signals for 60 Hz cycle

So, the dc current can be expressed as:

$$i_{dc} = gate_a(i_a) + gate_b(i_b) + gate_c(i_c) \quad [9]$$

This approach is very similar to the transfer function method used in the open-form solution as can be seen in the following block diagram Fig. 12.

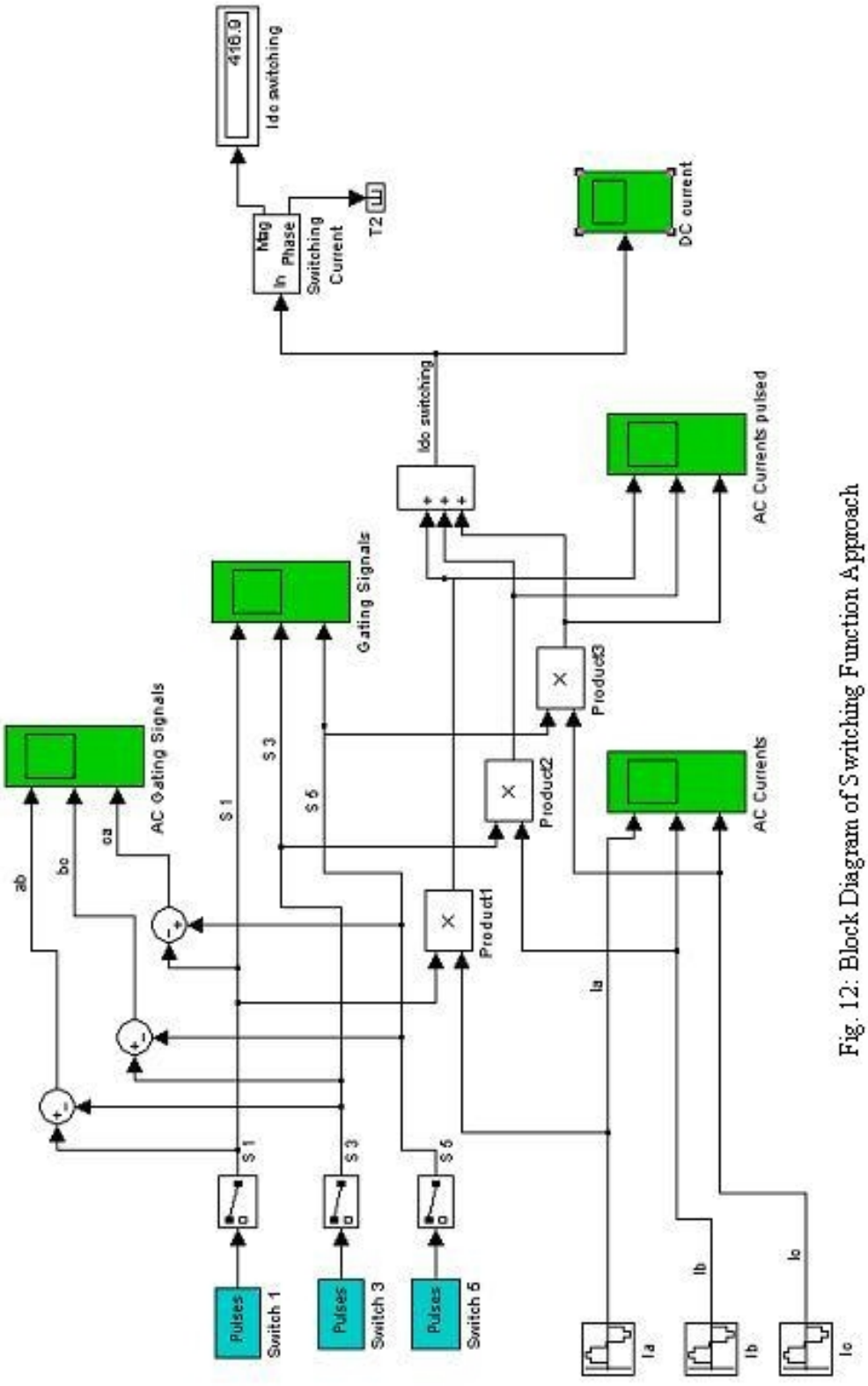

Fig. 12: Block Diagram of Switching Function Approach

Fig. 13 shows the gating signal output voltage and its harmonic spectrum which is also listed in Table 5.

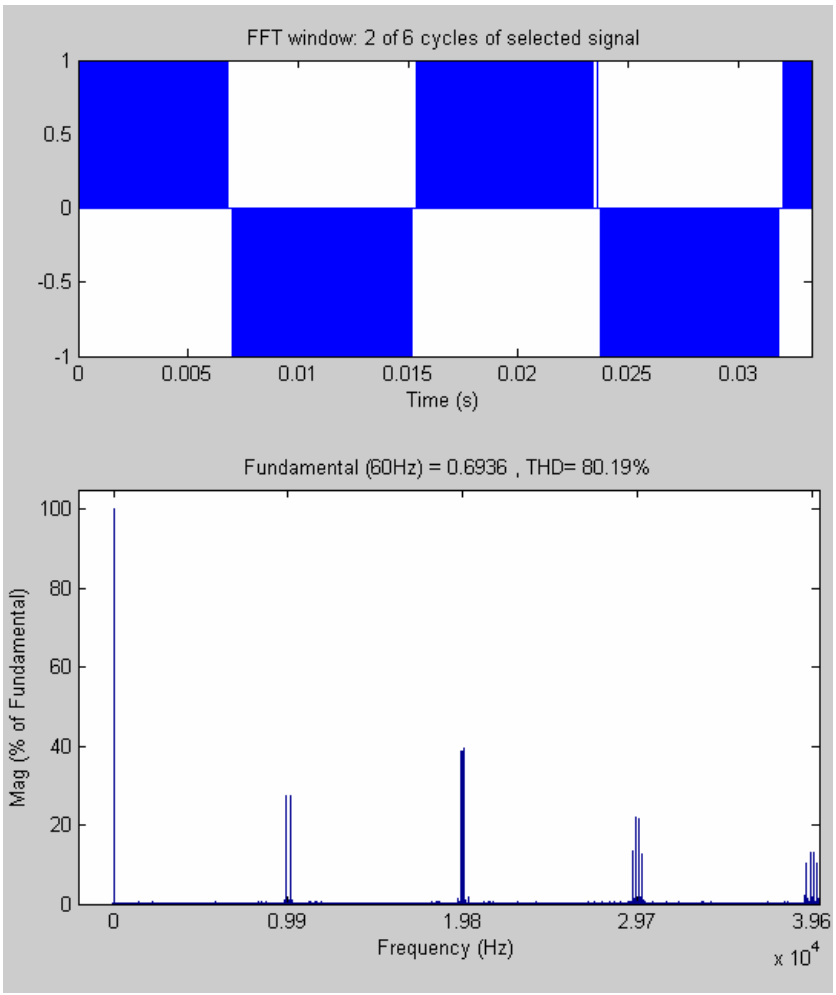

Fig. 13: Gating Voltage, $v_{gate,sw}$

Table 5: Harmonics of $v_{gate,sw}$

Order	Freq (kHz)	Magn (% of Fund)
FUND	0.060	100.00
161	9.66	1.27
163	9.78	27.5
167	10.02	27.41
169	10.14	0.86
325	19.5	1.52
329	19.74	38.8
331	19.86	39.36
335	20.1	1.57
491	29.46	13.32
493	29.58	21.94
497	29.82	21.69
499	29.94	12.68
653	39.18	2.2
655	39.3	10.28
659	39.54	13.0
661	39.66	12.87
665	39.9	10.38
667	40.02	2.25

Fig. 14 shows the switching function dc current, $i_{dc,sw}$, zoomed in. Fig. 15 shows $i_{dc,sw}$ and its harmonic spectra. Table 6 lists the harmonics of $i_{dc,sw}$.

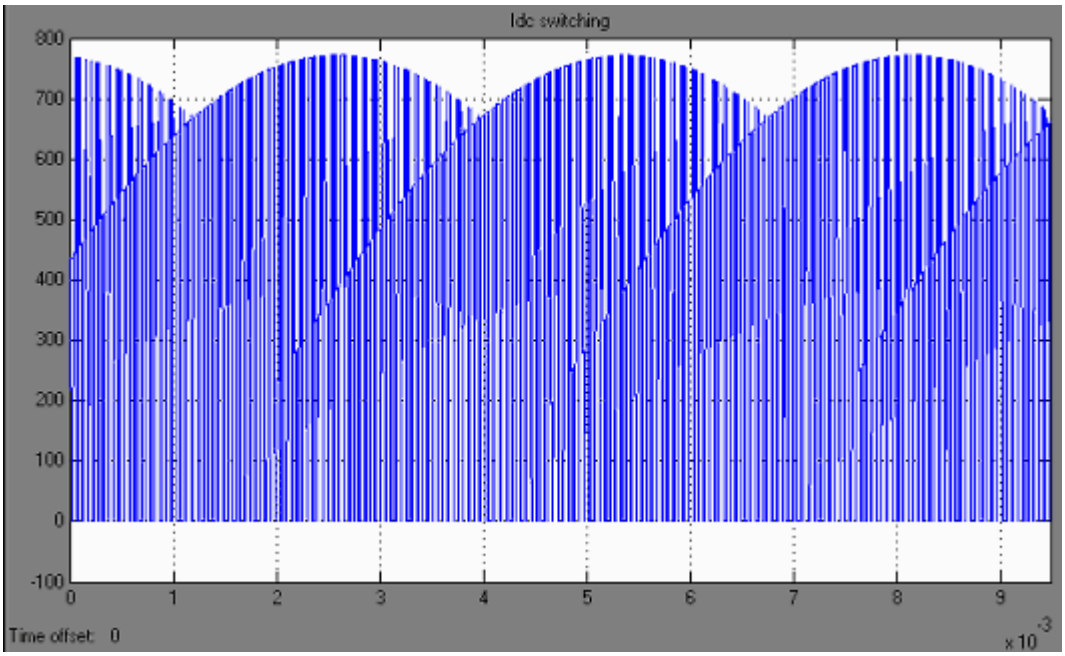

Fig. 14: DC Current, $i_{dc,sw}$, Zoomed in

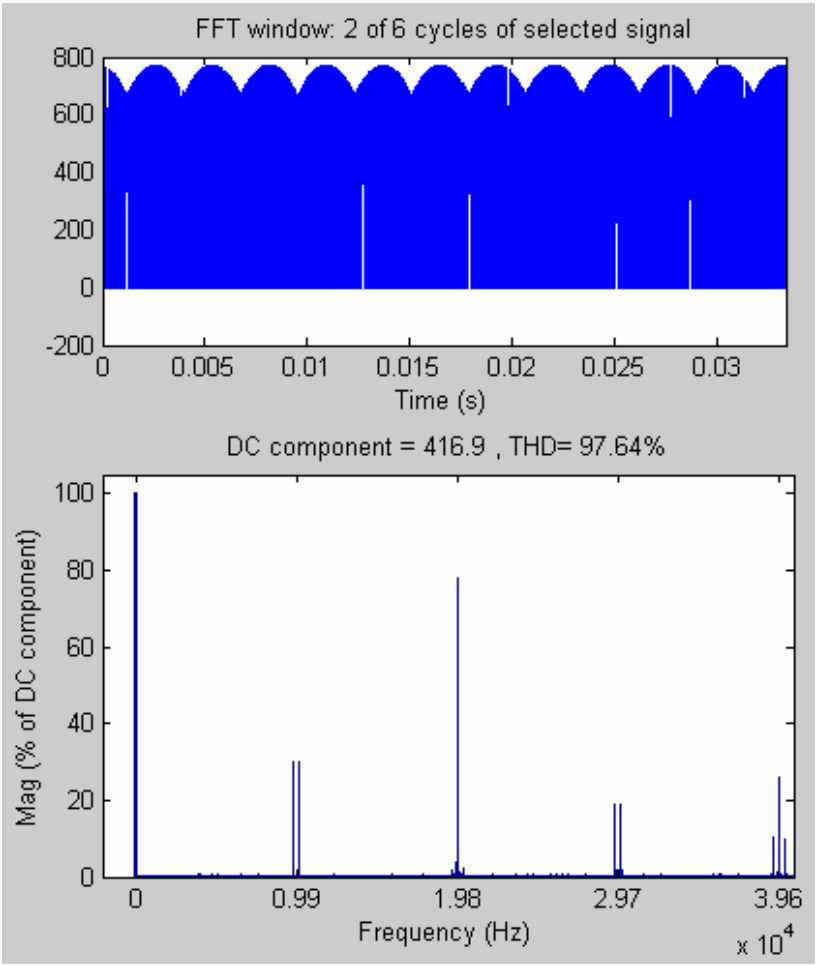

Fig. 15: DC Current, $i_{dc,sw}$

Table 6: Harmonics of $i_{dc,sw}$

Order	Frequency (kHz)	Magn (%of dc)
DC	0	100.00
162	9.72	29.8
168	10.08	29.87
324	19.44	1.67
330	19.8	78.3
336	20.16	1.87
492	29.52	19.1
498	29.88	19.1
654	39.24	10.4
660	39.6	20.06
666	39.96	10.2

2.3 Simulink Simulation

The system has been modeled in Simulink to perform the simulations implementing synchronous and asynchronous PWM, with $f_{fund} = 60\,\text{Hz}$, $f_{fund} = 2\,\text{Hz}$, $f_{fund} = 500\,\text{Hz}$, and $f_{fund} = 900\,\text{Hz}$. The switching frequency remains constant: $f_{sw} = 9900\,\text{Hz}$. Fig. 16 shows the block diagram of the Simulink simulation.

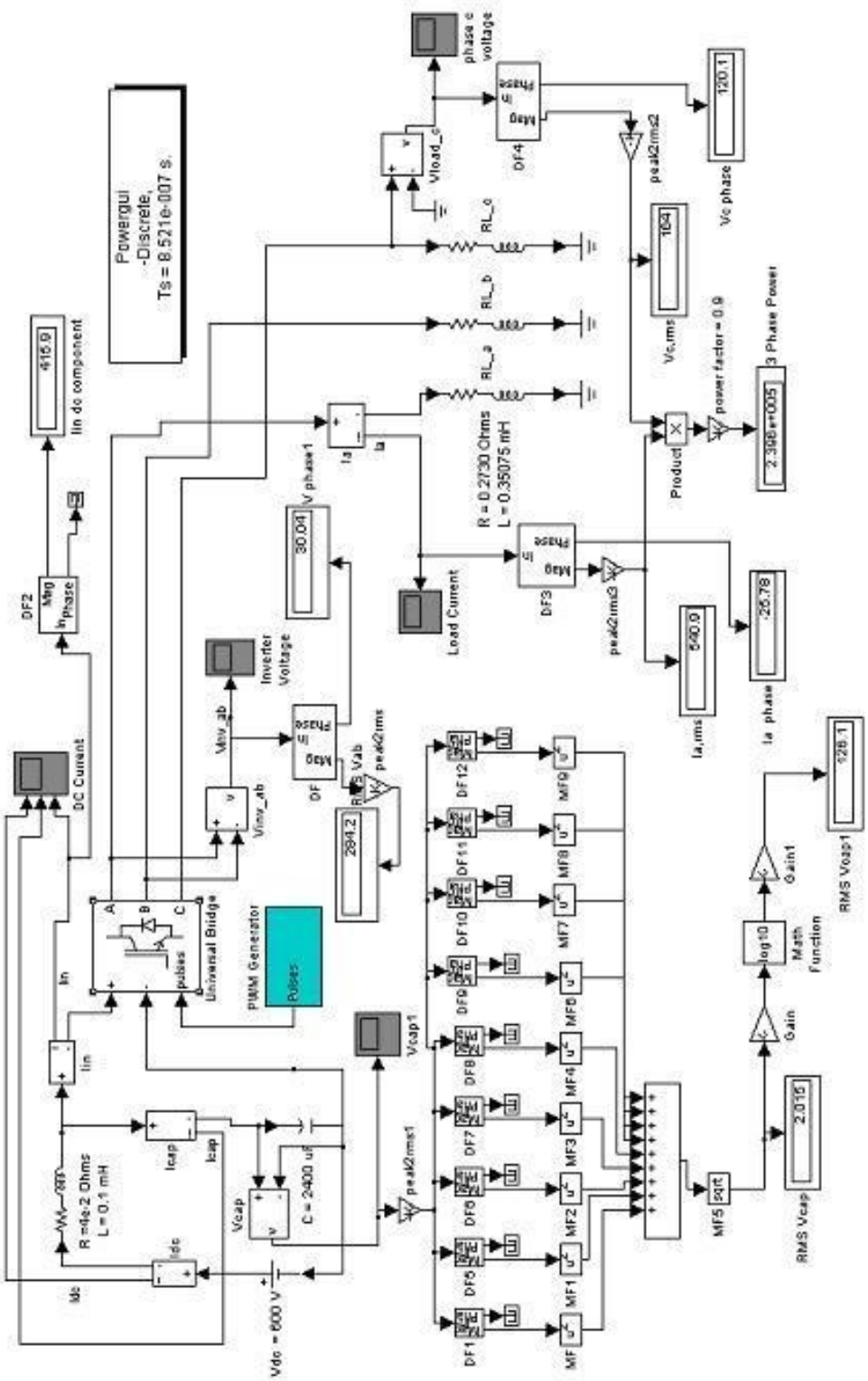

Fig. 16: Block Diagram of Simulink Simulation, 60 Hz

60 Hz Case:

Fig. 17 shows the line-to-line voltage $v_{ab,sim1}$ and its harmonic spectrum. The harmonics are also detailed in Table 7.

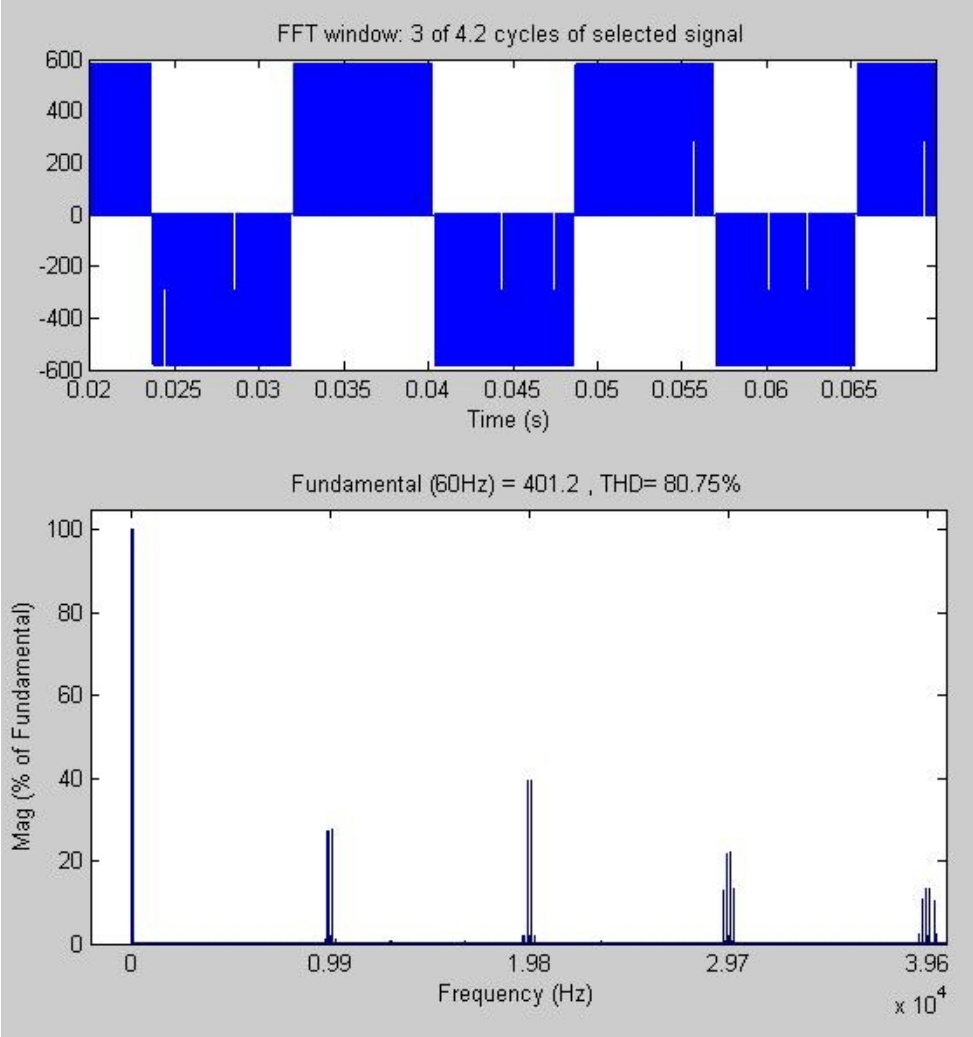

Fig. 17: Line-to-Line Voltage, $v_{ab,sim1}$, 60 Hz

Table 7: Harmonics of $v_{ab,sim1}$

Order	Freq (kHz)	Magn (% of Fund)
FUND	0.060	100.00
161	9.66	0.98
163	9.78	27.4
167	10.02	27.5
169	10.14	1.06
325	19.5	1.70
329	19.74	39.54
331	19.86	39.3
335	20.1	1.76
491	29.46	13.0
493	29.58	21.9
497	29.82	22.0
499	29.94	13.12
653	39.18	2.19
655	39.3	10.7
659	39.54	13.18
661	39.66	13.26
665	39.9	10.35
667	40.02	2.38

Fig. 18 shows the line current, $I_{a,sim1}$.

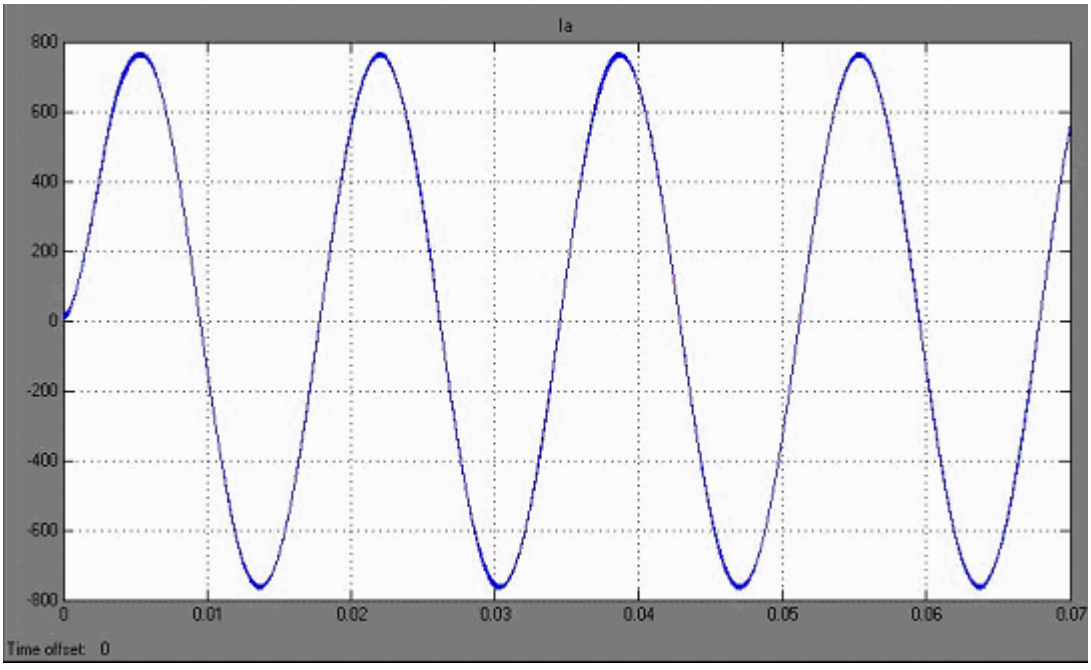

Fig. 18: Line Current, $I_{a,sim1}$, 60 Hz

Fig. 19 shows the input dc current (after the capacitor), $I_{dc,sim1}$, and its harmonic spectrum which is also listed in Table 8.

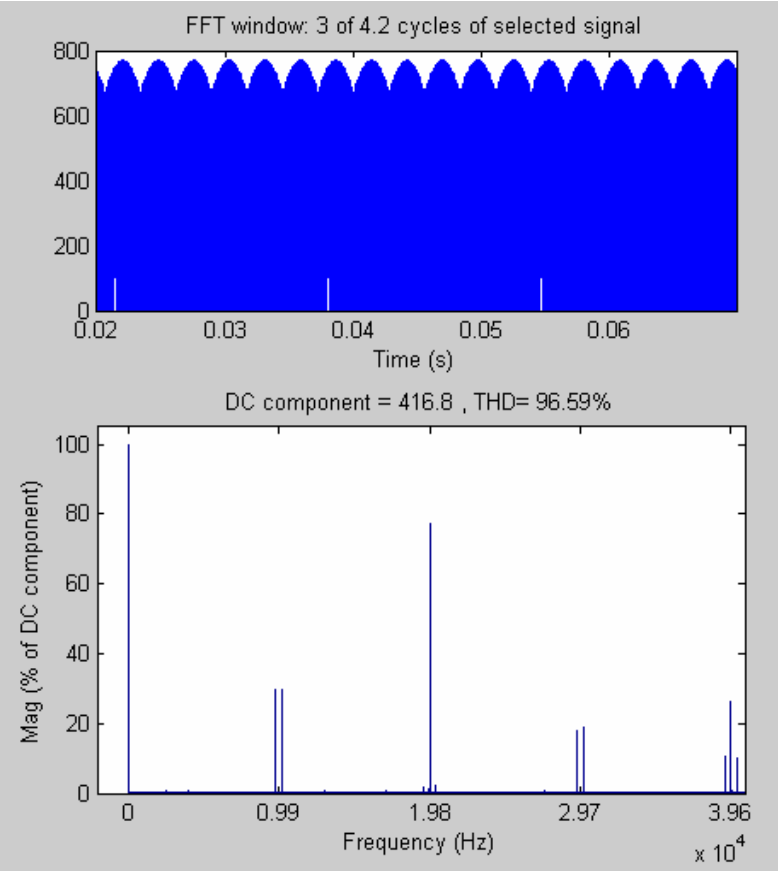

Fig. 19: DC Current, $I_{dc,sim1}$, 60 Hz

Table 8: Harmonic Comparison of $I_{dc,sim1}$

Order	Freq (kHz)	Magn (% of DC)
DC	0	100.00
162	9.72	29.45
168	10.08	29.84
324	19.44	1.77
330	19.8	77.03
336	20.16	2.0
492	29.52	18.1
498	29.88	18.76
654	39.24	10.3
660	39.6	26.3
666	39.96	10.02

Note: Since these results correspond well to the switching function approach, this simulation will extend through calculating the capacitor voltage and determining whether MIL-STD-461 is met for a relaxed curve of 16 dB μV for 600 V. Also, Fig. 20, MIL-STD-461 Conducted Emission (CE102) curve is inserted for quick reference.

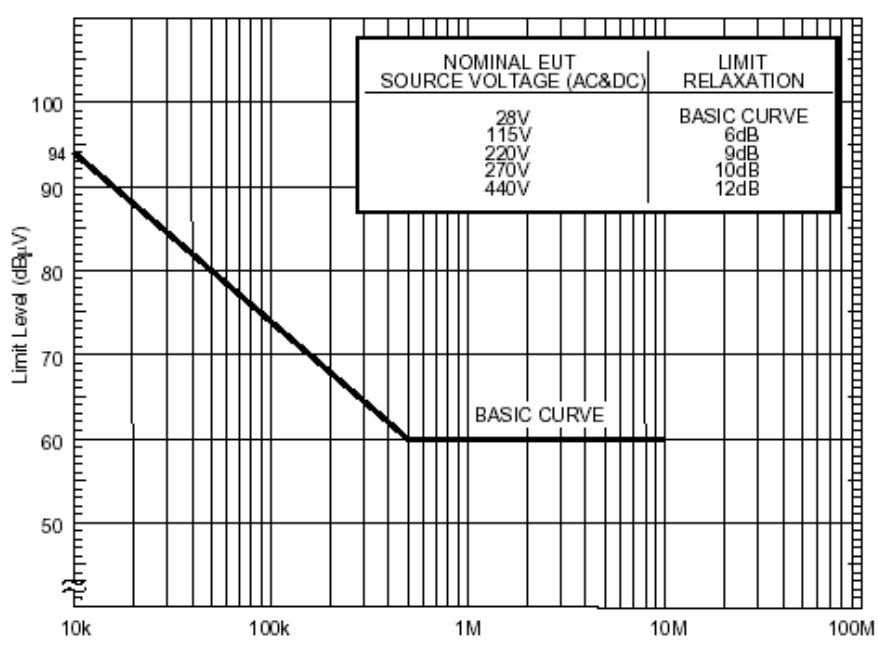

Fig. 20: Propulsion Bus Distortion Spectrum

Note: The distortion spectrum y-axis is calculated as: $dB = 20 \cdot \log\left(\frac{V_{rms}}{10^{-6}}\right)$. For MIL-STD-461, this corresponds to the limits listed in Table 9, which will be used in the graphs of capacitor voltage.

Table 9: Harmonic Content Limits for MIL-STD-461

Frequency (kHz)	Magnitude (dBμV)	Magn (mV)
10.0	110.0	316.22
20.0	104.5	158.48
30.0	100.0	100.00
40.0	96.0	63.09

Fig. 21 shows the capacitor current, $I_{cap,sim1}$, and its harmonic spectrum, which is listed in Table 10.

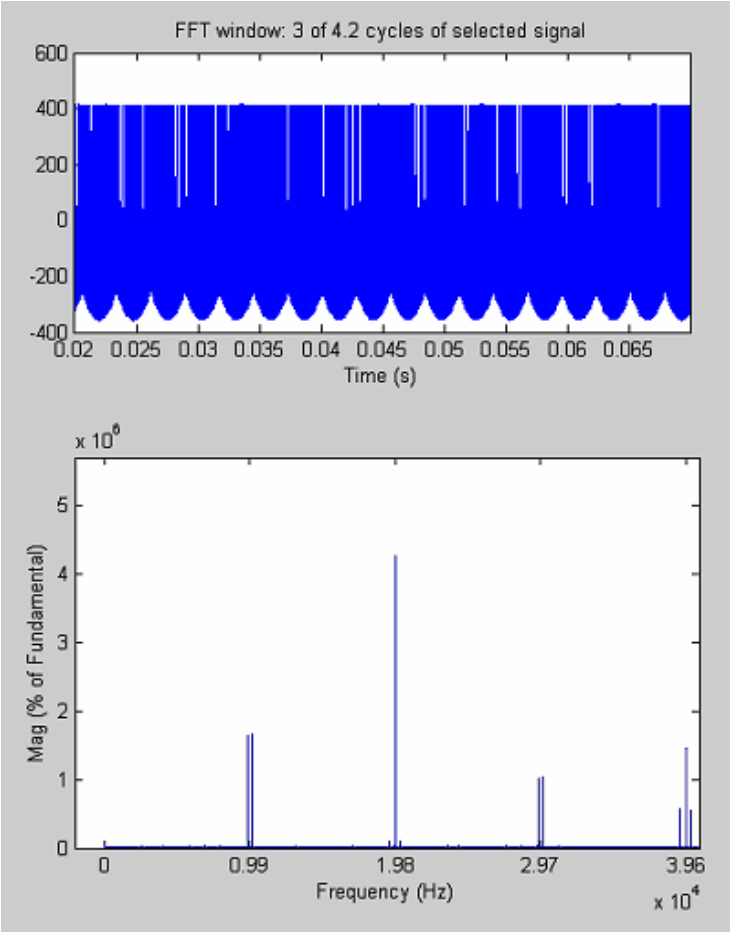

Fig. 21: Capacitor Current, $I_{cap,sim1}$, 60 Hz

Table 10: Harmonic Comparison of $I_{cap,sim1}$

Order	Freq (kHz)	Magn (% of DC-bus)
DC	0	0.0
162	9.72	29.45
168	10.08	29.84
324	19.44	1.77
330	19.8	77.03
336	20.16	2.0
492	29.52	18.1
498	29.88	18.76
654	39.24	10.3
660	39.6	26.3
666	39.96	10.02

Fig. 22 shows the capacitor voltage, $v_{cap,sim1}$, and its harmonic spectrum, which is listed in Table 11.

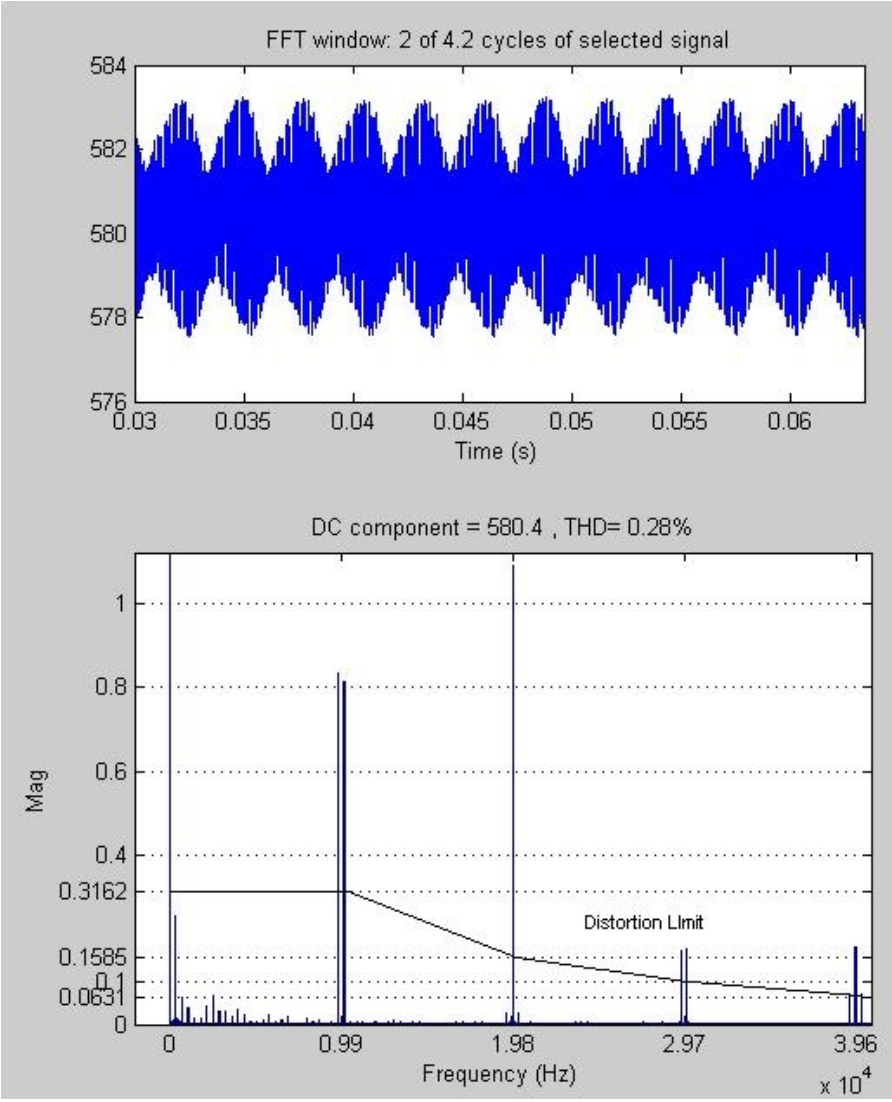

Fig. 22: Capacitor Voltage, $v_{cap,sim1}$, 60 Hz

Table 11: Harmonics of $v_{cap,sim1}$

Order	Freq (kHz)	Magn (%of dc)	Magn(V)	Magn (dB μV)
DC	0.0	100.00	580.4	-------
6	0.360	0.0453	0.2633	108.41
162	9.72	0.1434	0.8324	118.41
168	10.08	0.1402	0.8137	118.21
330	19.8	0.1873	1.0871	120.73
492	29.52	0.0297	0.1728	104.75
498	29.88	0.0307	0.1785	105.03
654	39.24	0.0125	0.0724	97.19
660	39.6	0.0314	0.1821	105.21
666	39.96	0.0121	0.0698	96.88

From the simulation, the overall rms capacitor voltage from the harmonics is $v_{cap,sim1}$ = 1.15 V. Note: This does not include the 6th harmonic in the capacitor voltage, which is not dominant in the capacitor current. The resonant frequency between the dc-link inductor and the capacitor is 324.87Hz, which may be amplifying this 6th harmonic. The distortion (with respect to 1 μV) is calculated as: $20\log\left(\frac{v_{cap,rms}}{1x10^{-6}}\right) = dB$, so for this case we have, $20\log\left(\frac{1.15}{1x10^{-6}}\right) = 121.2$.

As can be seen from Fig. 22, the MIL-STD-461 CE102 Distortion Spectrum limit has been graphed as well. At 60 Hz, the present harmonics are well over this limit. To mitigate this, the capacitor was increased to $17000\,\mu F$. The resulting capacitor voltage and its harmonic spectrum are shown below in Fig. 23 and are listed in Table 12.

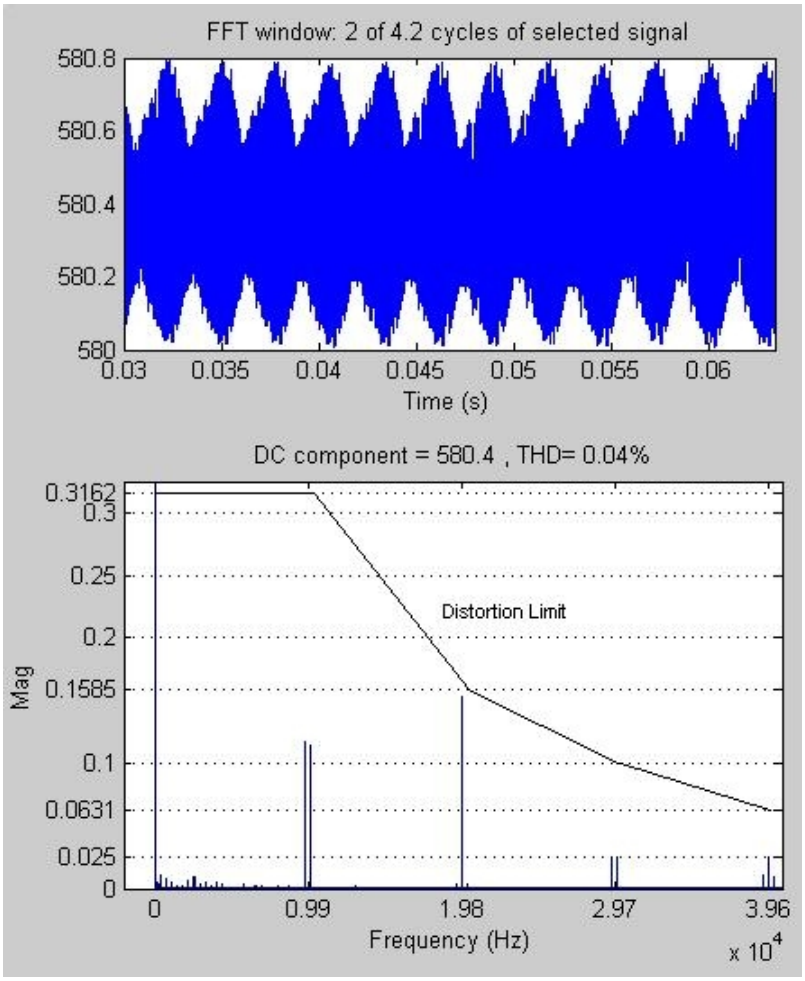

Fig. 23: Adjusted Capacitor Voltage, $v_{cap,sim1}$, 60 Hz

Table 12: Harmonics of Adjusted $v_{cap,sim1}$

Order	Frequency (kHz)	Magnitude (%of dc)	Magnitude (V)	Magnitude (dB μV)
DC	0.0	100.00	580.4	-------
6	0.360	--------	------	-------
162	9.72	0.0202	0.1175	101.4
168	10.08	0.0198	0.1146	101.18
330	19.8	0.0264	0.1534	103.72
492	29.52	0.00421	0.0244	87.75
498	29.88	0.00433	0.0251	87.99
654	39.24	0.00175	0.0101	80.09
660	39.6	0.00443	0.0257	88.19
666	39.96	0.00171	0.00994	79.95

The distortion (with respect to 1 μV) is calculated as: $20\log\left(\frac{0.1622}{1x10^{-6}}\right)=104.2$.

Fundamental Frequency Range Simulations

2 Hz Case:

Fig. 24 shows the line-to-line voltage $v_{ab,sim1}$ and its harmonic spectrum, which is also listed in Table 13.

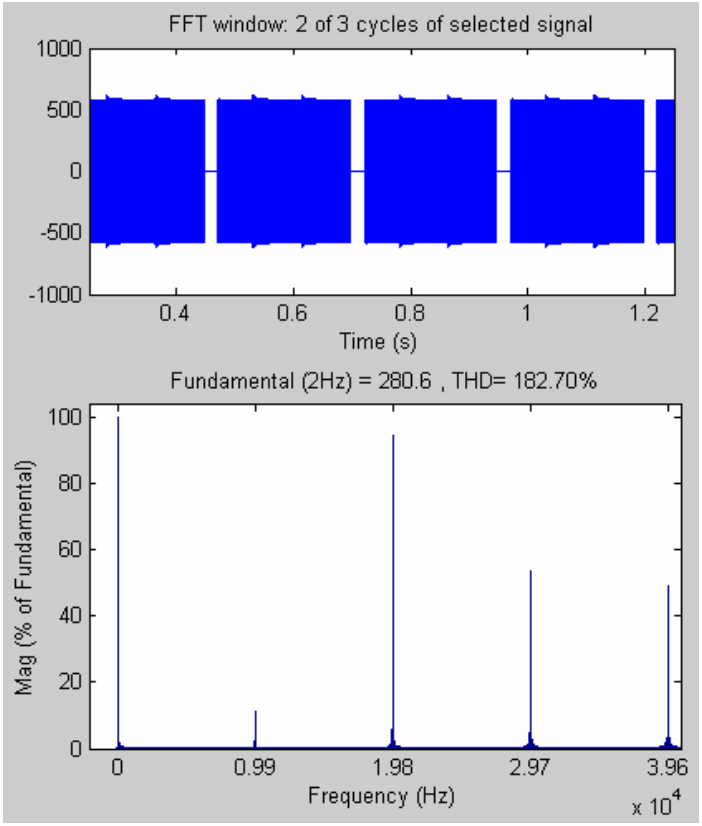

Fig. 24: Line-to-Line Voltage, $v_{ab,sim1}$, 2 Hz

Table 13: Harmonics of $v_{ab,sim1}$

Order	Frequency (kHz)	Magnitude (%of fund)
FUND	0.002	100.00
4948	9.896	11.3
4952	9.904	11.1
9899	19.798	87.3
9901	19.802	94.2
14848	29.696	53.3
14852	29.704	50.8
19795	39.590	27.5
19799	39.598	48.2
19801	39.602	48.9
19805	39.610	28.8

Fig. 25 shows the line current, $I_{a,sim1}$, and its harmonic spectrum.

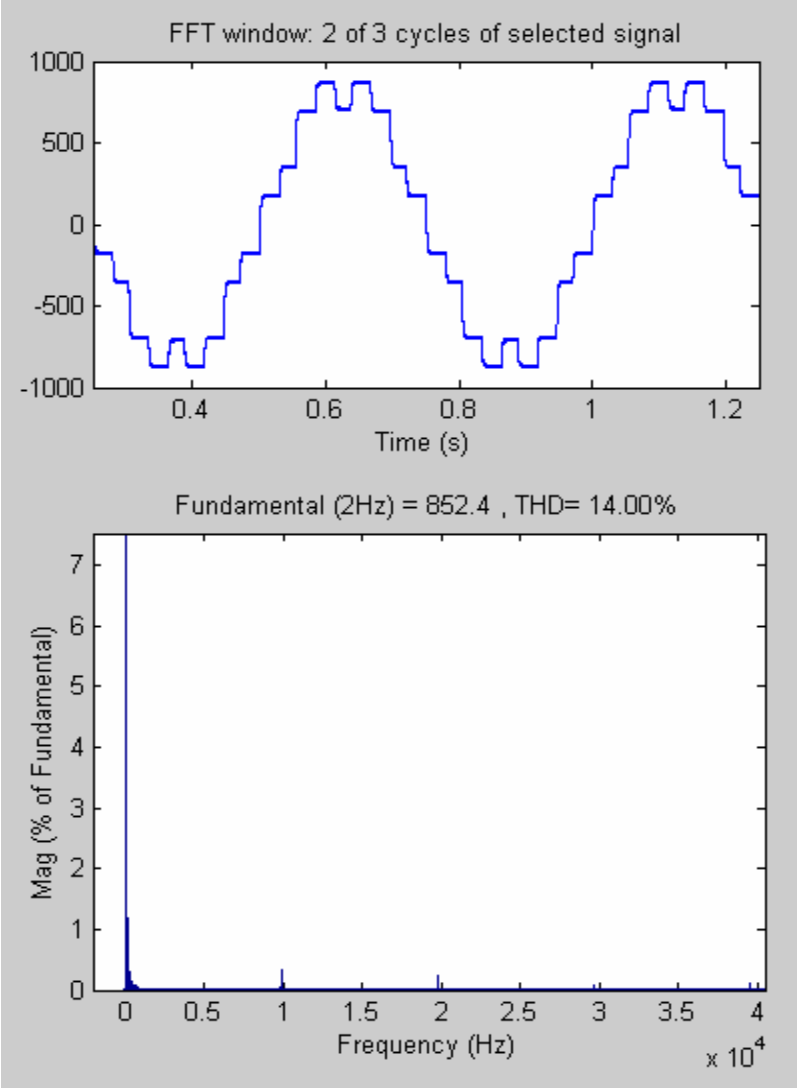

Fig. 25: Line Current, $I_{a,sim1}$, 2 Hz

Fig. 26 shows the input dc current (after the capacitor), $I_{dc,sim1}$, and its harmonic spectrum, which is also listed in Table 14.

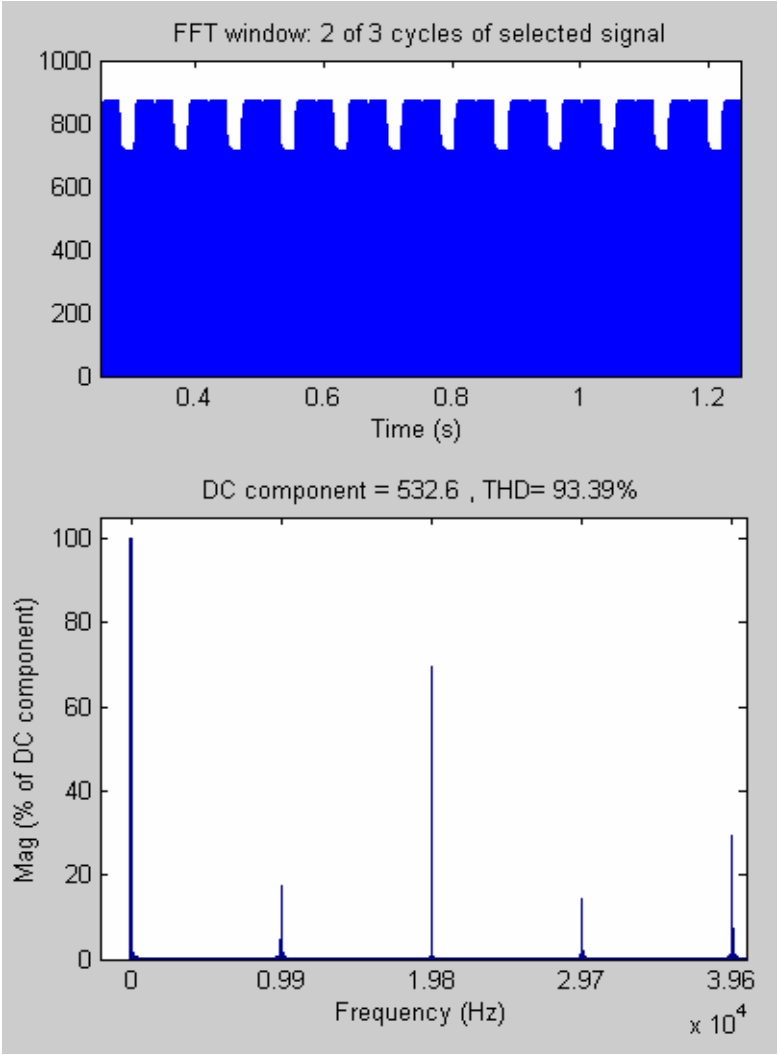

Fig. 26: DC Current, $I_{dc,sim1}$, 2 Hz

Table 14: Harmonics of $I_{dc,sim1}$

Order	Frequency (kHz)	Magnitude (%of dc)
DC	0	100.00
4947	9.894	16.9
4953	9.906	17.3
9900	19.8	69.3
14847	29.694	13.4
14853	29.706	14.2
19800	39.6	29.3

Fig. 27 shows the capacitor current, $I_{cap,sim1}$, and its harmonic spectrum, which is listed in Table 15.

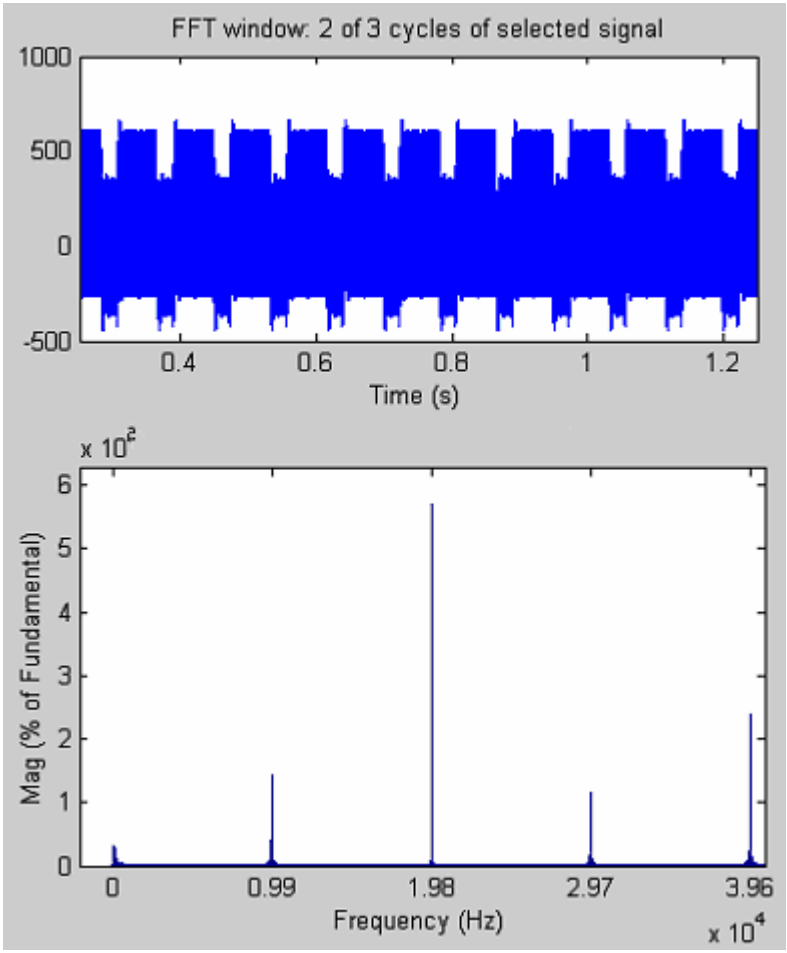

Fig. 27: Capacitor Current, $I_{cap,sim1}$,2 Hz

Table 15: Harmonics of $I_{cap,sim1}$

Order	Frequency (kHz)	Magnitude (%of dc)
DC	0	0
4947	9.894	16.9
4953	9.906	17.3
9900	19.8	69.3
14847	29.694	13.4
14853	29.706	14.2
19800	39.6	29.3

Fig. 28 shows the capacitor voltage, $v_{cap,sim1}$, and its harmonic spectrum, which is listed in Table 16.

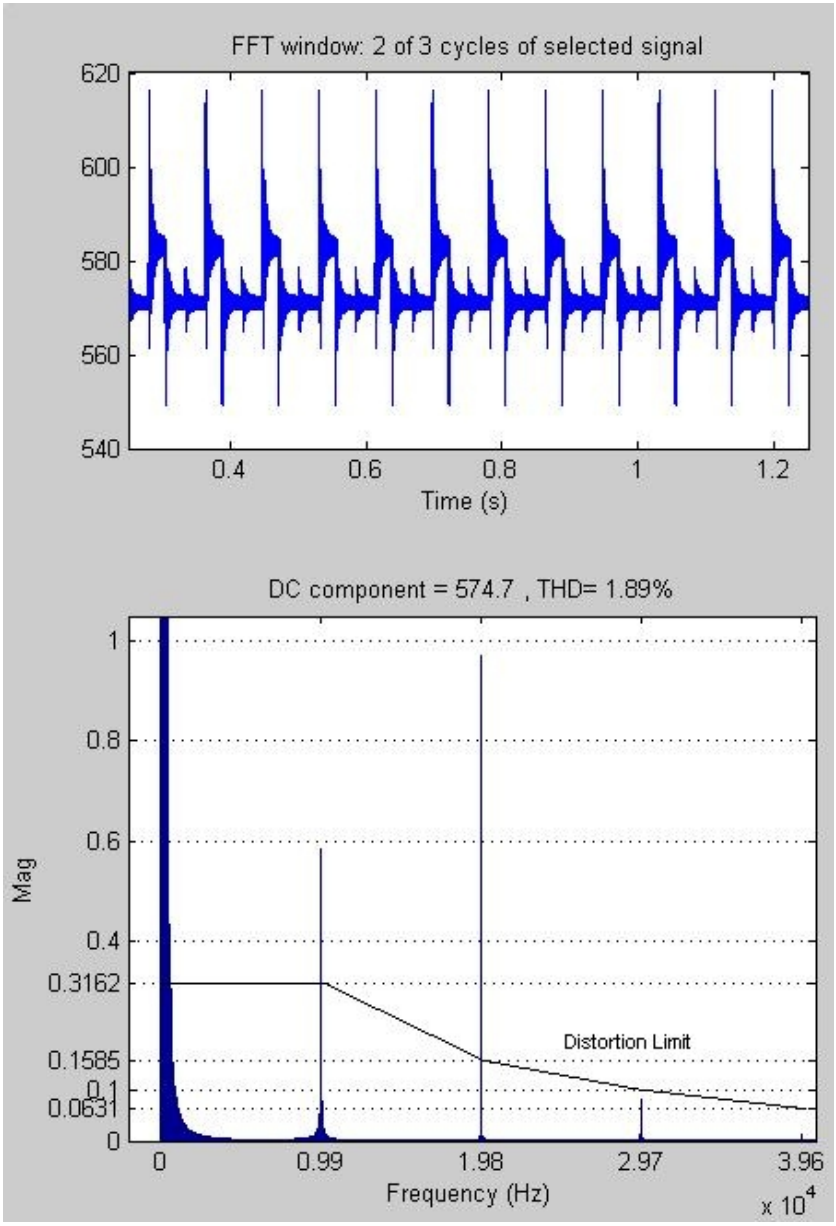

Fig. 28: Capacitor Voltage, $v_{cap,sim1}$, 2 Hz

Table 16: Harmonics of $v_{cap,sim1}$

Order	Frequency (kHz)	Magnitude (V)	Magnitude (dB μV)
DC	0.0	578.5	------
6	0.012	6.124	135.74*
12	0.024	3.885	131.79*
150	0.300	2.324	127.32*
156	0.312	2.625	128.39*
162	0.324	1.664	124.42*
166	0.336	1.812	125.16*
174	0.348	2.478	127.88*
180	0.36	2.011	126.07*
4947	9.894	0.576	115.21
4953	9.906	0.586	115.36
9900	19.8	0.971	119.74
14847	29.694	0.0781	97.85
14853	29.706	0.0823	98.31

* not included in following calculations

From the simulation, the rms capacitor voltage from the harmonics is $v_{cap,sim1}$ = 1.277 V. The distortion (with respect to 1 μV) is calculated as: $20\log\left(\frac{1.277}{1x10^{-6}}\right)=122.12$. As can be seen from Fig. 28 and Table 16 most of the harmonics do not pass the distortion limit. The lower order harmonics are not included in the distortion calculation as they seem to appear due to the previously discussed resonance condition, and it would require an unreasonable capacitor value to meet the distortion limit. To mitigate the harmonics around m_f, $2m_f$, and $3m_f$, the capacitor was increased to $17000\,\mu F$. The resulting capacitor voltage and its harmonic spectrum are shown below in Fig. 29 and are listed in Table 17.

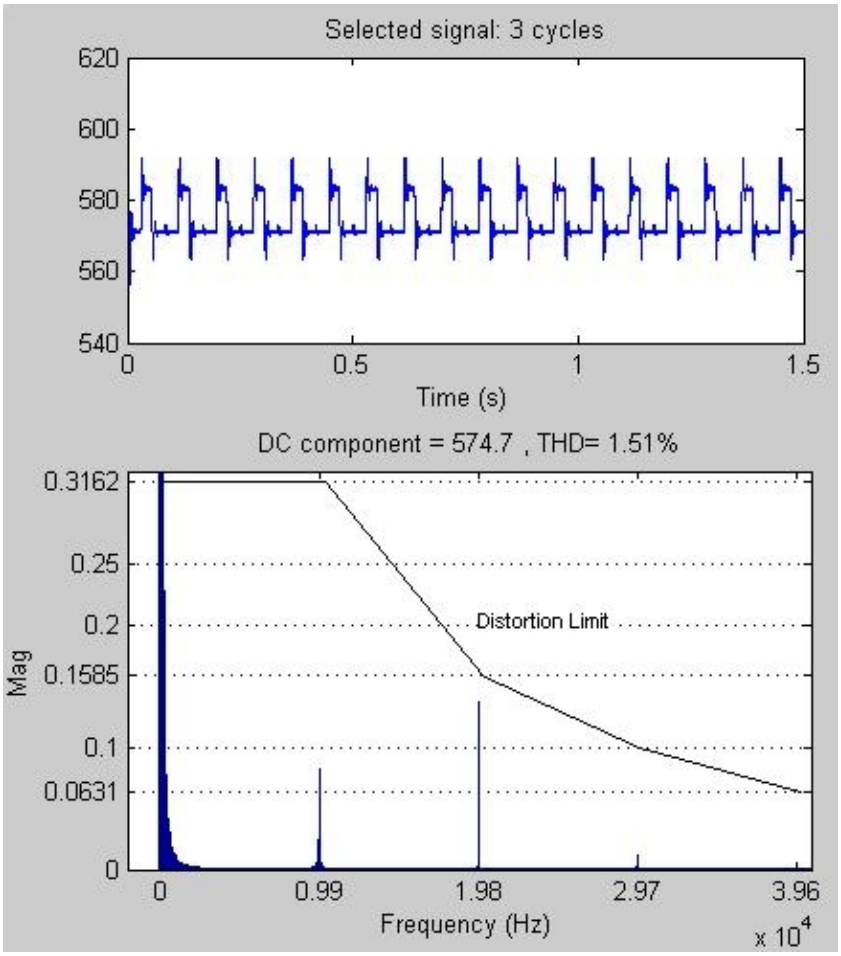

Fig. 29: Adjusted Capacitor Voltage, $v_{cap,sim1}$, 2 Hz

Table 17: Harmonics of Adjusted $v_{cap,sim1}$

Order	Frequency (kHz)	Magnitude (V)	Magnitude (dB μV)
DC	0.0	578.5	------
6	0.012	6.16	135.79*
12	0.024	3.984	132.01*
4947	9.894	0.0812	98.19
4953	9.906	0.0826	98.34
9900	19.8	0.137	102.73
14847	29.694	0.011	80.83
14853	29.706	0.0115	81.21

*not included in calculation

The distortion (with respect to 1 μV) is calculated as: $20\log\left(\frac{0.1801}{1x10^{-6}}\right)=105.11.$

500 Hz Case (Asynchronous):

Fig. 30 shows the line-to-line voltage $v_{ab,sim1}$ and its harmonic spectrum, which is also listed in Table 18.

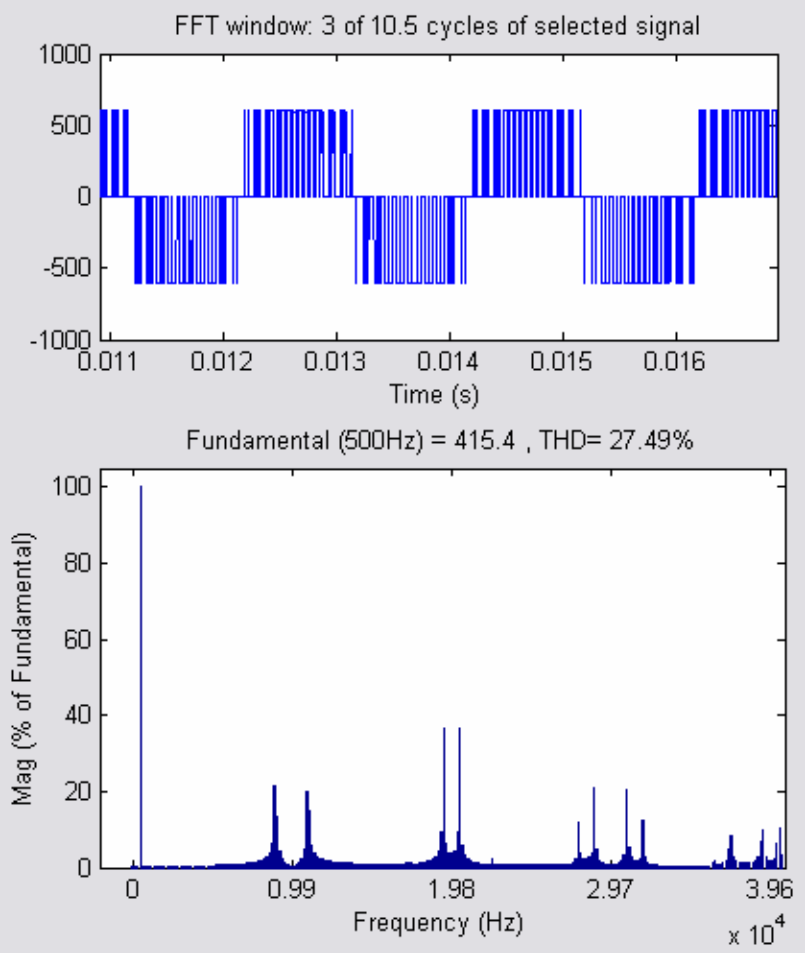

Fig. 30: Line-to-Line Voltage, $v_{ab,sim1}$, 500 Hz

Table 18: Harmonics of $v_{ab,sim1}$

Order	Frequency (kHz)	Magnitude (%of fund)
FUND	0.500	100.00
17.664	8.8322	21.24
18	9.0	13.3
21.664	10.832	19.84
22	1.1	14.7
38.664	19.332	36.82
40.664	20.332	36.65
55.33	27.665	12.0
57.33	28.665	21.06
61.33	30.665	20.4
63.33	31.665	12.39
74.33	37.165	8.26
78.33	39.165	9.8

Fig. 31 shows the line current, $I_{a,sim1}$, and its harmonic spectrum.

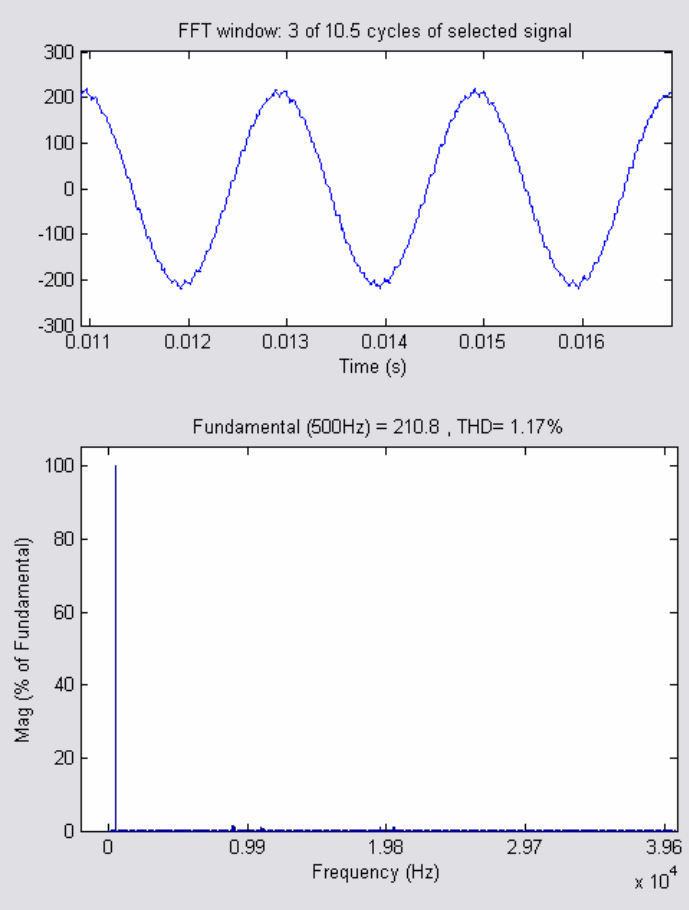

Fig. 31: Line Current, $I_{a,sim1}$, 500 Hz

Fig. 32 shows the input dc current (after the capacitor), $I_{dc,sim1}$, and its harmonic spectrum, which is also listed in Table 19.

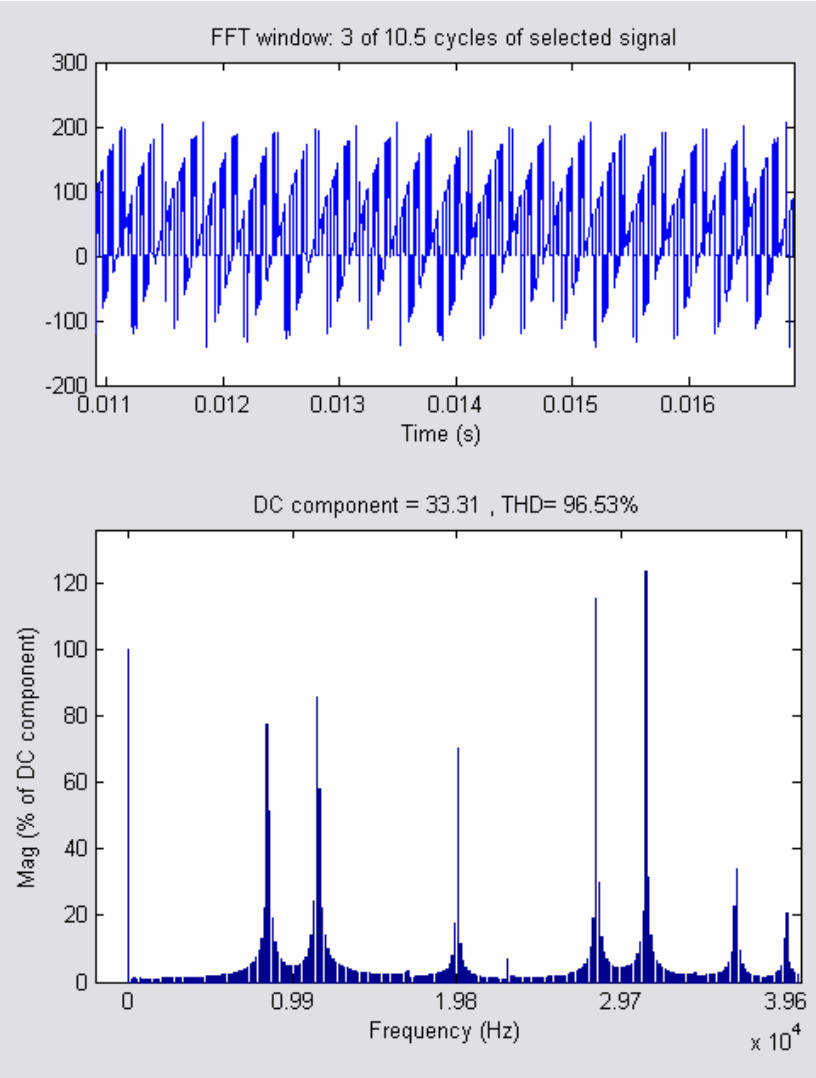

Fig. 32: DC Current, $I_{dc,sim1}$, 500 Hz

Table 19: Harmonics of $I_{dc,sim1}$

Order	Frequency (kHz)	Magnitude (%of dc)
DC	0	100.00
16.5	8.332	77.35
17	8.5	51.4
22.664	11.332	85.6
23	11.5	58.2
39.664	19.832	70.3
56.33	28.165	115.4
62.33	31.165	123.7
73.33	36.665	34.2
79	39.5	13.0
79.33	39.665	20.5

Fig. 33 shows the capacitor current, $I_{cap,sim1}$, and its harmonic spectrum, which is listed in Table 20.

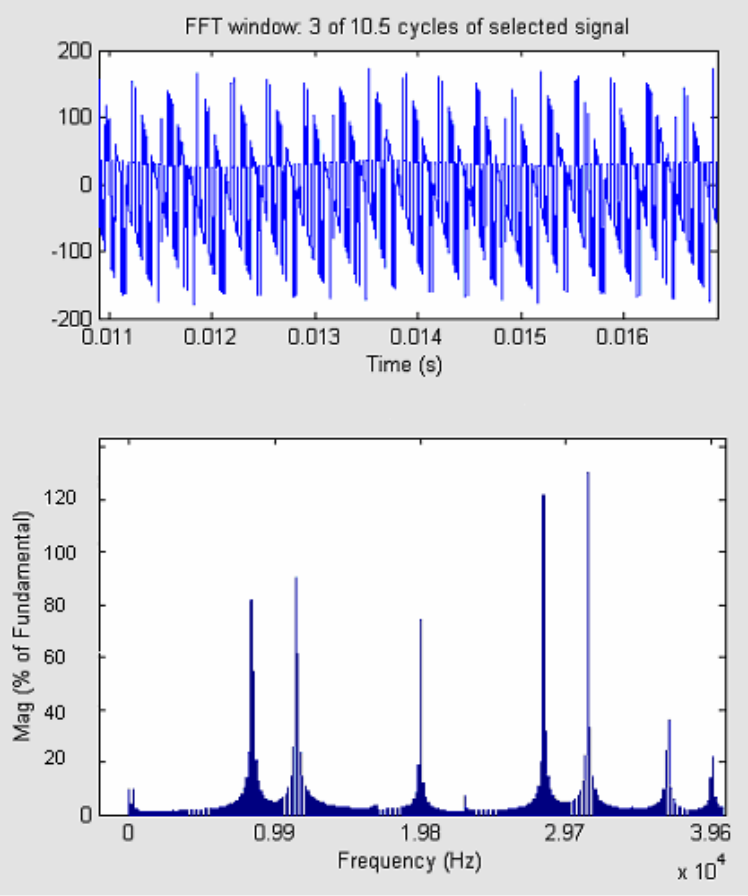

Fig. 33: Capacitor Current, $I_{cap,sim1}$, 500 Hz

Table 20: Harmonics of $I_{cap,sim1}$

Order	Frequency (kHz)	Magnitude (%of dc)
DC	0	100.00
16.5	8.332	77.35
17	8.5	51.4
22.664	11.332	85.6
23	11.5	58.2
39.664	19.832	70.3
56.33	28.165	115.4
62.33	31.165	123.7
73.33	36.665	34.2
79	39.5	13.0
79.33	39.665	20.5

Fig. 34 shows the capacitor voltage, $v_{cap,sim1}$, and its harmonic spectrum, which is listed in Table 21.

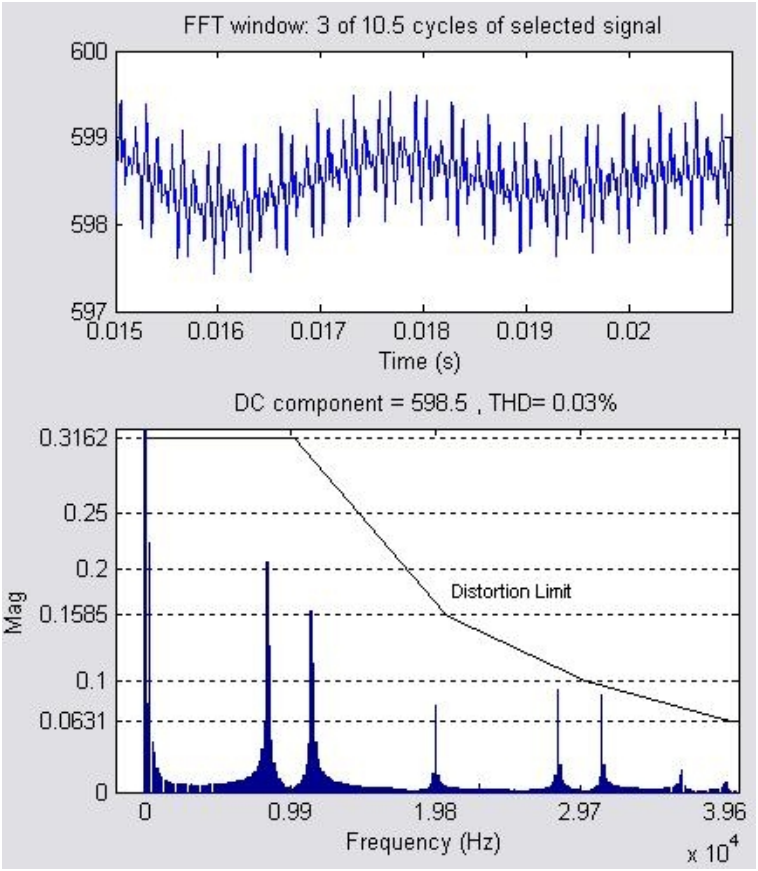

Fig. 34: Capacitor Voltage, $v_{cap,sim1}$, 500 Hz

Table 21: Harmonics of $v_{cap,sim1}$

Order	Frequency (kHz)	Magnitude (V)	Magnitude (dB μV)
DC	0.0	598.5	------
0.664	0.3322	0.2233	106.98
16.664	8.332	0.2056	106.26
17	8.5	0.1305	102.31
22.664	11.332	0.1623	104.21
23	11.5	0.1148	101.19
39.666	19.833	0.0771	97.74
56.33	28.165	0.091	99.18
63.3	31.165	0.0863	98.72

From the simulation, the rms $v_{cap,sim1}$ = 0.4127 V. The distortion (with respect to 1 μV) is calculated as:

$$20\log\left(\frac{0.4127}{1x10^{-6}}\right)=112.31 \ .$$

As can be seen from Fig. 34, the present harmonics all pass the distortion limit.

900 Hz Case:

Fig. 35 shows the line-to-line voltage $v_{ab,sim1}$ and its harmonic spectrum, which is also listed in Table 22.

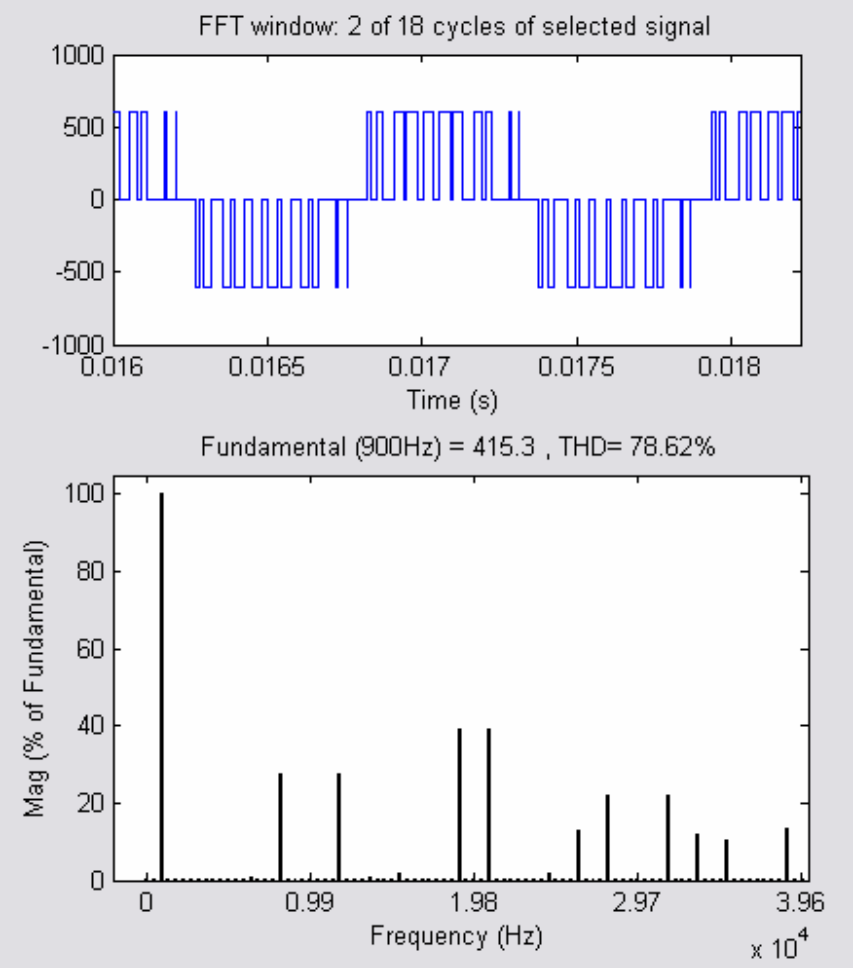

Fig. 35: Line-to-Line Voltage, $v_{ab,sim1}$, 900 Hz

Table 22: Harmonics of $v_{ab,sim1}$

Order	Frequency (kHz)	Magnitude (%of fund)
FUND	0.900	100.00
9	8.1	27.5
13	11.7	27.5
21	18.9	39.3
23	20.7	39.3
29	26.1	13.1
31	27.9	22.1
35	31.5	22.1
37	33.3	12.1
39	35.1	10.5
43	38.7	13.2

Fig. 36 shows the line current, $I_{a,sim1}$, and its harmonic spectrum.

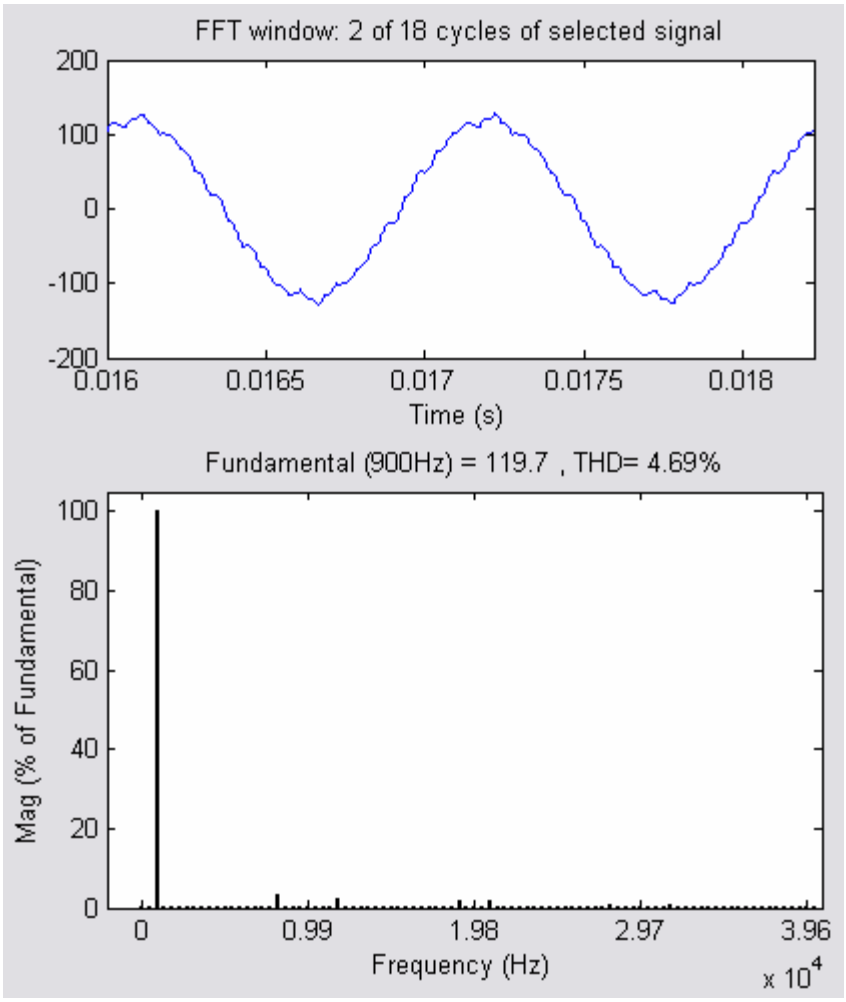

Fig. 36: Line Current, $I_{a,sim1}$, 900 Hz

Fig. 37 shows the input dc current (after the capacitor), $I_{dc,sim1}$, and its harmonic spectrum, which is also listed in Table 23.

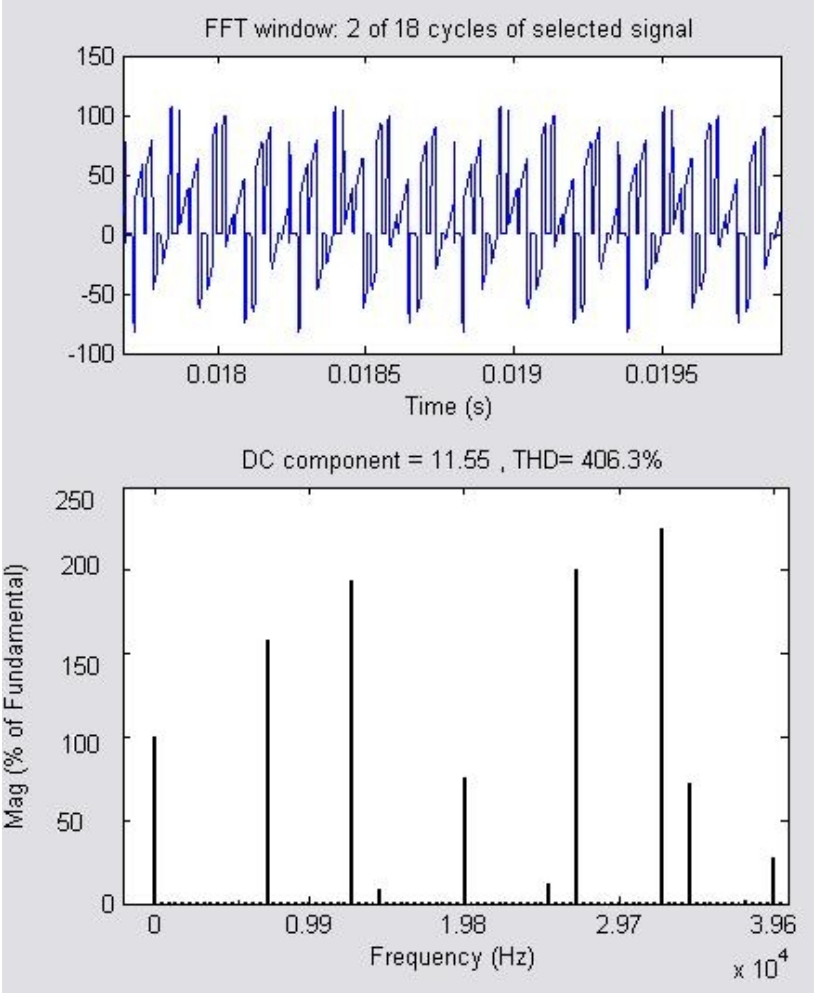

Fig. 37: DC Current, $I_{dc,sim1}$, 900 Hz

Table 23: Harmonics of $I_{dc,sim1}$

Order	Frequency (kHz)	Magnitude (%of dc)
DC	0	100.00
8	7.2	157.6
14	12.6	193.9
22	19.8	74.5
30	27.0	200.8
36	32.4	225.1
38	34.2	72.73
44	39.6	27.7

Fig. 38 shows the capacitor current, $I_{cap,sim1}$, and its harmonic spectrum, which is listed in Table 24.

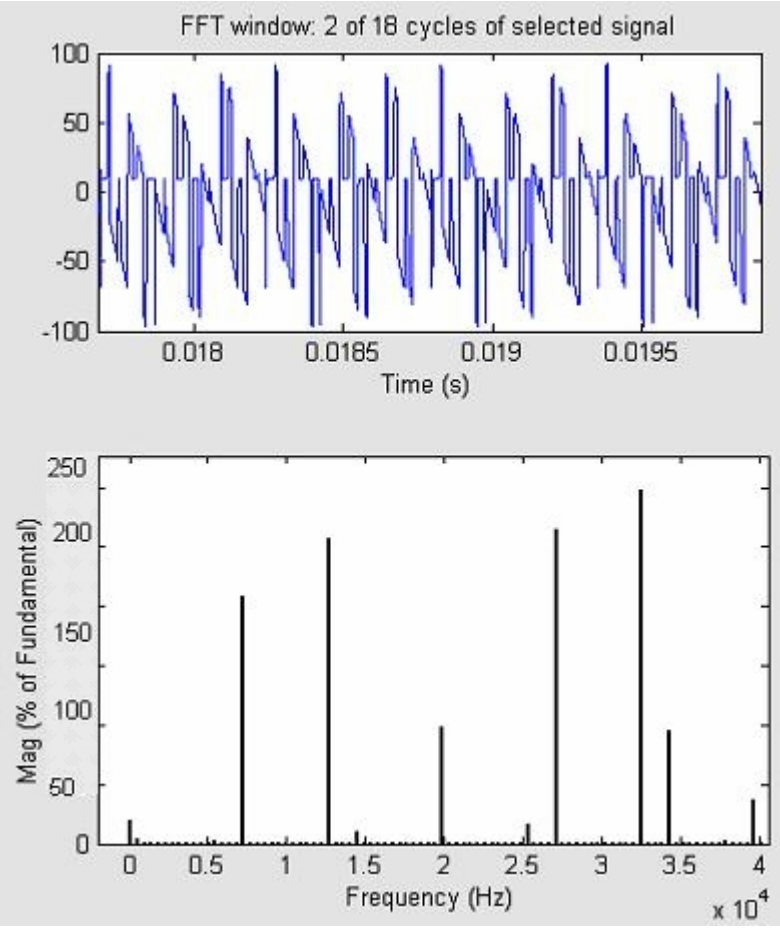

Fig. 38: Capacitor Current, $I_{cap,sim1}$, 900 Hz

Table 24: Harmonics of $I_{cap,sim1}$

Order	Frequency (kHz)	Magnitude (%of dc-bus)
DC	0	0
8	7.2	157.6
14	12.6	193.9
22	19.8	74.5
30	27.0	200.8
36	32.4	225.1
38	34.2	72.73
44	39.6	27.7

Fig. 39 shows the capacitor voltage, $v_{cap,sim1}$, and its harmonic spectrum, which is listed in Table 25.

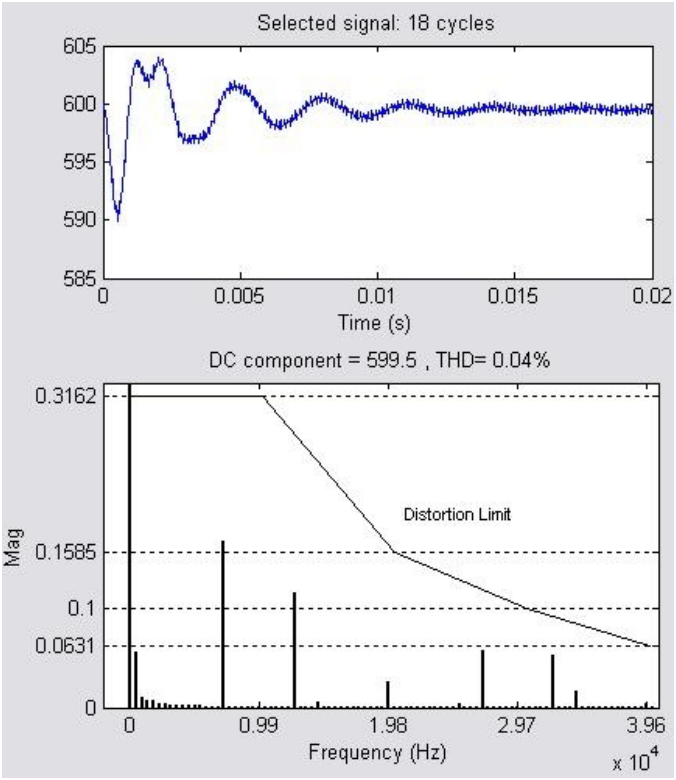

Fig. 39: Capacitor Voltage, $v_{cap,sim1}$, 900 Hz

Table 25: Harmonics of $v_{cap,sim1}$

Order	Frequency (kHz)	Magnitude (V)	Magnitude (dB μV)
DC	0.0	599.7	------
0.5	0.45	0.0555	94.89
8	7.2	0.1681	104.511
14	12.6	0.1169	101.36
22	19.8	0.0258	88.23
30	27.0	0.0575	95.19
36	32.4	0.0535	94.57
38	34.2	0.0162	84.19

From the simulation, the rms $v_{cap,sim1}$ = 0.2283 V. The distortion (with respect to 1 μV) is calculated as:

$20\log\left(\frac{v_{cap,rms}}{1x10^{-6}}\right) = dB$, so for this case we have, $20\log\left(\frac{0.2283}{1x10^{-6}}\right) = 107.17$.

As can be seen from Fig. 39, the present harmonics are beneath the distortion limit.

2.4 PSpice Implementation

Fig. 40 shows the schematic used in the PSpice simulation with f_{sw} = 9900 Hz, f_{fund} = 60 Hz, m_a = 0.8. Fig. 41 shows the line-to-line voltage, and its harmonic spectrum is shown in Fig. 42

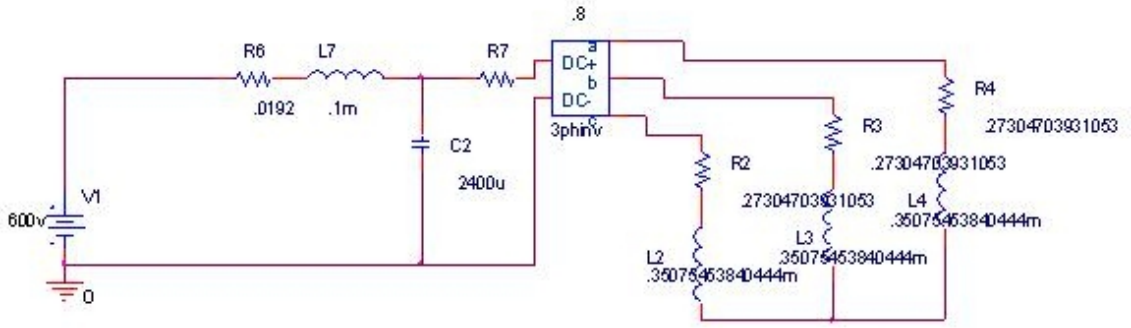

Fig. 40: PSpice Simulation Schematic

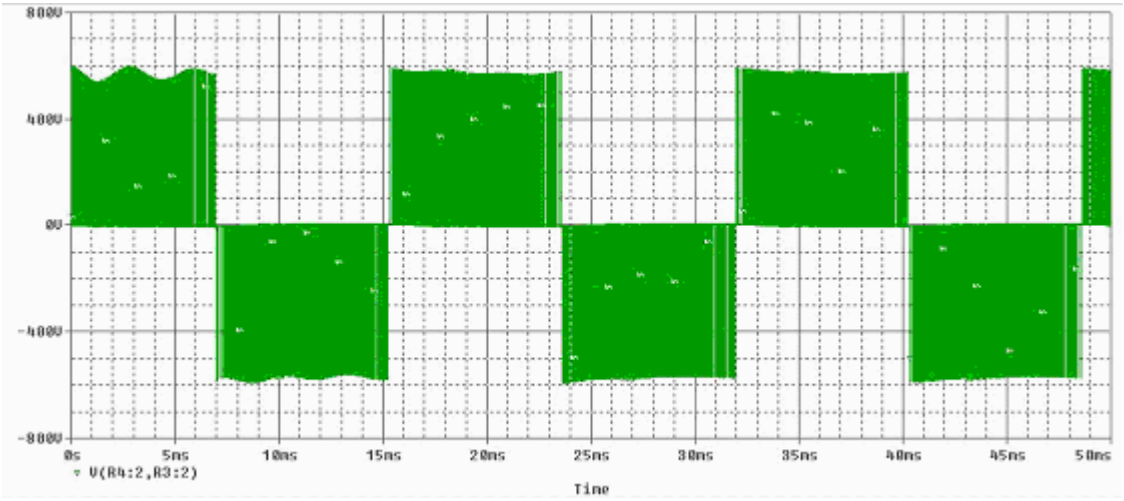

Fig. 41: PSpice Line-to-Line Voltage, $v_{ab,sim}(\omega t)$

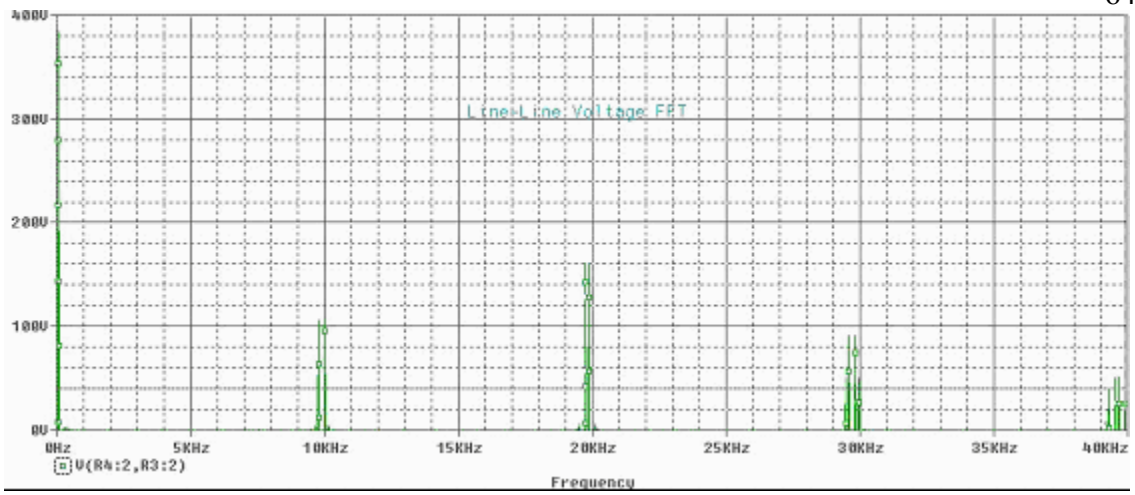

Fig. 42: Harmonic Spectrum of $v_{ab,sim}(\omega t)$

Fig. 43 shows the PSpice simulation line current, $I_{a,sim}(\omega t)$.

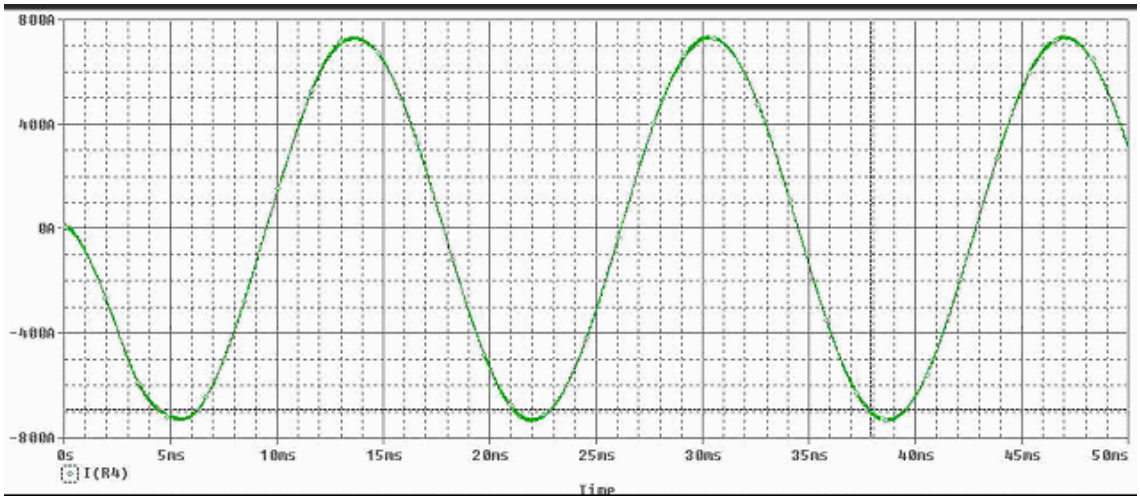

Fig. 43: PSpice Line Current, $I_{a,sim}(\omega t)$

Fig. 44 shows the input dc bus current and its harmonic spectrum is shown in Fig. 45.

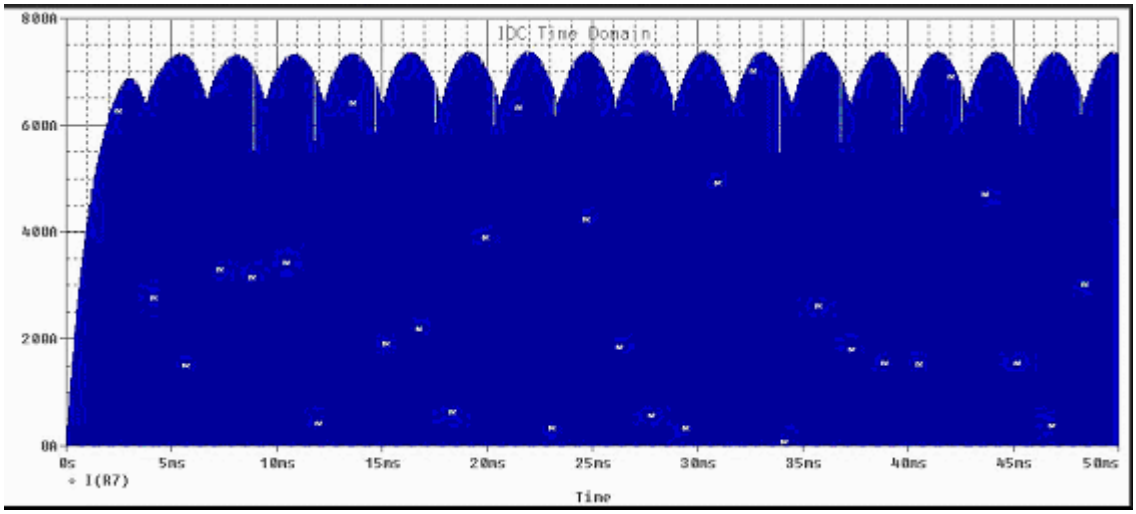

Fig. 44: PSpice DC Current, $I_{dc,sim}(\omega t)$

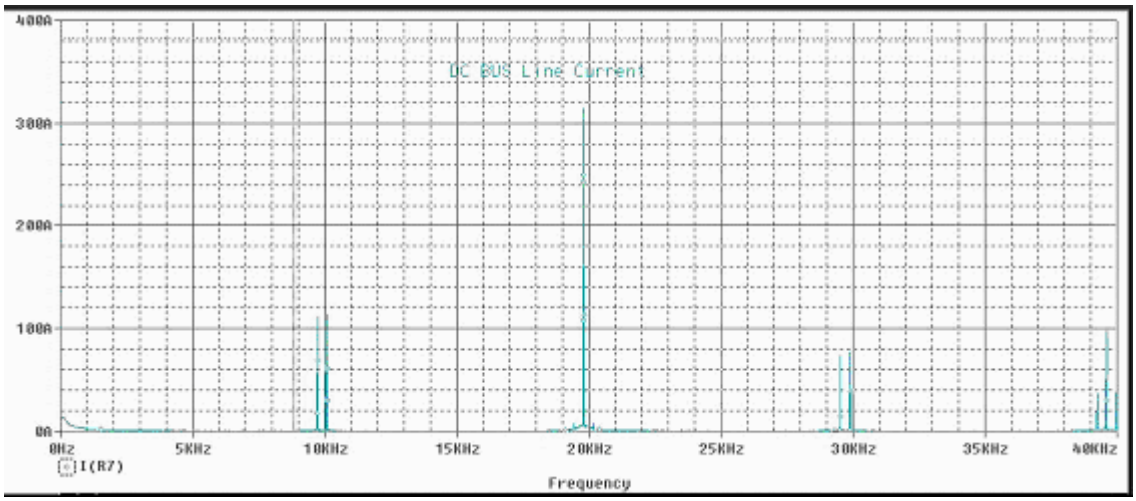

Fig. 45: Harmonic Spectrum of $I_{dc,sim}(\omega t)$

The harmonics of $v_{ab,sim}(\omega t)$ and $I_{dc,sim}(\omega t)$ are listed in the overall Comparison Section.

2.5 Space Vector Switching Function Approach

With space vector modulation (SVM), a set of three-phase ac voltages yields a single voltage vector, v_{ref} in the d-q plane [10]. This is achieved through using Park's Transformation as seen in Equation 4. The instantaneous output voltages are determined by the state of the six inverter switches. There are eight possible switching states, which are shown in Fig. 46 (includes two zero states) [10].

$$\begin{bmatrix} V_0 \\ V_d \\ V_q \end{bmatrix} = \sqrt{\frac{2}{3}} \begin{bmatrix} 1/\sqrt{2} & 1/\sqrt{2} & 1/\sqrt{2} \\ 1 & -1/2 & -1/2 \\ 0 & -\sqrt{3}/2 & \sqrt{3}/2 \end{bmatrix} \begin{bmatrix} V_a \\ V_b \\ V_c \end{bmatrix} \qquad (4)$$

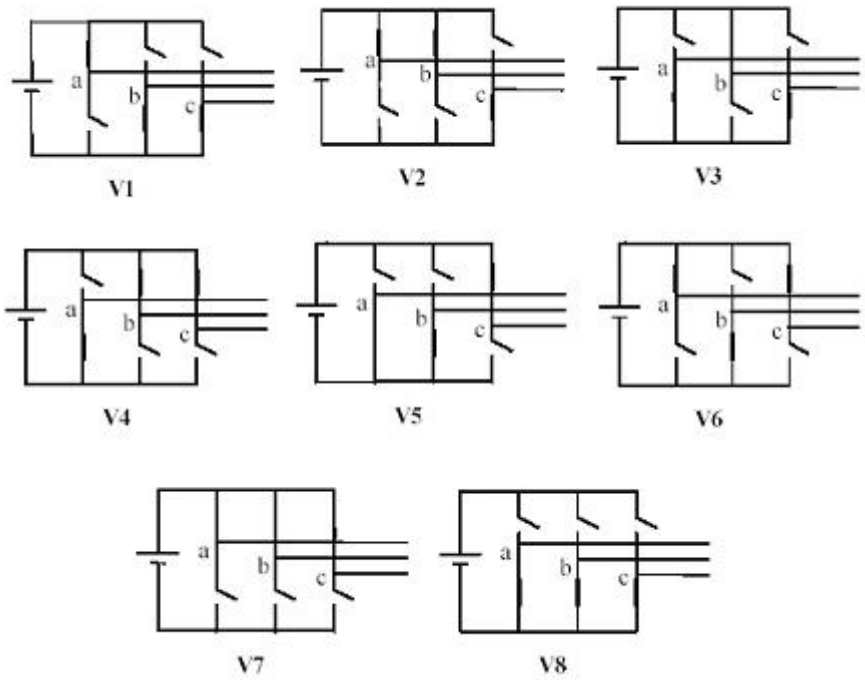

Fig. 46: Eight Possible Switching States

Each one of these states represents a vector in the d-q plane; and these vectors are shown in Fig. 47. Note that the states V7 and V8 are null states and are represented in the origin of Fig. 47.

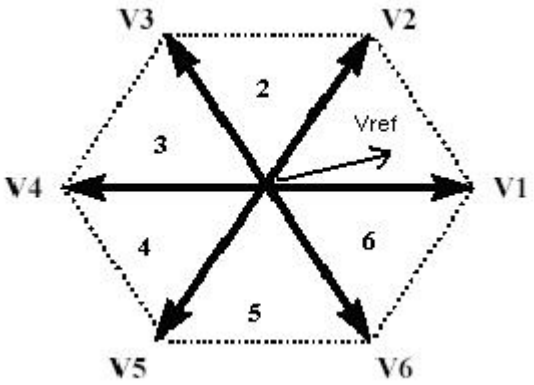

Fig. 47: Switching Voltage Vectors

When the desired voltage vector, v_{ref}, is in the position above (Fig. 47) over some time interval, T_s, it can be defined in terms of the adjacent voltage vector components (V1, V2, V7, V8) by equating voltage-time intervals:

$$\text{V8}*\frac{t_0}{2} + \text{V1}*t_a + \text{V2}*t_b + \text{V7}*\frac{t_0}{2} = v_{ref} * T_s$$

where V8, V1, V2, and V7 are selected for times $\frac{t_0}{2}$, t_a, t_b, and $\frac{t_0}{2}$, respectively.

The time durations can be solved as follows [11]:

$$t_a = \frac{9}{\pi^2} V_s T_s \left(\cos\alpha - \frac{1}{\sqrt{3}} \sin\alpha \right)$$

$$t_b = \frac{6\sqrt{3}}{\pi^2} V_s T_s (\sin\alpha)$$

$$t_0 = T_s - t_a - t_b$$

where V_s is the desired line voltage magnitude normalized to $0.61*V_{dc}$ and α is the angle between v_{ref} and the switching voltage vector Va. The pulse pattern generated by this is shown in Fig. 48 [12].

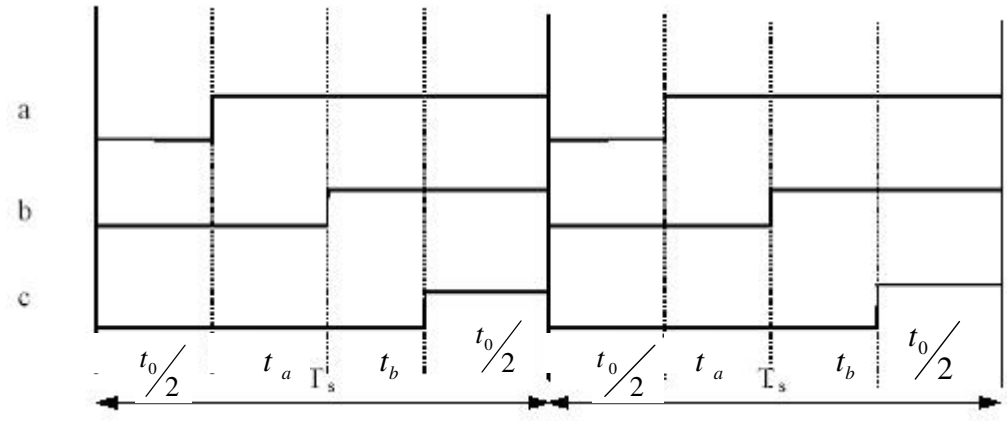

Fig. 48: SVM Pulse Pattern

It is important to note that there are other switching algorithms that could be used; however, this is what is used for the following simulation.

In this approach, the same methodology as for the SPWM switching function approach is used based on the SVM gating signals generated. Also, the same parameters are used here as in the analytical solution. The gating signals are generated using Matlab, and then they are inserted into Simulink to generate the dc input current. Fig. 49 shows the Simulink block diagram of the SVM approach.

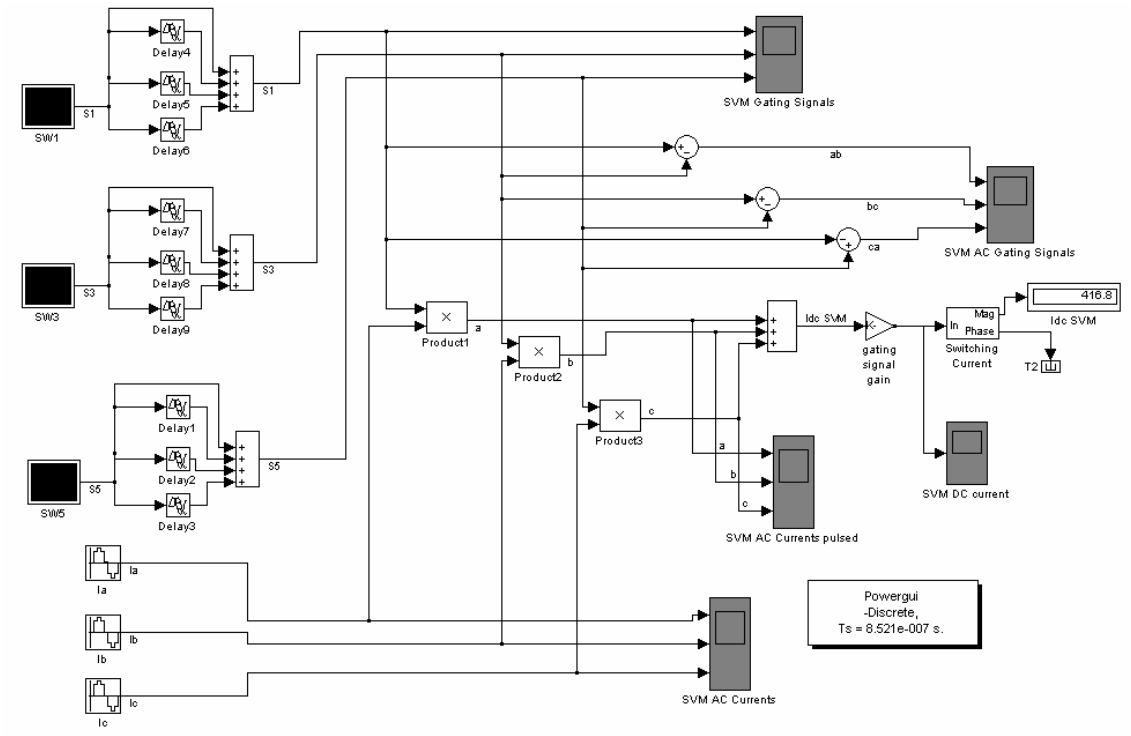

Fig. 49: Block Diagram of SVM

Fig. 50 shows the line-to-line gating signal and harmonic spectrum for switch one to switch three, which are listed in Table 26.

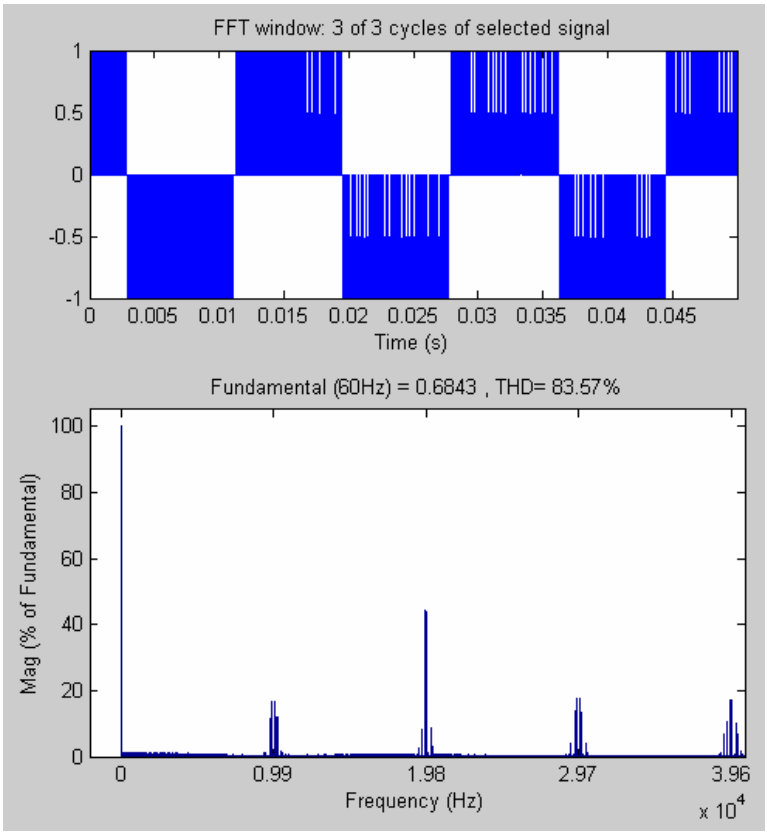

Fig. 50: SVM Gating Signal Voltage, $v_{gate,SV}$

Table 26: Harmonics of $v_{gate,SV}$

Order	Freq (kHz)	Magn (% of Fund)
FUND	0.060	100.00
161	9.66	11.6
163	9.78	16.4
167	10.02	16.5
169	10.14	12.2
325	19.5	8.3
329	19.74	44.5
331	19.86	43.9
335	20.1	8.5
491	29.46	13.7
493	29.58	17.8
497	29.82	17.6
499	29.94	13.5
653	39.18	6.7
655	39.3	10.4
659	39.54	17.2
661	39.66	17.2
665	39.9	10.2
667	40.02	6.8

Fig. 51 shows phase a line current.

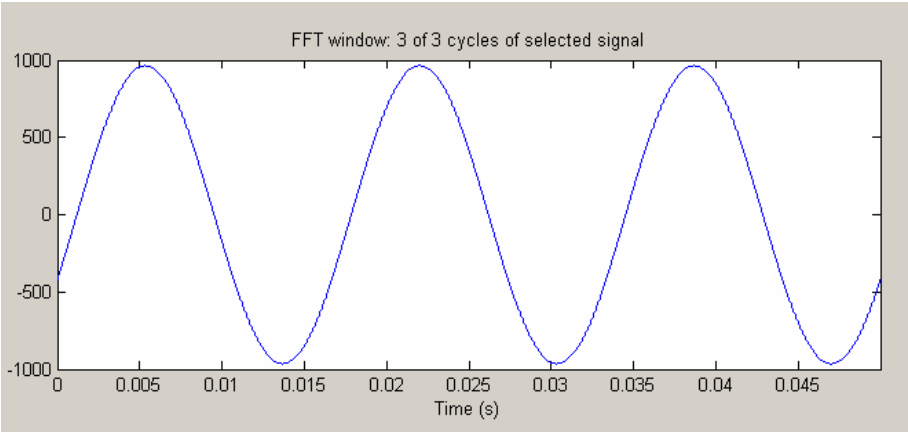

Fig. 51: SVM Line Current, $I_{a,sv}$

Fig. 52 shows the dc current which is the sum of the line currents multiplied by there respective gating signals and the resulting harmonic spectrum, which is listed in Table 27.

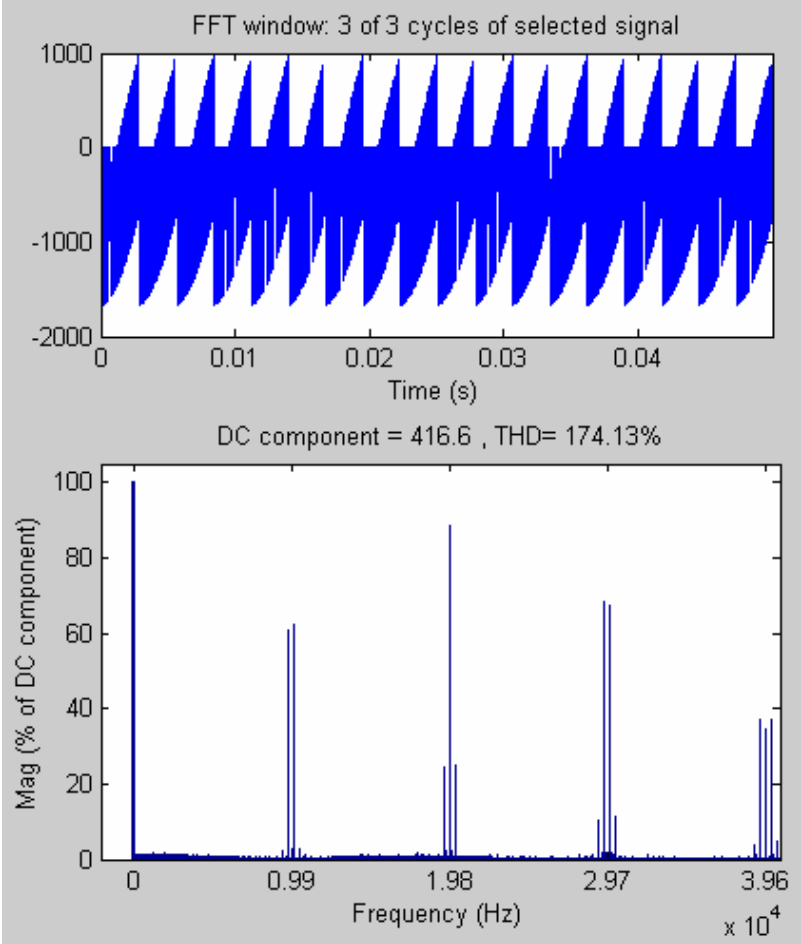

Fig. 52: SVM DC Current, $I_{dc,sv}$

Table 27: Harmonics of $I_{dc,SV}$

Order	Frequency (kHz)	Magnitude (%of dc)
DC	0	100.00
162	9.72	60.8
168	10.08	62.4
324	19.44	24.4
330	19.8	88.4
336	20.16	25.0
486	29.16	10.2
492	29.52	68.2
498	29.88	67.4
504	30.24	11.2
654	39.24	37.2
660	39.6	34.6
666	39.96	37.0

2.6 Experimental Verification

In this section, experimental data is provided from a SPWM controlled drive and compared with simulation results using similar operating parameters; however there are a few differences due to the specific dc bus filtering. This actual filtering information (LC values) is not available with the current hardware. So, the first simulation is run without any additional parameters added, then a second simulation is run with approximated values for the dc bus filter. Fig. 53 shows the block diagram of the experimental setup.

The experimental parameters are:

Reliance Electric AC – VS Drive: 5 hp 230 V

US Electric Induction Motor: 5 hp 230 V 60 Hz

$V_{dc,\exp} = 330V$ $V_{LL,rms} = 147.2\ \text{V}$ $pf = 0.836$ $I_{L,rms} = 12.12\ \text{A}$

$f_{sw} = 3.51\,\text{kHz}$ $P_{out} = 3.00\ \text{kW}\ @\ m_a = 0.73$

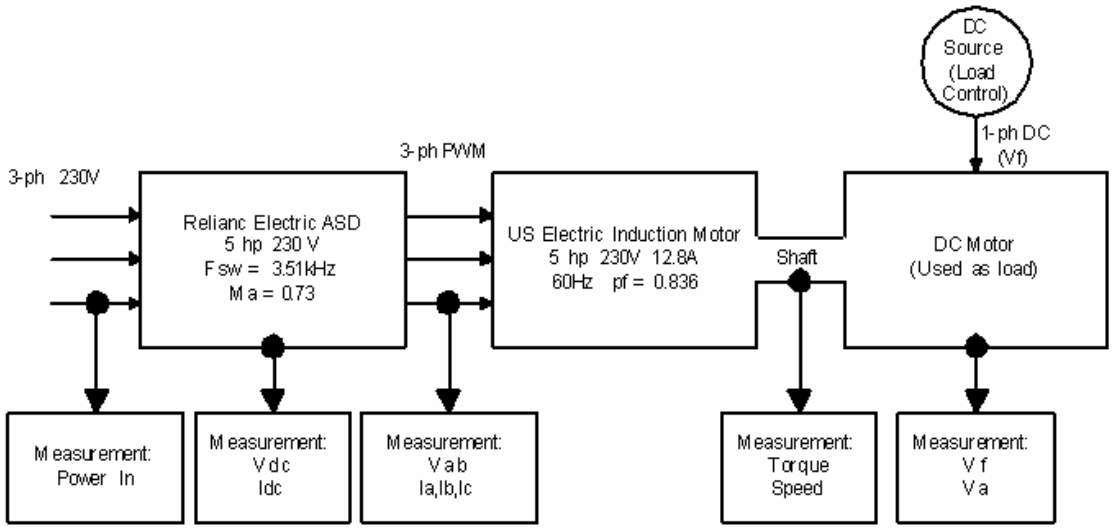

Fig. 53: Experimental Setup Block Diagram

Fig. 54 shows the harmonic spectrum of the line-to-line voltage, $V_{LL,\text{exp}}$, from the experimental setup and Table 28 lists the harmonics present.

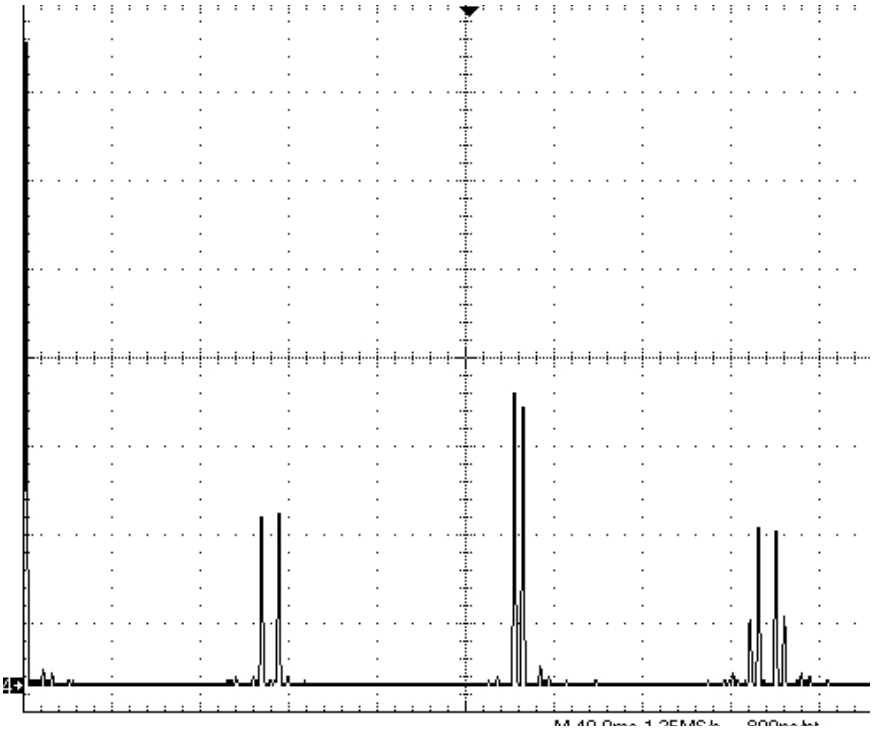

Fig. 54: Harmonic Spectrum of Experimental Line-to-Line Voltage, $V_{LL,\text{exp}}$

Table 28: Harmonics of $V_{LL,\text{exp}}$

Order	Frequency (kHz)	Magnitude (V)	Magnitude (%of Fund)
FUND	0.060	147.2	100.00
56.5	3.39	39.6	26.9
60.5	3.63	41.6	28.3
116	6.96	68.6	46.6
117	7.08	65.6	44.6
171.5	10.29	16.4	11.1
173.5	10.41	37.4	25.4
177.5	10.65	36.4	24.7
179.5	10.77	16.8	11.4

Fig. 55 shows the harmonic spectrum of the dc bus current, $I_{dc,\text{exp}}$, and its harmonics are listed in Table 29.

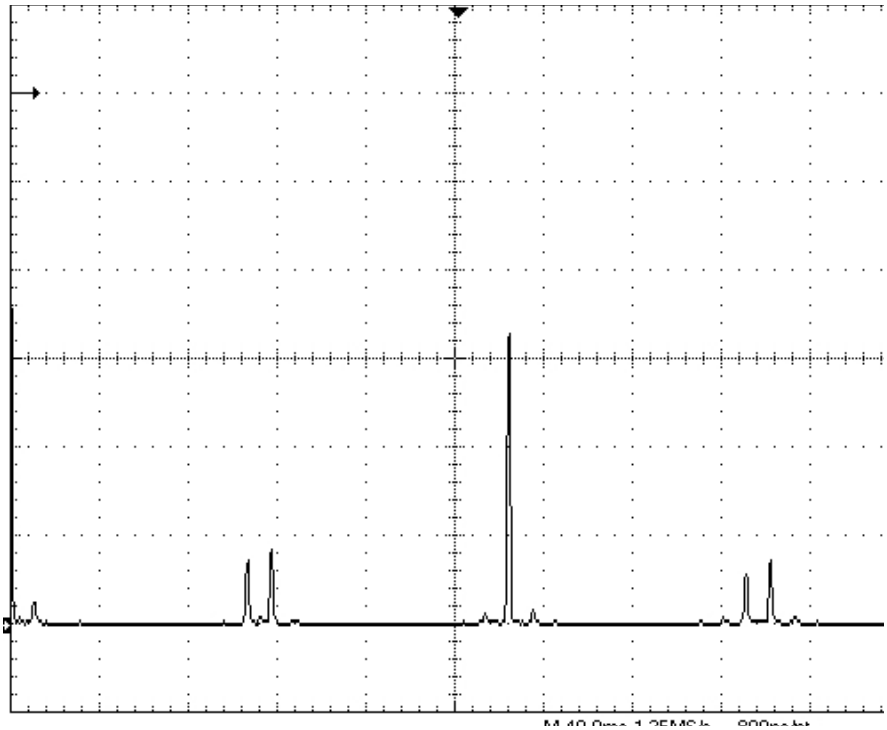

Fig. 55: Harmonic Spectrum Experimental DC Bus Current, $I_{dc,\exp}$

Table 29: Harmonics of $I_{dc,\exp}$

Order	Frequency (kHz)	Magnitude (A)	Magnitude (%of dc)
DC	0.06	7.81	100.00
4.5	0.27	0.31	3.9
55.5	3.33	0.99	12.6
61.5	3.69	1.1	14.1
117	7.02	4.1	52.5
172.5	10.35	0.7	8.9
178.5	10.71	0.85	10.9

Simulink Simulation Verification

As stated above, this first simulation was performed without the specific dc bus filtering. Fig. 56 shows the block diagram of the simulation.

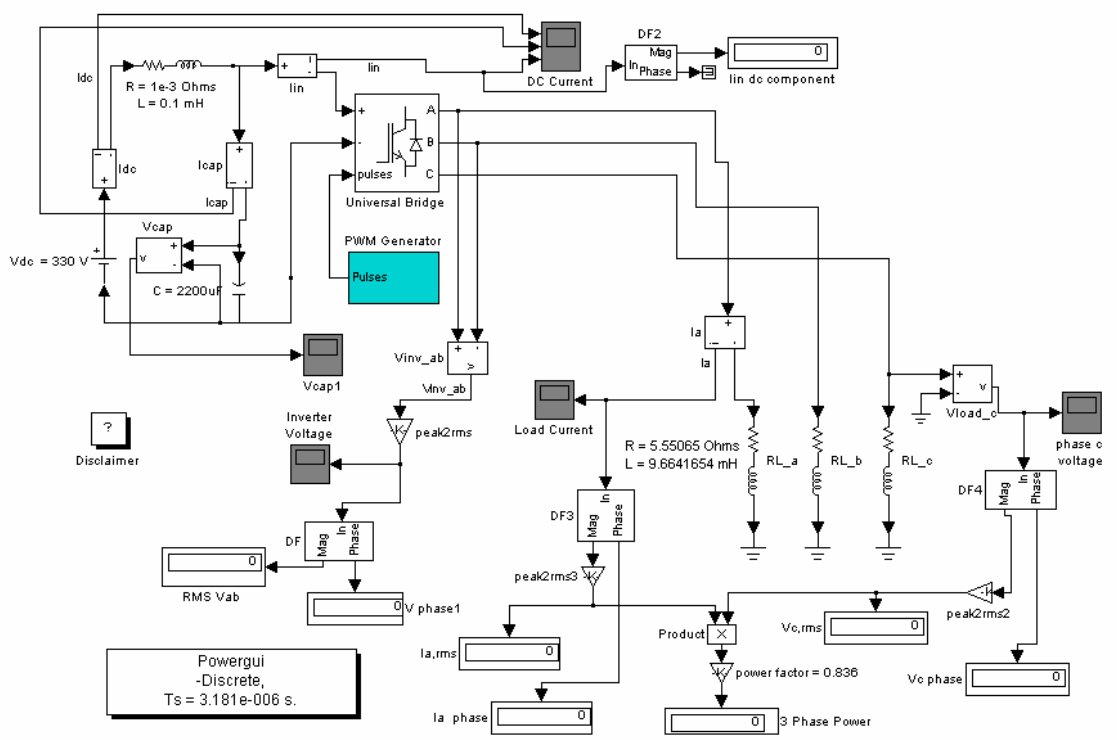

Fig. 56: Block Diagram of Experimental Verification Simulation

Fig. 57 shows the harmonic spectrum of the line-to-line voltage from the simulation, $V_{LL,ver1}$, and Table 30 lists the harmonics present.

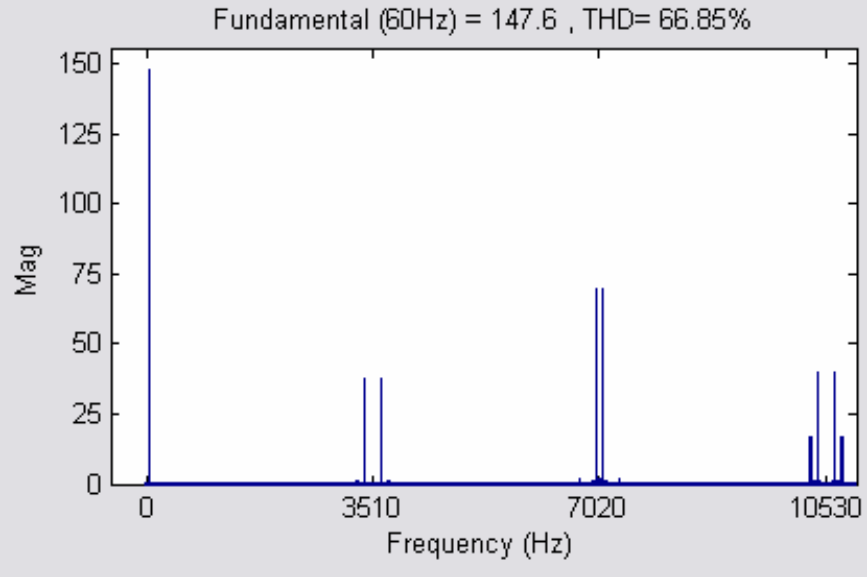

Fig. 57: Harmonic Spectrum of Simulation Verification Line-to-Line Voltage, $V_{LL,ver1}$

Table 30: Harmonics of $V_{LL,ver1}$

Order	Frequency (kHz)	Magnitude (V)	Magnitude (%of Fund)
FUND	0.060	147.61	100.00
56.5	3.39	37.81	25.61
60.5	3.63	37.81	25.62
116	6.96	69.65	47.19
117	7.08	69.66	47.19
171.5	10.29	16.83	11.41
173.5	10.41	39.81	26.96
177.5	10.65	39.72	26.90
179.5	10.77	16.79	11.37

Fig. 58 shows the harmonic spectrum of the dc bus current, $I_{dc,ver1}$, and its harmonics are listed in Table 31.

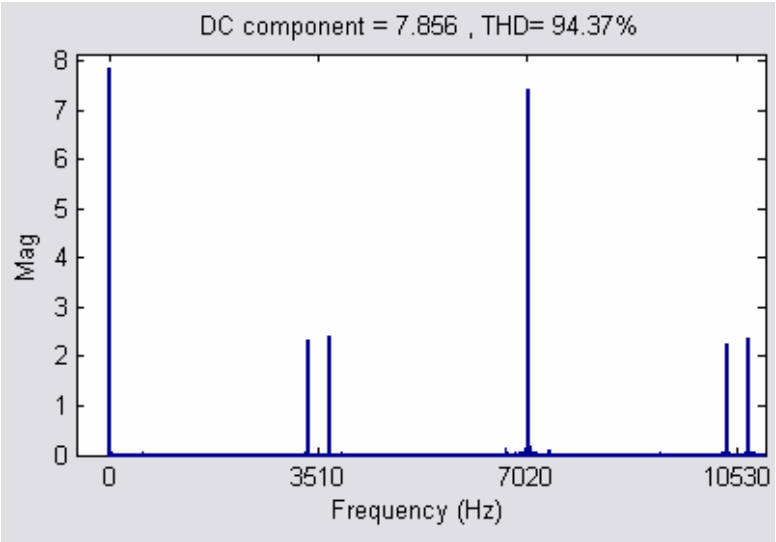

Fig. 58: Harmonic Spectrum of Simulation Verification DC Current, $I_{dc,ver1}$

Table 31: Harmonics of $I_{dc,ver1}$

Order	Frequency (kHz)	Magnitude (A)	Magnitude (%of dc)
DC	0.060	7.86	100.00
55.5	3.33	2.33	29.61
61.5	3.69	2.42	30.76
117	7.02	7.4	94.25
172.5	10.35	2.26	28.76
178.5	10.71	2.39	30.39

As can be seen from the first simulation, the harmonics are approximately twice the magnitude of the experimental data and there is no harmonic present at 270 Hz. This is probably due to the specific dc bus filtering components not being included that are incorporated in the particular adjustable speed drive used for these test. Since there was no ready access to or documentation for these elements, an approximation was made by adding an inductance of L = 128 pH and a capacitance of C = 1200 µF across the dc bus for the second simulation. The current was then measured between this approximate filter and the main dc bus capacitor. As expected, adding the inductance and capacitance values did not change the line-to-line voltage harmonic spectrum.

Fig. 59 shows the harmonic spectrum of the dc bus current from the second simulation and Table 32 listed the harmonics present.

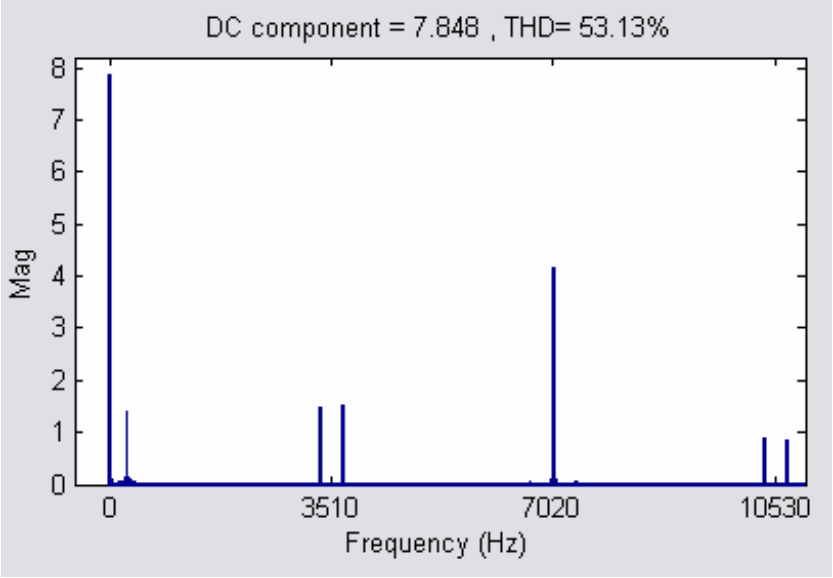

Fig. 59: Harmonic Spectrum of Simulation Verification DC Current, $I_{dc,ver2}$

Table 32: Harmonics of $I_{dc,ver2}$

Order	Frequency (kHz)	Magnitude (A)	Magnitude (%of dc)
DC	0.060	7.85	100.00
4.5	0.27	1.39	17.66
55.5	3.33	1.46	18.60
61.5	3.69	1.51	19.21
117	7.02	4.16	52.98
172.5	10.35	0.87	11.13
178.5	10.71	0.84	10.72

As can be seen from Table 32, the harmonics correlate better with the added approximated dc bus filter. There is now a harmonic component present at 270 Hz and the magnitudes of the other harmonics match better. The harmonics of the experimental data will be directly compared with the simulation results in the Comparison Section.

3 Overall Comparison of Harmonics

Table 33: Harmonic Spectra Comparison of v_{ab} (at 60Hz fundamental)

		SPWM Analytical	SPWM Switching Function	SPWM Simulink	SPWM PSpice	SVM Switching Function*
Order	Freq (kHz)	Magnitude (% of Fundamental)				
FUND	0.060	100.00	100.00	100.00	100.00	100.00
161	9.66	1.02	1.27	0.98	1.12	11.6
163	9.78	27.56	27.5	27.4	27.73	16.4
167	10.02	27.56	27.41	27.5	27.73	16.5
169	10.14	1.02	0.86	1.06	1.11	12.2
325	19.5	1.64	1.52	1.70	1.34	8.3
329	19.74	39.19	38.8	39.54	41.83	44.5
331	19.86	39.19	39.36	39.3	41.83	43.9
335	20.1	1.64	1.57	1.76	1.33	8.5
491	29.46	13.06	13.32	13.0	13.09	13.7
493	29.58	22.04	21.94	21.9	23.64	17.8
497	29.82	22.04	21.69	22.0	23.7	17.6
499	29.94	13.06	12.68	13.12	13.09	13.5
653	39.18	2.04	2.2	2.19	2.09	6.7
655	39.3	10.38	10.28	10.7	10.54	10.4
659	39.54	13.03	13.0	13.18	13.17	17.2
661	39.66	13.03	12.87	13.26	13.20	17.2
665	39.9	10.38	10.38	10.35	10.5	10.2
667	40.02	2.04	2.25	2.38	--	6.8

*SVM is included for comparison purposes only, not for "correlation" with SPWM

Table 34: Harmonic Spectra Comparison of I_{dc} (at 60Hz fundamental)

		SPWM Analytical	SPWM Switching Func.	SPWM Simulink	SPWM PSpice	SVM Switching Function*
Order	Freq (kHz)	Magn (% of DC)				
DC	0	100.00	100.00	100.00	100.00	100.00
162	9.72	29.92	29.80	29.45	29.21	60.80
168	10.08	29.92	29.87	29.84	29.60	62.40
324	19.44	1.81	1.67	1.77	-	24.40
330	19.80	37.95	78.30	77.03	82.13	88.40
336	20.16	1.81	1.87	2.00	-	25.00
492	29.52	19.22	19.10	18.10	19.47	68.20
498	29.88	19.22	19.10	18.76	19.85	67.40
654	39.24	10.31	10.40	10.30	9.54	37.20
660	39.60	12.65	20.06	26.30	25.61	34.60
666	39.96	10.31	10.20	10.02	9.80	37.00

*SVM is included for comparison purposes only, not for "correlation" with SPWM

It is shown above, in Table 33, that the line-to-line output voltage harmonics correspond very well between the SPWM analytical, switching function, Simulink and PSpice approaches. Looking at Table 34, it can be seen that small differences exist in the analytical reflected dc current, namely at $2m_f$ (330^{th} harmonic) and $4m_f$ (660^{th} harmonic). This may be due to the fact that for the analytical approach, the output line-to-line voltage harmonic magnitudes were used as specified in [7], however the phase angles are not provided. Also, there is an added phase shift in the actual transfer function as documented in [8]. It was found that by adding a phase shift of 60° to the 331^{st} and 661^{st} harmonics in the voltage corrected the magnitudes of the harmonics in the dc current. The line-to-line output voltage harmonics are extremely similar for each case (within 0.1% error). Table 35 lists the corrected harmonics of the dc bus current and Table 36 shows the comparison of the dc bus current from the experimental verification.

Table 35: Corrected Harmonic Spectra Comparison of I_{dc} (at 60Hz fundamental)

		SPWM Analytical	SPWM Switching Func.	SPWM Simulink	PSpice	SVM Switching Function*
Order	Freq (kHz)	Magn (% of DC)				
DC	0	100.00	100.00	100.00	100.00	100.00
162	9.72	29.92	29.8	29.45	29.21	60.8
168	10.08	29.92	29.87	29.84	29.6	62.4
324	19.44	1.81	1.67	1.77	-	24.4
330	19.8	**72.05**	78.3	77.03	82.13	88.4
336	20.16	1.81	1.87	2.0	-	25.0
492	29.52	19.22	19.1	18.1	19.466	68.2
498	29.88	19.22	19.1	18.76	19.847	67.4
654	39.24	10.31	10.4	10.3	9.54	37.2
660	39.6	**24.02**	20.06	26.3	25.61	34.6
666	39.96	10.31	10.2	10.02	9.8	37.0

*SVM is included for comparison purposes only, not for "correlation" with SPWM

Table 36: Experimental Verification Harmonic Spectra Comparison of I_{dc}

		Experimental Data	Simulation 1	Simulation 2
Order	Freq (kHz)	Magn (%of dc)		
DC	0.06	100.00	100.00	100.00
4.5	0.27	3.9	-------	17.66
55.5	3.33	12.6	29.61	18.60
61.5	3.69	14.1	30.76	19.21
117	7.02	52.5	94.25	52.98
172.5	10.35	8.9	28.76	11.13
178.5	10.71	10.9	30.39	10.72

4 Conclusion

4.1 Conclusion

Since it is proposed that HEV's will be used in applications that have high performance requirements, investigations into the harmonics generated by converters are very important. Several different approaches (Analytical, Switching Function, Simulink, and PSpice) were used to investigate dc bus harmonics. The first approach was to derive the dc bus current analytically using SPWM, which produced accurate results for the output line-to-line voltages and all but two of the reflected dc bus harmonics. The magnitudes of the harmonics at $2m_f$ and $4m_f$ were lower than what was found in the Switching Function approach and the Simulink and PSpice simulations due to a phase shift introduced by the transfer function. When this phase shift was added to the analytical approach it produced more representative predictions of the magnitudes of the 330^{th} and 660^{th} harmonics.

The SPWM Switching Function approach utilizes the switching characteristics of the inverter to construct the dc bus currents. More specifically, the dc current is constructed from the contributions of each of the top switches while in the "on state", contributing the ac line current associated with each switch. The results from this approach correlated very well with the Simulink and PSpice simulations. The Simulations performed in Simulink modeled the system, including the inverter using SPWM, a load calculated to meet the required power levels, and the components of the dc bus. Since the results of this simulation matched extremely well with the SPWM Switching Function approach (and PSpice, and correlated fairly well with the Analytical

approach), Simulink was used to investigate fundamental frequency changes including 2Hz, 60Hz, 500Hz, and 900Hz. For each case, the harmonics present in the dc bus capacitor were noted and compared with the MIL-STD-461 distortion limits. In the cases that didn't meet the distortion limit (2 Hz and 60 Hz), the dc bus capacitor was increased to 17,000 μF for mitigation. Next, PSpice was used to simulate the system and the results correlated extremely well with both the SPWM Switching Function and SPWM Simulink Simulation approaches.

For comparison, the SVM Switching Function approach was implemented. Although SVM is a completely different switching scheme than SPWM, the resulting harmonic orders correlated very well with the other approaches.

For further verification, an experimental test was setup and compared with a Simulink simulation. Due to lack of information on the values of the dc bus filter used in the adjustable speed drive for the experimental test, the comparison yielded close, but not exact results.

4.2 Suggestions for Future Work

As can be seen from this research, there are significant harmonics reflected onto the dc bus from a single converter. In large HEV applications, there may be several converters connected to a single dc bus. Future work should involve investigating these harmonics generated by multiple converters and relevant mitigation techniques. In addition, future hardware implementation work will include actual drive design and filter specifications for more accurate hardware vs. simulation comparison.

It is suggested that Simulink be used as the platform for future work as it can model the system(s) very well and has built in tools to view waveforms in both the time domain and frequency domain.

5 References

[1] Walker, Geoffrey R., "Modulation and Control of Multilevel Converters", Department of Computer Science and Electrical Engineering, University of Queensland, 1999.

[2] Tolbert, L. M. and Peng, F. Z., "Multilevel Inverters for Large Automotive Drives," in *Conf. Rec. All Electric Combat Vehicle 2nd Int. Conf.*, Dearborn, MI, June 8–12, 1997, vol. 2, pp. 209–214.

[3] Tolbert, L. M., Peng, F. Z., Habetler, Thomas G., "Multilevel Converters for Large Electric Drives," *IEEE Transactions on Industry Applications*, vol. 35, no. 1, Jan./Feb. 1999, pp. 36-44.

[4] Leon M. Tolbert and T.G Habetler, "Novel Multilevel Inverter Carrier-Based PWM Methods," *IEEE Transactions on Industry Applications*, vol. 35, no. 5, Sept/Oct. 1999, pp. 1098-1107.

[5] Tolbert, Leon M., Chiasson, John N., McKenzie, Keith, Du, Zhong, "Elimination of Harmonics in a Multilevel Converter for HEV Applications," *The 7th IEEE Workshop on Power Electronics in Transportation*, October 24-25, 2002, Auburn Hills, Michigan, pp. 135-142.

[6] Weichmann, Eduardo, *et al.*, "Generalized Functional Model for Three-Phase PWM Inverter/Rectifier Converters," *IEEE Transactions of Industry Applications*, vol. IA-23, no. 2, March/April 1987, pp. 236-246.

[7] Mohan, Undeland, Robbins, *Power Electronics: Converters, Applications and Design*, 3rd Edition, New York: John Wiley & Sons, Inc., 2003.

[8] Ziogas, Phoivos D. and Photiadis, Photis N. D., "An Exact Input Current Analysis of Ideal Static PWM Inverters," *IEEE Transactions on Industry Applications*, vol. IA-19, no. 2, March/April 1983, pp. 281-295.

[9] von Jouanne, A., and Enjeti, P., "A New Three-Phase Series Resonant Active Power Filter", *Industry Applications Society* Conf. Proc., Oct. 1994, pp. 929-935.

[10] Granado, J., Harley, R.G., Diana, G., "Understanding and Designing a Space Vector Pulse-Width-Modulator to Control a Three Phase Inverter," *The Transaction of the SA Institute of Electrical Engineers*, September 1989.

[11] Enjeti, P. and von Jouanne, A. "A New Real Time Space Vector PWM Strategy for High Performance Inverters," Department of Electrical Engineering, Texas A&M University.

[12] Broeck, Hienz, *et al.*, "Analysis and Realization of a Pulsewidth Modulator Based on Voltage Space Vectors," *IEEE Transactions on Industry Applications*, vol. 24, no. 1, January/Feburary 1988, pp. 271-280.

[13] T. Cunnyngham, "Cascade Multilevel Inverters for Large Hybrid-Electric Vehicle Applications with Variant DC Sources," Master's Thesis, University of Tennessee, 2001.

[14] John N. Chiasson, Leon M. Tolbert, Keith J. McKenzie, Zhong Du, "Eliminating Harmonics in a Multilevel Inverter Using the Theory of Symmetric Polynomials and Resultants," *IEEE Conference on Decision and Control*, December 9-12, 2003, Maui, Hawaii, pp. 3507-3512.

[15] Boys, J.T., Handley, P.G., "Harmonic Analysis of Space Vector Modulated PWM Waveforms," *IEE Preceedings*, vol 137, Pt.B, No. 4, July 1990.

[16] Boost, Michael and Ziogas, Phoivos D., "State-of-the-Art Carrier PWM Techniques: A Critical Evaluation," *IEEE Transactions on Industry Applications*, vol. 24, no. 2, March/April 1988, pp. 271-280.

[17] Kieferndorf, Frederick, *et. Al.*, "Reduction of DC Bus Capacitor Ripple Current with PAM/PWM Converter," University of Wisconsin-Madison, Dept. of Electrical and Computer Engineering.

[18] SuperHarm product flyer from www.electrotek.com

[19] Wilsun Xu, "Status and Future Directions of Power System Harmonic Analysis," publish date unknown.

[20] Frederick D. Kieferndorf, Matthias Förster and Thomas A. Lipo, "Reduction of DC Bus Capacitor Ripple Current with PAM/PWM Converter," 2002, WEMPEC

6 Appendix

Matlab Code for Analytical Closed Form Solution (pwm.m)

```
%DC Ripple Current Using Sine-Triangle Pulse Width Modulation Simulation
%Version 1.4    04/13/2004

%Waylon Bowers
%Motor Systems Research Facility
%Oregon State University
%Corvallis, OR 97330

%This material is provided without any guarantee or warranty either
%expressed or implied, and no author or distributor of this material will
%be held responsible for any damage that might possibly result from the use
%or misuse of this material.  The user acknowledges and accepts sole
%responsibility for his/her usage of this material.

%Parameters

Vdc = 600.0;                          %DC Bus Voltage (assumed ripple free)
f = 60.0;                             %Fundamental Frequency (Hz)
w = 2.0*pi*f;                         %Fundamental Frequency (rad/sec)
fsw = 9900.0;                         %Switching Frequency
fsamp = 2.0*123280.0;                 %Nyquist Sampling Frequency
t = [0.0:1/fsamp:1.0-1/fsamp];        %Time vector
Ma = 0.8;                             %Amplitude Modulation Ratio
Mf = fsw/f;                           %Frequency Modulation Ratio

%Vharmonic/Vdc ratio from Ned Mohan - "Power Electronics"
Mah = sqrt(2.0)*[0.490 0.135 0.192 0.108 0.064 0.064 0.051 0.005 0.008 0.010];
Kh = [1 (Mf+2) (Mf-2) (2*Mf+1) (2*Mf-1) (3*Mf+2) (3*Mf-2) (3*Mf+4) (3*Mf-4)
(4*Mf+1) (4*Mf-1) (4*Mf+5) (4*Mf-5) (Mf+4) (Mf-4) (2*Mf+5) (2*Mf-5) (4*Mf+7)
(4*Mf-7)];      %Order of harmonic

Pout = 250000.0;                      %Output Power
pf = 0.9;                             %Power Factor
phase = 120.0*pi/180.0;               %Phaseshift (rad)
phase30 = 30.0*pi/180.0;
theta_I = -acos(.9);                  %Reference Current phase angle (rad)
ms = length(t);                       %Scaling factor for fft magnitudes
format long g
```

```
%Phase Voltages

Va = (1/sqrt(3))*Vdc*(Mah(1)*sin(Kh(1)*w*t) + Mah(2)*sin(Kh(2)*w*t) +
Mah(2)*sin(Kh(3)*w*t) + Mah(3)*sin(Kh(4)*w*t) + Mah(3)*sin(Kh(5)*w*t) +
Mah(4)*sin(Kh(6)*w*t) + Mah(4)*sin(Kh(7)*w*t)+ Mah(5)*sin(Kh(8)*w*t)+
Mah(5)*sin(Kh(9)*w*t)+ Mah(6)*sin(Kh(10)*w*t)+ Mah(6)*sin(Kh(11)*w*t)+
Mah(7)*sin(Kh(12)*w*t)+ Mah(7)*sin(Kh(13)*w*t)+
Mah(8)*sin(Kh(14)*w*t)+Mah(8)*sin(Kh(15)*w*t)+Mah(9)*sin(Kh(16)*w*t)+Mah(9)
*sin(Kh(17)*w*t)+Mah(10)*sin(Kh(18)*w*t)+Mah(10)*sin(Kh(19)*w*t));

Vb = (1/sqrt(3))*Vdc*(Mah(1)*sin(Kh(1)*(w*t-phase)) + Mah(2)*sin(Kh(2)*(w*t-
phase)) + Mah(2)*sin(Kh(3)*(w*t-phase)) + Mah(3)*sin(Kh(4)*(w*t-phase)) +
Mah(3)*sin(Kh(5)*(w*t-phase))+ Mah(4)*sin(Kh(6)*(w*t-phase)) +
Mah(4)*sin(Kh(7)*(w*t-phase)) + Mah(5)*sin(Kh(8)*(w*t-phase)) +
Mah(5)*sin(Kh(9)*(w*t-phase)) + Mah(6)*sin(Kh(10)*(w*t-phase)) +
Mah(6)*sin(Kh(11)*(w*t-phase)) + Mah(7)*sin(Kh(12)*(w*t-phase)) +
Mah(7)*sin(Kh(13)*(w*t-phase))+Mah(8)*sin(Kh(14)*(w*t-
phase))+Mah(8)*sin(Kh(15)*(w*t-phase))+Mah(9)*sin(Kh(16)*(w*t-
phase))+Mah(9)*sin(Kh(17)*(w*t-phase))+Mah(10)*sin(Kh(18)*(w*t-
phase))+Mah(10)*sin(Kh(19)*(w*t-phase)));

Vc = (1/sqrt(3))*Vdc*(Mah(1)*sin(Kh(1)*(w*t+phase)) +
Mah(2)*sin(Kh(2)*(w*t+phase)) + Mah(2)*sin(Kh(3)*(w*t+phase)) +
Mah(3)*sin(Kh(4)*(w*t+phase)) + Mah(3)*sin(Kh(5)*(w*t+phase))+
Mah(4)*sin(Kh(6)*(w*t+phase)) + Mah(4)*sin(Kh(7)*(w*t+phase)) +
Mah(5)*sin(Kh(8)*(w*t+phase)) + Mah(5)*sin(Kh(9)*(w*t+phase)) +
Mah(6)*sin(Kh(10)*(w*t+phase)) + Mah(6)*sin(Kh(11)*(w*t+phase)) +
Mah(7)*sin(Kh(12)*(w*t+phase)) +
Mah(7)*sin(Kh(13)*(w*t+phase))+Mah(8)*sin(Kh(14)*(w*t+phase))+Mah(8)*sin(Kh(
15)*(w*t+phase))+Mah(9)*sin(Kh(16)*(w*t+phase))+Mah(9)*sin(Kh(17)*(w*t+phase
))+Mah(10)*sin(Kh(18)*(w*t+phase))+Mah(10)*sin(Kh(19)*(w*t+phase)));

%Line-to-Line Voltages

Vab = Vdc*(Mah(1)*sin(Kh(1)*(w*t+phase30)) + Mah(2)*sin(Kh(2)*(w*t+phase30))
+ Mah(2)*sin(Kh(3)*(w*t+phase30)) + Mah(3)*sin(Kh(4)*(w*t+phase30)) +
Mah(3)*sin(Kh(5)*(w*t+phase30)) + Mah(4)*sin(Kh(6)*(w*t+phase30)) +
Mah(4)*sin(Kh(7)*(w*t+phase30))+ Mah(5)*sin(Kh(8)*(w*t+phase30))+
Mah(5)*sin(Kh(9)*(w*t+phase30))+ Mah(6)*sin(Kh(10)*(w*t+phase30))+
Mah(6)*sin(Kh(11)*(w*t+phase30))+ Mah(7)*sin(Kh(12)*(w*t+phase30))+
Mah(7)*sin(Kh(13)*(w*t+phase30))+
Mah(8)*sin(Kh(14)*(w*t+phase30))+Mah(8)*sin(Kh(15)*(w*t+phase30))+Mah(9)*sin
(Kh(16)*(w*t+phase30))+Mah(9)*sin(Kh(17)*(w*t+phase30))+Mah(10)*sin(Kh(18)*(
w*t+phase30))+Mah(10)*sin(Kh(19)*(w*t+phase30)));
```

```
Vbc = Vdc*(Mah(1)*sin(Kh(1)*(w*t-phase+phase30)) + Mah(2)*sin(Kh(2)*(w*t-
phase+phase30)) + Mah(2)*sin(Kh(3)*(w*t-phase+phase30)) +
Mah(3)*sin(Kh(4)*(w*t-phase+phase30)) + Mah(3)*sin(Kh(5)*(w*t-phase+phase30))+
Mah(4)*sin(Kh(6)*(w*t-phase+phase30)) + Mah(4)*sin(Kh(7)*(w*t-phase+phase30))
+ Mah(5)*sin(Kh(8)*(w*t-phase+phase30)) + Mah(5)*sin(Kh(9)*(w*t-
phase+phase30)) + Mah(6)*sin(Kh(10)*(w*t-phase+phase30)) +
Mah(6)*sin(Kh(11)*(w*t-phase+phase30)) + Mah(7)*sin(Kh(12)*(w*t-
phase+phase30)) + Mah(7)*sin(Kh(13)*(w*t-
phase+phase30))+Mah(8)*sin(Kh(14)*(w*t-
phase+phase30))+Mah(8)*sin(Kh(15)*(w*t-
phase+phase30))+Mah(9)*sin(Kh(16)*(w*t-
phase+phase30))+Mah(9)*sin(Kh(17)*(w*t-
phase+phase30))+Mah(10)*sin(Kh(18)*(w*t-
phase+phase30))+Mah(10)*sin(Kh(19)*(w*t-phase+phase30)));

Vca = Vdc*(Mah(1)*sin(Kh(1)*(w*t+phase+phase30)) +
Mah(2)*sin(Kh(2)*(w*t+phase+phase30)) + Mah(2)*sin(Kh(3)*(w*t+phase+phase30))
+ Mah(3)*sin(Kh(4)*(w*t+phase+phase30)) +
Mah(3)*sin(Kh(5)*(w*t+phase+phase30))+ Mah(4)*sin(Kh(6)*(w*t+phase+phase30))
+ Mah(4)*sin(Kh(7)*(w*t+phase+phase30)) +
Mah(5)*sin(Kh(8)*(w*t+phase+phase30)) + Mah(5)*sin(Kh(9)*(w*t+phase+phase30))
+ Mah(6)*sin(Kh(10)*(w*t+phase+phase30)) +
Mah(6)*sin(Kh(11)*(w*t+phase+phase30)) +
Mah(7)*sin(Kh(12)*(w*t+phase+phase30)) +
Mah(7)*sin(Kh(13)*(w*t+phase+phase30))+Mah(8)*sin(Kh(14)*(w*t+phase+phase30)
)+Mah(8)*sin(Kh(15)*(w*t+phase+phase30))+Mah(9)*sin(Kh(16)*(w*t+phase+phase
30))+Mah(9)*sin(Kh(17)*(w*t+phase+phase30))+Mah(10)*sin(Kh(18)*(w*t+phase+p
hase30))+Mah(10)*sin(Kh(19)*(w*t+phase+phase30)));

%Plots of Line-to-line voltages

figure
plot(t*10^3,Vab)
axis ([0 70 1.1*min(Vab) 1.1*max(Vab)])
xlabel('Time (ms)')
ylabel('Voltage (V)')
title('Vab(wt)')

figure
plot(t*fsamp,2*abs(fft(Vab))/ms)
axis ([-100 4.05*10^4 0 1.1*max(2*abs(fft(Vab))/ms)])
xlabel('Frequency (Hz)')
ylabel('Magnitude (V)')
title('Harmonic Spectrum of Vab(wt)')
```

```
%Phase Voltage Plots

figure
plot(t*10^3,Va)
axis ([0 70 1.1*min(Va) 1.1*max(Va)])
xlabel('Time (ms)')
ylabel('Voltage (V)')
title('Va(wt)')

figure
plot(t*fsamp,2*abs(fft(Va))/ms)
axis ([0 4.05*10^4 0 1.1*max(2*abs(fft(Va))/ms)])
xlabel('Frequency (Hz)')
ylabel('Magnitude (V)')
title('Harmonic Spectrum of Va(wt)')

%Transfer Function

Ha = Va/(Vdc);
Hb = Vb/(Vdc);
Hc = Vc/(Vdc);

%Line Currents

Il =Pout/(sqrt(3) * (Vdc*Mah(1)/sqrt(2.0)) * pf);                    %Magnitude of line
current

Ia = sqrt(2.0)*Il * sin(w*t+theta_I);
Ib = sqrt(2.0)*Il * sin(w*t+theta_I-phase);
Ic = sqrt(2.0)*Il * sin(w*t+theta_I+phase);

figure
plot(t*10^3,Ia,'b',t*10^3,Ib,'g',t*10^3,Ic,'c')
axis([0 25 1.1*min(Ia) 1.1*max(Ia)])
xlabel('Time (ms)')
ylabel('Line Current (A)')
title('Ia(wt), Ib(wt), Ic(wt)')
Legend('Ia(wt)','Ib(wt)','Ic(wt)')

%DC Input Current

Idc = Ia.*Ha + Ib.*Hb + Ic.*Hc;
```

```
figure
plot(t*10^3,Idc)
axis([0 20 1.1*min(Idc) 1.1*max(Idc)])
xlabel('Time (ms)')
ylabel('DC Bus Current A')
title('Idc(wt)')


%FFT of Idc
Idc_fft = fft(Idc);
Idc_fft(1)=Idc_fft(1)/2;                %DC component needs modified due to matlabs fft
algorithm

figure
plot(t*fsamp,2*abs(Idc_fft)/ms)
axis([-200 4.05*10^4 0 1.1*max(2*abs(Idc_fft)/ms)])
xlabel('Frequency (Hz)')
ylabel('Magnitude (A)')
title('Harmonic Spectrum of Idc(wt)')
```

Matlab Code for SVM Gating Signals (svm_switching_function.m)

```
%DC Ripple Current Using Space Vector Modulation Simulation
%Version 1.2    04/13/2004

%Waylon Bowers
%Motor Systems Research Facility
%Oregon State University
%Corvallis, OR 97330

%This material is provided without any guarantee or warranty either
%expressed or implied, and no author or distributor of this material will
%be held responsible for any damage that might possibly result from the use
%or misuse of this material.  The user acknowledges and accepts sole
%responsibility for his/her usage of this material.

%To be used in conjuncture with Simulink File <svm_sw_fund.mdl>

%Space Vector Approach
clear
format long

C = 1;                                  %Number of cycles
```

```
Vm = 600*0.49*(sqrt(2.0)/sqrt(3.0));                %Phase Voltage (max)
Vdc = 600.0;                                  %DC Bus Voltage
Im = 250e3/(0.9*sqrt(3.0)*(600.0*0.49/sqrt(2.0)));      %Phase Current (rms)
Im = Im*sqrt(2.0);                            %Phase Current (max)
      phaseI = -acos(0.9);                        %Current phase shift
      fmod= 60.0;                               %Fundamental Frequency
                fsw = 9900.0;                           %Switching Frequency
                rt = 1.0e-7;                          %Rise time for switch
                Vg = 1;                               %Magnitude of gating signal
                w=2.0*pi*fmod;                          %Frequency in radians
      TsSVM = 1/60/(2*fsw);                       %Sample time for simulink
       N = fsw/fmod;                              %Modulation ratio
         fsw_act = N*fmod;
         dt = (1.0/fsw_act);
         tt = 0.0:dt:C*N*dt;                        %Time vector

   wt = w*tt;
         delt = dt/2.0;
   x=7;                                       %x,y = constants for gating vectors
   y=12;

   for i=1:C*(N),

      %Angle Calculation
                ang(i) = tt(i)*(1.0/(1.0/fmod))*2.0*pi;
                q = 1;
                if ( ang(i) >= (2.0*pi/6.0) && ang(i)  < 2.0*(2.0*pi/6.0))
                 ang(i) = ang(i) - 2.0*pi/6.0;
                q = 2;
      end
                if ( ang(i) >= 2.0*(2.0*pi/6.0) && ang(i)  < 3.0*(2.0*pi/6.0))
                 ang(i) = ang(i) - 2.0*(2.0*pi/6.0);
                q = 3;
      end
                if ( ang(i) >= 3.0*(2.0*pi/6.0) && ang(i)  < 4.0*(2.0*pi/6.0))
                 ang(i) = ang(i) - 3.0*(2.0*pi/6.0);
                q = 4;
      end
                if ( ang(i) >= 4.0*(2.0*pi/6.0) && ang(i)  < 5.0*(2.0*pi/6.0))
                 ang(i) = ang(i) - 4.0*(2.0*pi/6.0);
                q = 5;
      end
                if ( ang(i) >= 5.0*(2.0*pi/6.0) && ang(i)  < 6.0*(2.0*pi/6.0))
                ang(i) = ang(i) - 5.0*(2.0*pi/6.0);
                q = 6;
```

```
    end

    %Reference phase voltages
            refa(i) = Vm*sin(wt(i));
            refb(i) = Vm*sin(wt(i)-(2.0*pi/3.0));
            refc(i) = Vm*sin(wt(i)+(2.0*pi/3.0));

    %Transformation to dq domain using Parks
            refd(i) = 2.0/3.0.*(refa(i)-0.5.*refb(i)-0.5.*refc(i));
            refq(i) = 2.0/3.0.*(((sqrt(3.0))/2.0).*refb(i)-((sqrt(3.0))/2.0).*refc(i));
            refm(i) = sqrt(refd(i).*refd(i) + refq(i).*refq(i));
            U(i) = refm(i)./(0.61*Vdc);

  %Time
      t1(i) = (9.0/(pi*pi))*U(i)*delt*(cos(ang(i))-(1.0/(sqrt(3.0)))*sin(ang(i)));
      t1(i) = abs(t1(i));
      t2(i) = (6.0*(sqrt(3.0))/(pi*pi))*U(i)*delt*sin(ang(i));
      t2(i) = abs(t2(i));
      t0(i) = (delt - t1(i) - t2(i))/2.0;
      t0(i) = abs(t0(i));

      %Sector 1
        if (q == 1)
          timeS11(i,:)= [tt(i) tt(i)+t0(i) tt(i)+t0(i)+rt tt(i)+2.0*delt-t0(i) tt(i)+2.0*delt-
t0(i)+rt tt(i)+2.0*delt];
      timeS13(i,:)= [tt(i) tt(i)+t0(i)+t1(i) tt(i)+t0(i)+t1(i)+rt tt(i)+delt+t0(i)+t2(i)
tt(i)+delt+t0(i)+t2(i)+rt tt(i)+2.0*delt];
      timeS15(i,:)= [tt(i) tt(i)+delt-t0(i) tt(i)+delt-t0(i)+rt tt(i)+delt+t0(i)
tt(i)+delt+t0(i)+rt tt(i)+2*delt];
    else
      timeS11(i,:) = [0 0 0 0 0 0];
      timeS13(i,:) = [0 0 0 0 0 0];
      timeS15(i,:) = [0 0 0 0 0 0];
      end

%Sector 2
        if (q == 2)
          timeS21(i,:)= [tt(i) tt(i)+t0(i)+t2(i) tt(i)+t0(i)+t2(i)+rt tt(i)+delt+t0(i)+t1(i)
tt(i)+delt+t0(i)+t1(i)+rt tt(i)+2.0*delt];
      timeS23(i,:)= [tt(i) tt(i)+t0(i) tt(i)+t0(i)+rt tt(i)+2.0*delt-t0(i) tt(i)+2.0*delt-
t0(i)+rt tt(i)+2.0*delt];
      timeS25(i,:)= [tt(i) tt(i)+delt-t0(i) tt(i)+delt-t0(i)+rt tt(i)+delt+t0(i)
tt(i)+delt+t0(i)+rt tt(i)+2.0*delt];
    else
      timeS21(i,:)= [0 0 0 0 0 0];
```

```
        timeS23(i,:)= [0 0 0 0 0 0];
        timeS25(i,:)= [0 0 0 0 0 0];

      end
%Sector 3
        if (q == 3)
           timeS31(i,:) = [tt(i) tt(i)+delt-t0(i) tt(i)+delt-t0(i)+rt tt(i)+delt+t0(i)
tt(i)+delt+t0(i)+rt tt(i)+2.0*delt];
      timeS33(i,:) = [tt(i) tt(i)+t0(i) tt(i)+t0(i)+rt tt(i)+2.0*delt-t0(i) tt(i)+2.0*delt-t0(i)+rt
tt(i)+2.0*delt];
      timeS35(i,:) = [tt(i) tt(i)+t0(i)+t1(i) tt(i)+t0(i)+t1(i)+rt tt(i)+delt+t0(i)+t2(i)
tt(i)+delt+t0(i)+t2(i)+rt tt(i)+2.0*delt];
      else
        timeS31(i,:)= [0 0 0 0 0 0];
        timeS33(i,:)= [0 0 0 0 0 0];
        timeS35(i,:)= [0 0 0 0 0 0];
  end

 %Sector 4
  if (q == 4)
      timeS41(i,:) = [tt(i) tt(i)+delt-t0(i) tt(i)+delt-t0(i)+rt tt(i)+delt+t0(i)
tt(i)+delt+t0(i)+rt tt(i)+2.0*delt];
      timeS43(i,:) = [tt(i) tt(i)+t0(i)+t2(i) tt(i)+t0(i)+t2(i)+rt tt(i)+delt+t0(i)+t1(i)
tt(i)+delt+t0(i)+t1(i)+rt tt(i)+2.0*delt];
      timeS45(i,:) = [tt(i) tt(i)+t0(i) tt(i)+t0(i)+rt tt(i)+2.0*delt-t0(i) tt(i)+2.0*delt-t0(i)+rt
tt(i)+2.0*delt];
      else
        timeS41(i,:)= [0 0 0 0 0 0];
        timeS43(i,:)= [0 0 0 0 0 0];
        timeS45(i,:)= [0 0 0 0 0 0];
  end

 %Sector 5
  if (q == 5)
           timeS51(i,:) = [tt(i) tt(i)+t0(i)+t1(i) tt(i)+t0(i)+t1(i)+rt tt(i)+delt+t0(i)+t2(i)
tt(i)+delt+t0(i)+t2(i)+rt tt(i)+2.0*delt];
      timeS53(i,:) = [tt(i) tt(i)+delt-t0(i) tt(i)+delt-t0(i)+rt tt(i)+delt+t0(i)
tt(i)+delt+t0(i)+rt tt(i)+2.0*delt];
      timeS55(i,:) = [tt(i) tt(i)+t0(i) tt(i)+t0(i)+rt tt(i)+2.0*delt-t0(i) tt(i)+2.0*delt-t0(i)+rt
tt(i)+2.0*delt];
      else
        timeS51(i,:)= [0 0 0 0 0 0];
        timeS53(i,:)= [0 0 0 0 0 0];
        timeS55(i,:)= [0 0 0 0 0 0];
  end
```

```
 %Sector 6
          if (q == 6)
             timeS61(i,:) = [tt(i) tt(i)+t0(i) tt(i)+t0(i)+rt tt(i)+2.0*delt-t0(i) tt(i)+2.0*delt-
t0(i)+rt tt(i)+2.0*delt];
       timeS63(i,:) = [tt(i) tt(i)+delt-t0(i) tt(i)+delt-t0(i)+rt tt(i)+delt+t0(i)
tt(i)+delt+t0(i)+rt tt(i)+2.0*delt];
       timeS65(i,:) = [tt(i) tt(i)+t0(i)+t2(i) tt(i)+t0(i)+t2(i)+rt tt(i)+delt+t0(i)+t1(i)
tt(i)+delt+t0(i)+t1(i)+rt tt(i)+2.0*delt];
       else
          timeS61(i,:)= [0 0 0 0 0 0];
          timeS63(i,:)= [0 0 0 0 0 0];
          timeS65(i,:)= [0 0 0 0 0 0];
   end

   %Compiling time vectors into signal gating signal vector
         gate1(1,1:6) = timeS11(1,:);
   gate3(1,1:6) = timeS13(1,:);
   gate5(1,1:6) = timeS15(1,:);
   if (i>=2 && q==1)
      gate1(1,x:y) = timeS11(i,:);
      gate3(1,x:y) = timeS13(i,:);
      gate5(1,x:y) = timeS15(i,:);
      x=x+6;
      y=y+6;
   elseif (i>=2 && q==2)
      gate1(1,x:y) = timeS21(i,:);
      gate3(1,x:y) = timeS23(i,:);
      gate5(1,x:y) = timeS25(i,:);
      x=x+6;
      y=y+6;
   elseif (i>=2 && q==3)
      gate1(1,x:y) = timeS31(i,:);
      gate3(1,x:y) = timeS33(i,:);
      gate5(1,x:y) = timeS35(i,:);
      x=x+6;
      y=y+6;
   elseif (i>=2 && q==4)
      gate1(1,x:y) = timeS41(i,:);
      gate3(1,x:y) = timeS43(i,:);
      gate5(1,x:y) = timeS45(i,:);
      x=x+6;
      y=y+6;
   elseif (i>=2 && q==5)
      gate1(1,x:y) = timeS51(i,:);
```

```
        gate3(1,x:y) = timeS53(i,:);
        gate5(1,x:y) = timeS55(i,:);
        x=x+6;
        y=y+6;
    elseif (i>=2 && q==6)
        gate1(1,x:y) = timeS61(i,:);
        gate3(1,x:y) = timeS63(i,:);
        gate5(1,x:y) = timeS65(i,:);
        x=x+6;
        y=y+6;

    end
 end

 %Removing duplicates
 for p=1:(length(gate1)-2)
    if gate1(p)>=gate1(p+1)
       gate1(p+1)=(gate1(p+2)+gate1(p))/(2.0);
   end
   if gate3(p)>=gate3(p+1)
       gate3(p+1)=(gate3(p+2)+gate3(p))/(2.0);
    end
    if gate5(p)>=gate5(p+1)
       gate5(p+1)=(gate5(p+2)+gate1(p))/(2.0);
    end
end

       gate1=gate1(1:length(gate1)-1);
       gate3=gate3(1:length(gate3)-1);
       gate5=gate5(1:length(gate5)-1);

  %Magnitude vector for gating signals
 magn = zeros(size(gate1));
 v = 3;
 for l=1:length(gate1)/6,

     magn(1,v:v+1)=1;
     v=v+6;
end

    %Phase Currents
    tspace = 1/(fmod);
    t = linspace(0,2*tspace,length(gate1));

    Ia = Im * sin(w*t+phaseI);
```

```
Ib = Im * sin(w*t+phaseI-(2.0*pi/3.0));
Ic = Im * sin(w*t+phaseI+(2.0*pi/3.0));
```